Simulating the Last Glacial Maximum and abrupt glacial climate shifts in a coupled Earth System Model

Dissertation zur Erlangung des akademischen Grades
Doktor der Naturwissenschaften (Dr. rer. nat.)

Dissertation zur Erlangung des akademischen Grades eines Doktors der Naturwissenschaften

Dr. rer. nat.

im Fachbereich Physik und Elektrotechnik
der Universität Bremen

vorgelegt von:

Xu Zhang

Feb. 2014, Bremen

Acknowledgement

First of all, I thank my supervisor, Prof. Dr. Gerrit Lohmann for his invaluable support on my PhD work. His very pleasant personality and high enthusiasm on science make our discussions, no matter in the office or on the train, very enjoyable and inspirable. I also acknowledge Dr. Gregor Knorr who always gives me constructive and pertinent advice on my PhD work. His convincing logic on climate dynamics helps me efficiently precede my PhD study. Their broad and clear perspectives on my PhD research guide me into an interesting, exciting and enjoyable science world.

I am grateful to Dr. Martin Werner, Dr. Martin Butzin, Christian Stepanek, Dr. Stephen Hagemann, Dr. Wei Wei, Dr. Xu Xu and the AWI computer center for their technique supports and Mr. Conor Purcell for his help on my English writing during my PhD study. Many thanks to all the former and current colleagues in Paleoclimate Dynamics group in the AWI, for creating such a great working environment I enjoyed quite much. I also want to express my gratitude to Andrea Bleyer and Stefanie Klebe for their excellent administrative work that provided the most comfortable research environment I ever had.

I thank Prof. Dr. Zhengyu Liu in University of Wisconsin Madison, as the host of my study in the US and for sharing his expertise on oceanography.

A special thank goes to my Bachelor and Master thesis adviser, Prof. Dr. Fei Huang, who introduced me into global climate research and provided me with the framework of my knowledge on climate dynamics.

As always, my wife, Yiqun Song, deserves the most gratitude from me. We enjoy every minute of our life and share with each other the happiness as well as the sadness. Immense thanks also to my parents and parents-in-law for their long-term unconditional love and support. It is their love that gives me the strength to move forward and enjoy my work as a climate researcher.

Huge thanks to all the other unmentioned friends, colleagues and my relatives for our unforgetful moment sharing together.

I thank the graduate school POLMAR in the AWI for providing useful courses and the outgoing scholarship for my study in the US, and to China Scholar Council (CSC) and PACES program in the AWI for their funding on my PhD study.

Abbreviation:

AABW: Antarctic Bottom Water

ACC: Antarctic Circumpolar Current

ACR: Antarctic Cold Reversal

AID: Antarctic Ice-sheet Discharge

AMOC: Atlantic Meridional Overturning Circulation

BA: Bølling-Allerød

DO events: Dansgaard-Oeschger events

ECMWF: European Centre for Medium-Range Weather Forecasts

FIS: Fennoscandian Ice Sheet

FWP: Freshwater Perturbation

GHG: Greenhouse Gas

GNAIW: Glacial North Atlantic Intermediate Water

HD-model: Hydrological Discharge model

HE: Heinrich Event

IRD: Ice-Rafted Debris

ITCZ: Intertropical Convergence Zone

LDG: Last Deglaciation

LGM: Last Glacial Maximum

LIS: Laurentide Ice Sheet

MIS: Marine Isotope Stage

NADW: North Atlantic Deep Water

NHIS: Northern Hemisphere Ice Sheets

PFT: Plant Functional Type

PI: Preindustrial

PMIP: Paleoclimate Modeling Intercomparison Projection

SAT: Surface Air Temperature

SIC: Sea Ice Concentration

SST: Sea Surface Temperature

SubST: Subsurface Temperature

YD: Younger Dryas

Abstract

The last deglaciation is one of the best constrained global-scale climate changes documented by climate archives. Nevertheless, understanding of the underlying dynamics is still limited, especially with respect to abrupt climate shifts and associated changes in the Atlantic Meridional Overturning Circulation (AMOC) during glacial and deglacial periods. A fundamental issue is how to obtain an appropriate climate state at the Last Glacial Maximum (LGM, 21,000 years before present, 21ka BP) that can be used as an initial condition for deglaciation. With the aid of a comprehensive climate model, we found that initial ocean states play an important role on the equilibrium time scale of the simulated glacial ocean. Independent of the initialization the climatological surface characteristics are similar and quasi-stationary, even when trends in the deep ocean are still significant, which provides an explanation for the large spread of simulated LGM ocean states among the Paleoclimate Modeling Intercomparison Project phase 2 (PMIP2) models. The simulated ocean state with most realistic AMOC is characterized by a pronounced vertical stratification, in line with reconstructions. Freshwater perturbation experiments further suggest that response of the glacial ocean is distinctly dependent on the ocean background state, i.e. only the state with robust stratification shows an overshoot behavior in the North Atlantic. We propose that the salinity stratification represents a key control on the AMOC pattern and its transient response to perturbations. Furthermore, additional experiments suggest that the stratified deep ocean formed prior to the LGM during a time of minimum obliquity (~27ka BP). This indicates that changes in the glacial deep ocean already occur before the last deglaciation. In combination, these findings represent a new paradigm for the LGM and the last deglaciation, which challenges the conventional evaluation of glacial and deglacial AMOC changes based on an ocean state derived from 21ka BP boundary conditions.

During glacial periods of the Late Pleistocene, an abundance of proxy data demonstrates the existence of large and repeated, millennial-scale climate changes, known as Dansgaard-Oeschger (DO) events. This ubiquitous feature of rapid glacial climate change can be extended back as far as 800 ka BP in the ice core record, and has drawn broad attention within the science and policy making communities alike. Many studies have been dedicated to investigating the underlying causes of these changes, however a coherent mechanism remains elusive. Using a fully-coupled climate model, we show that the non-linear responses of the glacial ocean to Northern Hemisphere Ice Sheets (NHIS) volume changes in the coupled atmosphere-ocean system can explain the occurrence of rapid glacial climate shifts. The global climate responses, including abrupt warming in the North Atlantic and a shift of the tropical rain belts, are generally consistent with empirical evidence. A hysteresis analysis with respect to changes of the NHIS suggests that two distinct glacial climate modes coexist at identical intermediate ice sheet volumes. Notably, minor shifts in the NHIS and atmospheric carbon dioxide can trigger the rapid climate transitions, which occur due to a local positive atmosphere-ocean-sea ice feedback in the North Atlantic at intermediate ice-sheet volume. Our results demonstrate that this distinct glacial climate sensitivity to forcing changes is associated with tempo-spatial variations in the internal variability of sea-ice cover and surface air temperature in the northern North Atlantic and Nordic Sea. In conclusion, the hysteresis

of the glacial ocean with respect to ice-sheet variation provides the first coherent concept for understanding the recorded millennial-scale variability and abrupt climate changes in the coupled atmosphere-ocean system, as well as their linkages to intermediate ice-sheet volume during glacials.

Table of Contents

Chapter 1. Introduction

Ocean circulation plays a crucial role in the climate system, by moving immense amounts of heat, prominently from lower latitudes to higher latitudes, where heat is released to the atmosphere. This poleward heat transport is a fundamental driver of the climate system and characterizes the variability of the climate, as we know it today. One prominent component of the ocean circulation is known as the Atlantic Meridional Overturning Circulation (AMOC) which is characterized by northward flowing warm, saline water in the upper layers of the Atlantic (red curve in Fig. 1.1), a cooling and freshening of the water at higher northern latitudes of the Atlantic in the Nordic and Labrador Seas, and southward flowing colder water at depth (light blue curve). Potential changes in the operational mode of the AMOC, as a consequence of alterations in the hydrological cycle and greenhouse gas (GHG) concentration, draw our concerns regarding the future fate of our climate [*Meehl et al.,* 2007].

During the glacial period of Late Pleistocene, an abundance of proxy data demonstrates the existence of large and repeated millennial-scale climate changes, known as Dansgaard-Oeschger (DO) events [*Dansgaard et al.*, 1993]. This ubiquitous feature of rapid glacial climate change can be extended back as far as 800 ka BP in the ice core record [*Barker et al.*, 2011], and has drawn broad attention within the science and policy making communities alike [*Masson-Delmotte et al.,* 2013]. The last deglaciation (LDG) and Marine Isotope Stage 3 (MIS3) during the last glacial-interglacial cycle, due to relatively more available proxy data, are well-suited time intervals for investigating the underlying causes of these rapid changes, via model simulations [e.g. *Liu et al.*, 2009; *Menviel et al.*, 2011; *Gong et al.*, 2013].

The LDG (19~11.5ka BP) is the most recent glacial termination during the last 800 ka BP, characterized by several rapid climate shifts especially in the Northern Hemisphere, known as Heinrich Event 1 (HE1), Bølling-Allerød warming (BA, or DO event 1) and Younger Dryas cooling (YD). These rapid events occurred during a globally warming background associated with changes in insolation, increases in atmospheric carbon dioxide and the melting of continental ice-sheet. In comparison, most of the DO events as well as the HEs occurred when global ice volume was varying at intermediate levels

during last glaciation, e.g. during the MIS3 (65 ~ 27ka BP). In this time interval, relatively smaller fluctuations in insolation, atmospheric CO_2 concentration and ice-sheet size are accompanied by large and rapid Northern Hemisphere warming, suggesting a different background climate in contrast to the LDG.

To date, many model simulations with different levels of complexity have been conducted to simulate the transient responses of glacial ocean to prescribed freshwater perturbation (FWP) as well as other forcing types (e.g. ice-sheet, orbital parameter, greenhouse gas concentration etc.), to study the underlying mechanism [*Ganopolski and Rahmstorf*, 2001; *Schmittner et al.*, 2002; *Knorr and Lohmann* 2003; *Weaver et al.*, 2003; *Knorr and Lohmann*, 2007; *Liu et al*., 2009; *Menviel et al.*, 2011]. In all the cases, the abrupt northern warming as well as the corresponding global responses are attributed to the abrupt AMOC variation in response to gradual/rapid forcing changes, commonly the FWP. Nevertheless, it is of great importance to note that there are large uncertainties in the representation of freshwater origin, timing and magnitude in different models to generate the simulated results comparable to reconstructions [e.g. *Ganopolski and Rahmstorf*, 2001; *Schmittner et al.*, 2002; *Roche et al.*, 2004; *Stouffer et al.*, 2006; *Liu et al.*, 2009; *Menviel et al.*, 2011; *Carlson and Clark*, 2012; *Roberts et al.*, 2014]. Additionally, palaeoceanographic evidence for ocean circulation changes and their relationship to freshwater perturbation remains elusive [*Dansgaard et al.*, 1993; *McManus et al.*, 1999; *Elliot et al.*, 2002; *Hemming*, 2004; *Ahn and Brook*, 2008; *Piotrowski et al.*, 2008; *Barker et al.*, 2011]. Therefore, further studies are highly desirable to disentangle this puzzle so as to strengthen our confidence of future climate projections associated with AMOC changes.

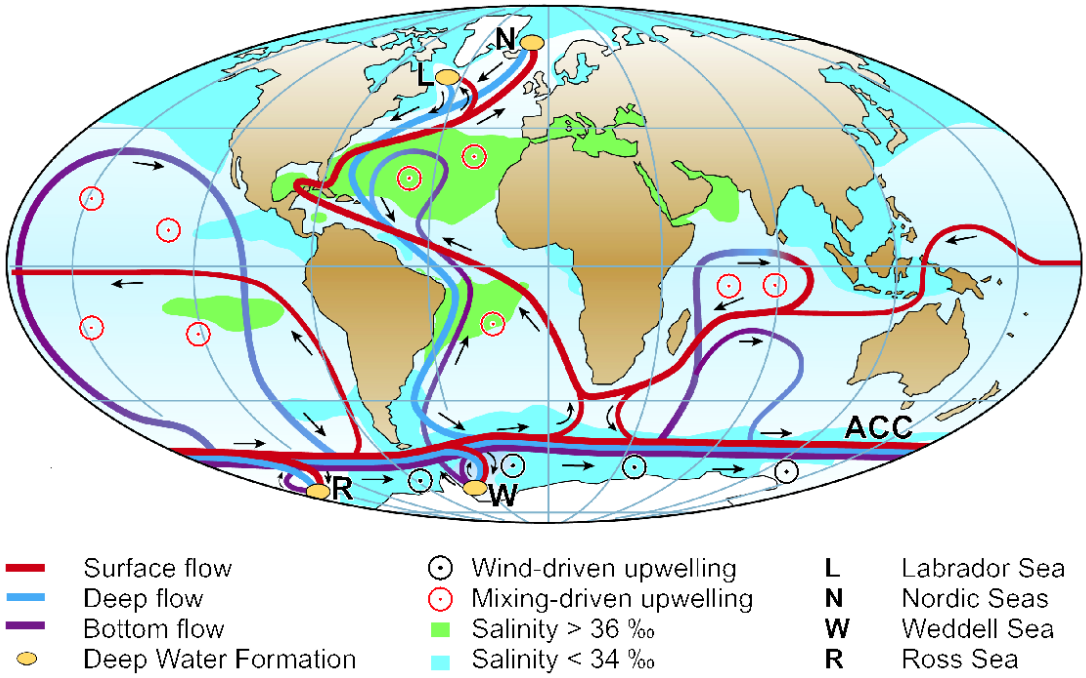

Fig. 1.1 Schematic of the ocean circulation associated with the global Meridional Overturning Circulation (MOC), with special focus on the Atlantic section of the flow (AMOC). The red curves in the Atlantic indicate the northward flow of water in the upper layers. The filled orange circles in the Nordic and Labrador Seas indicate regions where near-surface water cools and becomes denser, causing the water to sink to deeper layers of the Atlantic. This process is referred to as "water mass transformation," or "deep water formation." In this process heat is released to the atmosphere. The light blue curve denotes the southward flow of cold water at depth. At the southern end of the Atlantic, the AMOC connects with the Antarctic Circumpolar Current (ACC). Deep water formation sites in the high latitudes of the Southern Ocean are also indicated with filled orange circles. These contribute to the production of AABW, which flows northward near the bottom of the Atlantic (indicated by dark blue lines in the Atlantic). The circles with interior dots indicate regions where water upwells from deeper layers to the upper ocean.(from *Kuhlbrodt et al.*, 2007)

1.1 Working hypothesis 1: Initial ocean states affect the glacial ocean simulation

The Last Glacial Maximum (LGM, 23~19ka BP) is commonly used as the starting point for LDG simulations. Given the climate state's immense continental ice sheets and low GHG concentration, for future projections [*Braconnot et al*., 2012] it is also an excellent test-bed for climate models to simulate a climate that strongly deviates from our modern condition (e.g. the Paleoclimate Modeling Intercomparison Projection, or PMIP; [*Braconnot et al.,* 2007]). Thus, reproducing the LGM climate is one of the most fundamental issues in understanding the subsequent abrupt climate change during the

LDG. However, there has been a substantial difference in AMOC states among different models during the LGM [*Otto-Bliesner et al.*, 2007]. It is worth noting that PMIP utilized no specific protocol concerning the initial ocean condition for LGM simulations, and only CCSM3 and HadCM3M2, initialized from a previous glacial ocean state, were found to yield a simulated glacial ocean comparable to reconstructions [*Braconnot et al.*, 2007; *Weber et al.*, 2007]. Thus, it can be asked whether the different LGM AMOC states are potentially associated with different initial ocean states. This hypothesis will be discussed in detail in **Chapter 3**.

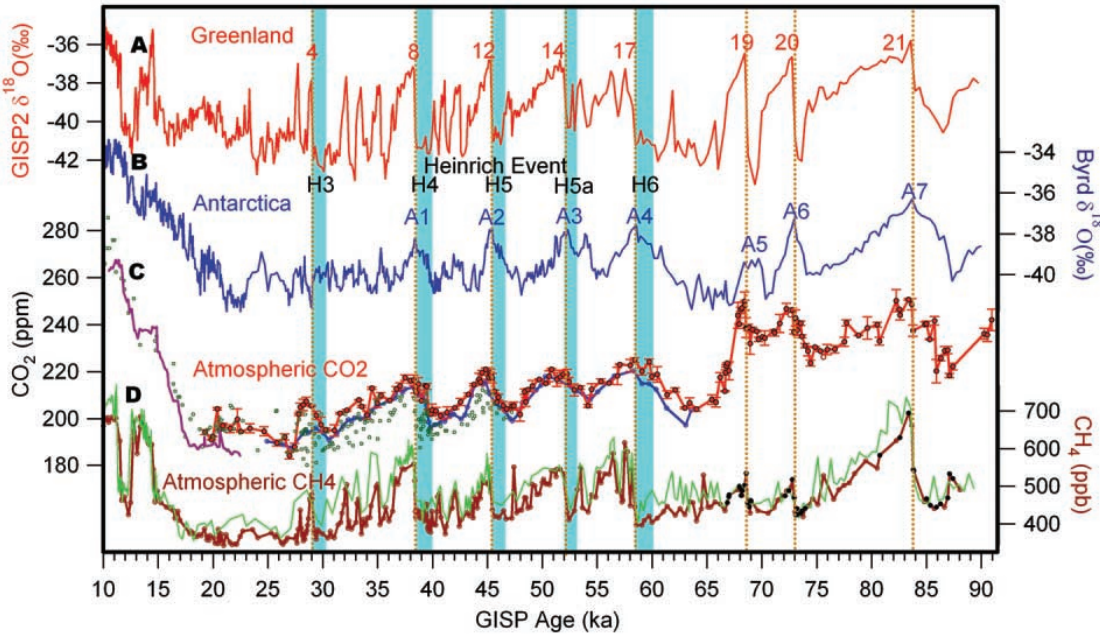

Fig.1.2 Atmospheric CO_2 composition and climate during the last glacial period. (A) Greenlandic temperature proxy, $d^{18}O_{ice}$ [*Grootes et al.*, 1993]. Red numbers denote DO events. (B) Byrd Station, Antarctica temperature proxy, $d^{18}O_{ice}$ [*Blunier and Brook*, 2001]. A1 to A7, Antarctic warming events. (C) Atmospheric CO_2 concentrations. Red dots [this study and early results for 47 to 65 ka [*Ahn and Brook*, 2007] at Oregon State University and green circles [*Stauffer et al.*, 1998] (results from University of Bern) are from Byrd ice cores. Red dots are averages of replicates, and red open circles at ~73 and 76 ka are single data[*Ahn and Brook*, 2007, 2008]. Blue line is from Taylor Dome ice core [*Indermühle and Monnin*, 2000] on the GISP2 time scale [*Ahn and Brook*, 2007]. Purple line is from EPICA Dome C [*Monnin et al.*, 2001]. (D) CH_4 concentrations from Greenland (green) [*Blunier and Brook*, 2001] and Byrd ice cores (brown) [*Blunier and Brook*, 2001; *Ahn and Brook*, 2008]. Black dots, new measurements for this study. Vertical blue bars, timing of Heinrich events (HE 3 to HE 6) [*Hemming*, 2004]. Brown dotted lines, abrupt warming in Greenland. (from *Ahn and Brook*, 2008)

1.2 Working hypothesis 2: Varying intermediate ice volume controls the rapid glacial climate shifts

Until now most studies of abrupt climate changes in the past (e.g. DO events) are mainly based on so-called "hosing experiments", due to the assumption that the AMOC variation, especially its hysteresis behavior, is controlled by the prescribed FWP amount in Atlantic basin [*Rahmstorf*, 1996]. This approach was first employed to explain the YD cooling which occurred when a major outbreak of glacial Lake Agassiz drains massive freshwater to the ocean, and thereafter extended to numerous other events in the paleoclimate records of which massive Ice-Rafted debris (IRD) during HEs [*Hemming,* 2004] is supposed to be equivalent to freshwater injection in the open ocean [e.g. *Clark et al.,* 2001; *Rahmstorf*, 2002]. However, it is still unknown whether HEs (i.e. FWP) act as a trigger or respond as a consequence of the climate mode transition in the past. A number of problems exist with regards to using freshwater forcing alone to explain the recorded abrupt climate shifts during glacials. Listed below are some of these controversies:

1. Some IRD data lags the onset of the stadials [e.g. *Zahn et al.*, 1997].
2. Some IRD data actually occurs during the interstadials [e.g. *Dokken et al.*, 2013].
3. IRD data does not always coincide with DO-events [e.g. *Dansgaard et al.*, 1993; *McManus et al.*, 1999; *Hemming*, 2004; *Barker et al.*, 2011].
4. Freshwater discharge rates indicated by proxy data are much weaker than those used in climate model simulations. [e.g. *Roche et al.*, 2004; *Zhang and Delworth*, 2005; *Stouffer et al.*, 2006; *Liu et al.*, 2009; *Zhang et al.*, 2013; *Roberts et al.*, 2014]
5. The freshwater history and origin to force consistent climate change with reconstructions is highly uncertain and varies with models [e.g. *Ganopolski and Rahmstorf*, 2001; *Schmittner et al.*, 2002; *Schmittner and Galbraith*, 2008; *Liu et al.*, 2009; *Menviel et al.*, 2011].
6. Sea surface warming occurs in the northern North Atlantic during ice-rafting events [e.g. *Peck et al.,* 2008; *Jonkers et al*., 2010], contradicting to model

results derived from hosing experiments [e.g. *Ganopolski and Rahmstorf,* 2001; *Zhang and Delworth*, 2005; *Stouffer et al.*, 2006; *Zhang et al.*, 2013].

7. The AMOC resumption upon cessation of modelled freshwater perturbation takes longer than the time indicated by proxy data [*Stouffer et al.*, 2006]

One fundamental characteristic of DO variability, possibly offering a profound clue to their origin, is that almost all events occurred during glacial periods when global ice volume was varying at intermediate levels [*Dansgaard et al.*, 1993; *McManus et al.*, 1999; *Schulz et al.*, 1999; *Barker et al.*, 2011]. This suggests a potential relationship between the intermediate ice sheets and the existence of millennial scale climate variability [*Wunsch*, 2006]. In **Chapter 4**, a systematical test of this hypothesis is tested via the prescription of varying ice sheet configurations in a fully coupled atmosphere-ocean climate model.

1.3 Working hypothesis 3: The glacial ocean responses to freshwater perturbation are dependent on perturbed locations, glacial ocean states and glacial background conditions.

As previously mentioned, although large uncertainties exist in the relationship between IRD and glacial ocean circulation changes, FWP is still an effective means of triggering AMOC variation for the investigation of resulting global responses in climate models. To simulate global deglacial signatures comparable to reconstructions, different models have employed distinct FWP schemes, i.e. the magnitude, timing and origins [e.g. *Liu et al*., 2009; *Menviel et al.,* 2011], especially for the BA warming (~14.6ka BP), a time interval with unclear source of meltwater injection as well as the magnitude and timing causing ~20m sea level rise in less than 500 years [e.g. *Carlson and Clark*, 2012]. The large spread of initial states of the LDG simulations amongst models, i.e. the simulated LGM state [*Otto-Bliesner et al.*, 2007], indicates potential effects of initial ocean states in the transient LDG simulations. Furthermore, it is worthy to note that mechanisms accounting for the rapid glacial climate shifts are likely different under distinct background climates [e.g. *Gong et al.,* 2013], i.e. between MIS3 and LDG. Thus, the explanations based on hosing experiments under present-day/LGM boundary condition are probably

inappropriate for DO events during the MIS3 [e.g, *Ganopolski and Rahmstorf*, 2001; *Zhang and Delworth*, 2005; *Stouffer et al.*, 2006]. Given this complexity a suite of hosing experiments in a fully coupled earth system model was conducted to evaluate this hypothesis in **Chapter 5**.

1.4 Outline of the thesis

The general structure of this thesis is as follows. Chapter 2 provides details of the fully coupled Earth System Model (ESM) which is used for the three main studies presented in Chapters 3 to 5. Chapter 6 summarizes the main findings of the thesis and provides an overall discussion and outlook for possible future research.

In more detail: Chapter 2 introduces the general information about atmosphere-ocean-land surface components of the earth system model COSMOS. In Chapter 3 (published in ***Climate of the Past***, referred to Zhang et al. [2013]), working hypothesis 1 is tested via initialization of the LGM simulations with different ocean states and integrating to quasi-equilibrium states with respect to deep ocean properties. It is confirmed that initial ocean states do affect the glacial simulations in fully coupled climate models by influencing the transient characteristics and the equilibrium time scale of the deep ocean. In Chapter 4 (in revision in ***Nature***, referred to Zhang et al. (*in revision*)), a suite of simulations with respect to varying Northern Hemisphere Ice Sheets (NHIS) is conducted in order to corroborate working hypothesis 2. The hysteresis behavior of glacial ocean circulation with respect to NHIS changes is for the first time identified in the fully coupled climate model, providing a coherent mechanism accounting for the recorded millennial-scale variability and abrupt climate changes in the coupled atmosphere-ocean system. This is followed by Chapter 5: freshwater sensitivity studies. This Chapter, which includes my contribution to Kageyama et al. [2013], work in ***Climate of the Past,*** Weber et al. (*accepted*) in ***Nature,*** parts of my work in Zhang et al. [2013] published in ***Climate of the Past,*** and Zhang et al. (*in revision*) in ***Nature***, provides an assessment of the impacts of meltwater origins, glacial ocean states and glacial background conditions on the glacial ocean response to FWP in COSMOS. Finally, Chapter 6 summarizes the thesis and provides in-depth discussion along with a future outlook.

Chapter 2. Model Description

Community Earth System Models (COSMOS, version: COSMOS-landveg r2413, 2009) that have been mainly developed by the Max Planck Institute for Meteorology (MPI) in Hamburg is used to investigate the working hypothesis in this thesis. The version used here includes the ECHAM5 atmosphere model in T31-resolution (~3.75°) with 19 levels, the MPI ocean model (MPI-OM) in GR30 resolution (3.0°× 1.8°) with 40 levels, and the land-vegetation model JSBACH. Our setup is identical to the COSMOS-1.2.0 release, which has been developed in the Millennium project [*Jungclaus et al.*, 2010], but additionally includes a dynamical vegetation module [*Brovkin et al.,* 2009]. In this version, COSMOS was already utilized to analyse the last millennium [*Jungclaus et al.*, 2010], warm climates in the Miocene [*Knorr et al.*, 2011] and the Pliocene [*Stepanek and Lohmann*, 2012; *Dowsett et al.*, 2013], glacial [*Gong et al.*, 2013; *Kageyama et al.*, 2013; *Zhang et al.*, 2013] and interglacial climate [*Varma et al.*, 2012; *Wei and Lohmann*, 2012; *Wei et al.*, 2012].

2.1 The atmosphere and land surface model ECHAM5-JSBACH

ECHAM5 was adapted for climate research from the weather forecasting model of the European Centre for Medium-Range Weather Forecasts (ECMWF). The model is based on a spectral dynamical core with a hybrid sigma-/pressure-level system in vertical dimension. In our model setup, we use ECHAM5 in T31/L19 resolution (i.e. there are 19 vertical levels and triangular truncation of the series of spherical harmonics is performed at wave number 31) (Fig. 2.1). The approximate horizontal resolution is 3.75° × 3.75° and each time step is 2400 s.

A high-resolution (0.5° × 0.5°) hydrological discharge model (HD-model), described in details by Hagemann and Duemenil [1998] and Hagemann and Gates [2003], closes the hydrological cycle in the coupled system (Fig. 2.2). It simulates the translation and retention of land-bound lateral water flows, which are separated into overland flow, base flow, and river flow. The sum over these quantities makes up the runoff at each grid cell. The HD-model ensures that water flowing into water-sinks over land is redistributed to the ocean. Land ice sheets are not simulated but prescribed in our model setup. Therefore,

precipitation over glacier cells is transferred toward adjacent ocean points rather than being accumulated as ice volume. Data exchange between the coarse atmosphere grid and the high-resolution HD-model is performed via an interpolation scheme.

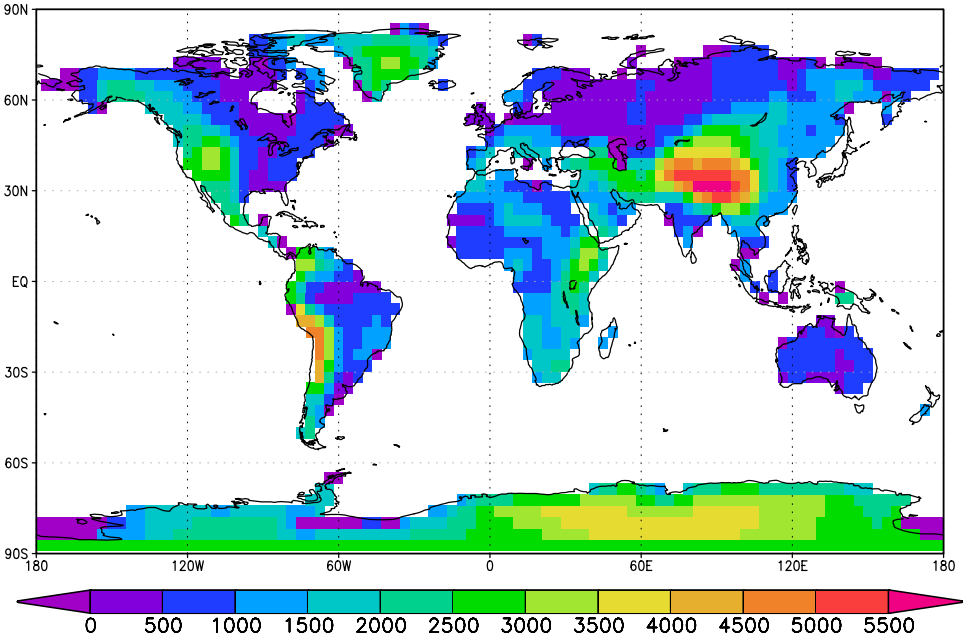

Fig. 2.1 Topography (units: m) in the atmosphere model ECHAM5 for preindustrial (PI) configuration.

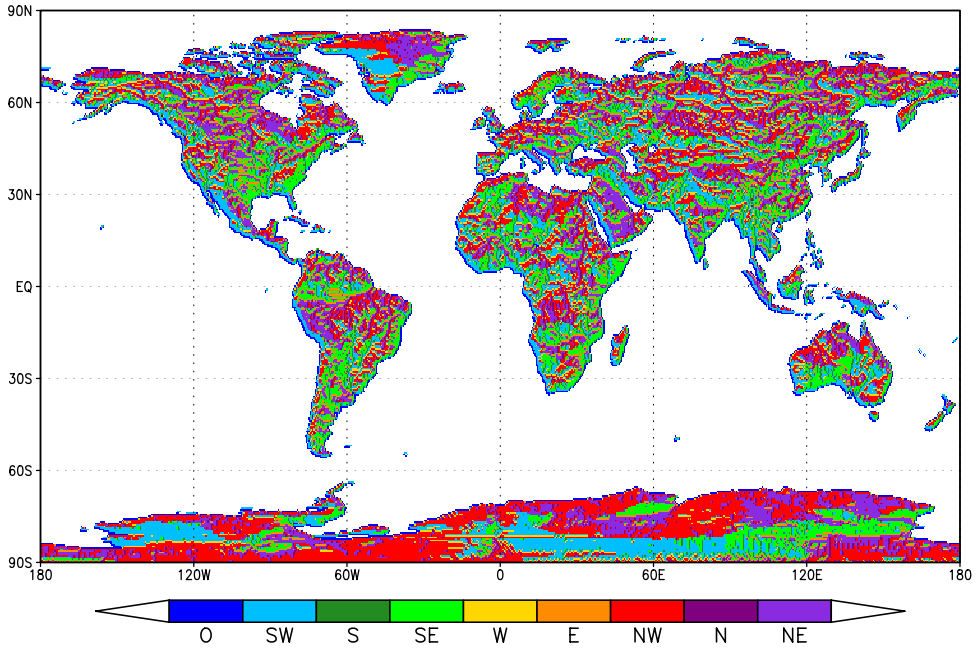

Fig. 2.2 River directions in the HD model grids (0.5° × 0.5°) of ECHAM5 for PI configuration. The colours indicate the flow direction at each grid point; ocean is indicated by white. In addition to the four main and diagonal directions, dark blue (O) marks grid

cells where the water flow is directly into the ocean (coastal grid-points).

The JSBACH land surface and vegetation model, described by Raddatz et al. [2007], is an extension of the ECHAM5 model. It runs at the same horizontal resolution as the atmosphere model ECHAM5. In JSBACH, eight of thirteen different plant functional types (PFTs) have been in use for the model runs (Table 2.1). These include different forms of deciduous and evergreen trees, shrubs and grasses. The model is capable of simulating dynamic changes in the vegetation distribution as a result of changes in ambient climatic conditions [*Brovkin et al.,* 2009]. A fixed vegetation distribution can be prescribed via the parameters land cover fraction (which defines the relative contribution of a PFT to the vegetated area) and the maximum vegetated cell area fraction. As the dynamic vegetation module of JSBACH is activated, both fields are simulated rather than being prescribed.

PFT index	description	type: forest (F) or grass (G)
1	tropical broadleaved evergreen forest	F
2	tropical deciduous broadleaved forest	F
3	temperate / boreal evergreen forest	F
4	temperate / boreal deciduous forest	F
5	raingreen shrubs	G
6	cold shrubs (tundra)	G
7	C3 perennial grass	G
8	C4 perennial grass	G

Table 2.1 Plant functional types considered by JSBACH. These include different types of evergreen and deciduous forest, shrubs and grasses. The rightmost column indicates to which generalized vegetation type (forest or grass) a PFT contributes.

2.2 The ocean model MPI-OM

MPI-OM is a hydrostatic, Boussinesq, free surface, primitive equation ocean and sea ice model [*Marsland et al.,* 2003; *Jungclaus et al.,* 2006]. The model dynamics are solved on an Arakawa C-grid. Our model setup is formulated on a bipolar, orthogonal, curvilinear GR30/L40-grid with poles over Greenland and Antarctica (Fig. 2.3). The advantage of this setup is an increased resolution at many deep-water formation sites, which facilitates a more realistic simulation of the physical processes operating in these regions. The formal horizontal resolution is 3.0°× 1.8°, with the vertical dimension being split into 40

unequally spaced z-coordinate model levels. Ocean bathymetry is resolved on partial grid cells [*Marsland et al.,* 2003] and defined via a global data set of ocean bottom depth. Flow near the bottom boundary is parameterized by a bottom boundary layer scheme in a similar way as described by Beckmann and Doescher [1997], Lohmann [1998], and Legutke and Maier-Reimer [2002]. Eddy-induced mixing is parameterized following Gent et al. [1995]. Furthermore, an isopycnal diffusion scheme for subgrid-scale mixing is applied [*Marsland et al.,* 2003]. Overturning by convection is implemented via increased vertical diffusion [*Jungclaus et al.,* 2006]. MPI-OM includes a dynamic-thermodynamic sea ice model after Hibler III [1979] that simulates the distribution and thickness of sea ice considering ambient climatic conditions. The model is run at a time step of 8640s; no flux adjustment is applied.

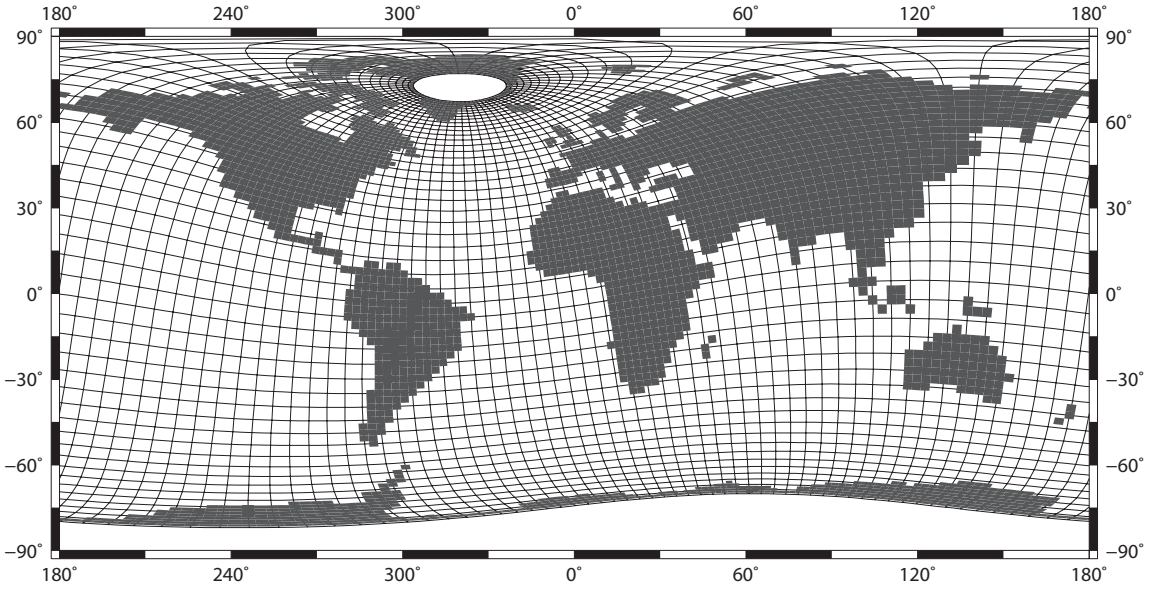

Fig. 2.3 Land-sea distribution on the ocean model grid for PI configuration. There are two grid poles (white areas) that are located over Greenland and Antarctica. The nominal grid resolution of 3° × 1.8° of the 122 × 101 grid varies; it is high in polar regions and highest around Greenland.

Chapter 3. Different ocean states and transient characteristics in Last Glacial Maximum simulations

Due to its capability to redistribute large amounts of heat around the globe [e.g. *Ganachaud and Wunsch*, 2000], the Atlantic meridional overturning circulation (AMOC) is a key player in the global climate system. Potential changes in the operational mode of the AMOC, as a consequence of alterations in the hydrological cycle and greenhouse gas concentration, draw our concerns regarding the future fate of our climate [*Meehl et al.,* 2007].

During glacial and deglacial periods, large and abrupt changes in the climate system are thought to have repeatedly occurred. These changes have been linked to large and abrupt shifts in the AMOC [e.g. *Dansgaard et al.,* 1993; *Bard et al.,* 2000; *Ganopolski and Rahmstorf*, 2001; *Knorr and Lohmann*, 2003; *Knorr and Lohmann*, 2007; *Liu et al.,* 2009; *Barker et al.,* 2010; *Menviel et al.,* 2011]. A well-suited period to investigate the underlying mechanisms by model simulations is the last deglaciation [*Knorr and Lohmann*, 2007; *Liu et al.,* 2009; *Menviel et al.,* 2011] due to the abundance of available data based reconstructions [e.g. *Lea et al.*, 2003; *McManus et al.,* 2004; *Peltier*, 2004; *Ahn and Brook*, 2008; *Gherardi et al.*, 2009]. One of the most fundamental issues in this respect is the definition of a climate state to be used as an initial state. On account of the abundance of available proxy data and maximum ice sheet volume [*Duplessy et al*., 1988; *Bard et al.,* 2000; *Adkins et al.,* 2002; *Pflaumann,* 2003; *Peltier*, 2004; *Gersonde et al.,* 2005; *Lynch-Stieglitz et al.,* 2007; *Clark et al.,* 2009; *Gutjahr and Lippold*, 2011; *Hesse et al.,* 2011], the Last Glacial Maximum (LGM, about 21000yr before present, hereafter 21kaBP) commonly serves as the starting point for simulations of the last deglaciation [*Liu et al.,* 2009; *Menviel et al.,* 2011]. Furthermore, it is also an excellent test bed for climate models to simulate a climate that strongly deviates from our modern condition (e.g. the Paleoclimate Modeling Intercomparison Projection, or PMIP; *Braconnot et al*., 2007) for the future projection [*Braconnot et al.,* 2012]. However, there was a substantial difference in AMOC states among different models during the LGM [*Otto-Bliesner et al.,* 2007]. It is worth noting that PMIP utilized no specific protocol concerning the initial ocean condition for LGM simulations, and only CCSM3 and HadCM3M2, initialized

from a previous glacial ocean state, were found to yield a simulated glacial ocean comparable to reconstructions (Fig. 3.1) [*Braconnot et al.,* 2007; *Weber et al.,* 2007]. Thus, it is open to question whether the different LGM AMOC states are potentially associated with different regimes due to the mean deep-ocean properties.

The work done in this Chapter is referred to the published paper by Zhang et al. [2013] in ***Climate of the Past***.

3.1 Experimental design

In the following section we describe the experimental set-up of the ten model simulations that represent the basis for our study. A summary of the experiment characteristics is also provided in Table 1.

	Boundary conditions	Initial conditions	Integrated years
PI (control)	Pre-industrial	Present-day ocean	3000
LGM2PI	Pre-Industrial	Glacial ocean	3000
LGMW	21ka	Glacial ocean	4000
LGMS	21ka	Present-day ocean	5000
LGMS27ka	21ka, except 27ka orbital forcing	Model year 4000 in LGMS	700

Table 1 Model simulations used in Chapter 3.

3.1.1 The LGM simulations

External forcing and boundary conditions are imposed according to the PMIP3 protocol for the LGM (available at http://pmip3.lsce.ipsl.fr/). The respective boundary conditions for the LGM comprise orbital forcing, greenhouse gas concentrations (CO2 = 185ppm; N2O = 200ppb; CH4 = 350ppb), ocean bathymetry, land surface topography, run-off routes according to PMIP3 ice sheet reconstruction and increased global salinity (+ 1 psu compared to modern value) to account for a sea level drop of ~116 m.

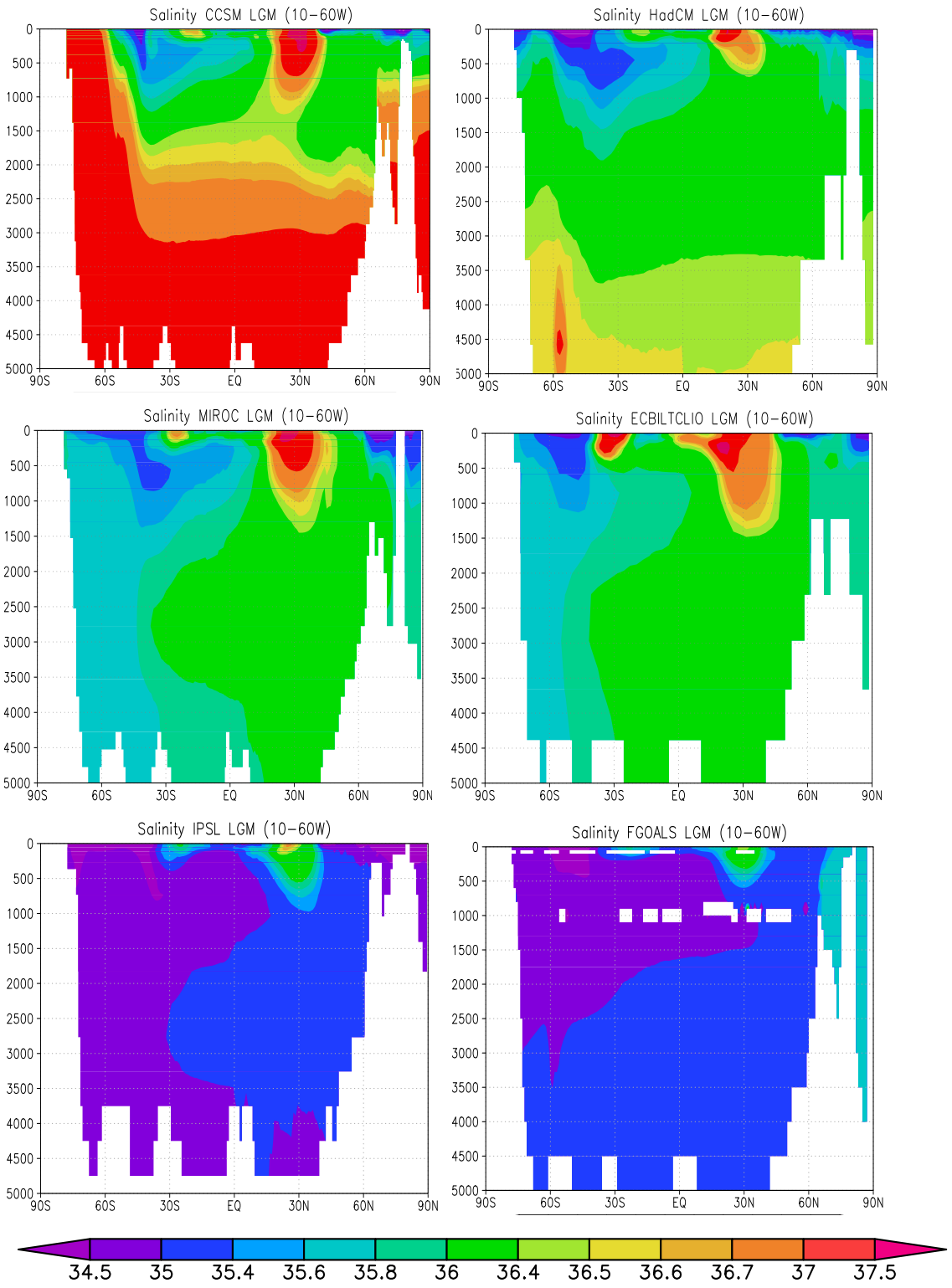

Fig. 3.1 Meridional section of zonal mean salinity in Atlantic Ocean for six PMIP2 models (CCSM3 [*Otto-Bliesner et al.*, 2006], HadCM3M2 [*Gordon et al.*, 2000], MIROC 3.2 [*K-1-Model-Developers*, 2004], ECBilt-CLIO [*de Vries and Weber*, 2005], FGOALS-1.0g [*Yu et al.*, 2004; *Yu et al.,* 2002] and IPSL-CM4-V1-MR [*Marti et al.,* 2005]. The stratification in CCSM3 and HadCM3M2 is comparable with reconstruction [*Otto-Bliesner et al.*, 2007],

while the ocean structure in MIROC 3.2, ECBilt-CLIO, FGOALS-1.0g and IPSL-CM4-V1-MR is more like to present day with the saltiest deep-water mass in the North Atlantic. According to their salinity structure, one can divide the PMIP2 models into two main classes, which are related to a highly stratified ocean, but weaker AMOC (i.e. CCSM3 and HadCM, as our quasi-equilibrium ocean state) and weaker stratified, but stronger AMOC (transient ocean state).

Using the same LGM boundary conditions we performed two experiments, LGMW and LGMS, with different initial ocean states and integrated them for 4000 and 5000 years, respectively (Table 1). LGMS is initialized from a ocean state with imposed present-day temperature and salinity fields [*Levitus et al.*, 1998], while LGMW from a glacial ocean state. The initial glacial ocean was generated through an ocean-only model, MPI-OM (ocean component of our COSMOS set-up), which was run for 3000 years under the LGM conditions. To generate the glacial ocean state with MPI-OM, we obtained its atmospheric forcing from an ECHAM3 (T31) run [*Lohmann and Lorenz*, 2000], forced by CLIMAP sea surface temperature (SST) [*CLIMAP Members*, 1981], and derived its initial ocean state and surface salinity restoring from PMIP2 model outputs of CCSM3 (the National Center for Atmospheric Research CCSM3 model) that is assumed to have a good performance on simulating the LGM climate state in comparison to other PMIP2 models [*Otto-Bliesner et al.*, 2007; *Weber et al.*, 2007].

To define the representative climatology from both LGM runs we employed the quasi-equilibrium criteria of the PMIP protocol [*Braconnot et al.*, 2007] to assess the stability of the simulated ocean states. That is, quasi-equilibrium state can be defined, as the global SST trend is less than 0.05k/century as well as a stable AMOC. Figures 3.2 and 3.3 show the AMOC indices and 100-year running means of global mean sea surface temperature (SST) for the simulations LGMW and LGMS. Compared to the gradual increase of AMOC and SST in LGMW, the decreasing trend in LGMS is particularly pronounced, especially after the model year 3000.

Based on the PMIP criteria [*Braconnot et al.,* 2007], LGMW and LGMS are in quasi-equilibrium after model years 2700 and 4500, respectively. In LGMW, due to the fact that there is almost no change in the climatology after model year 2700 (Figs. 3.2-3.7), the climatologically annual mean of model years 2900-3000 was chosen to represent the quasi-equilibrium ocean state LGMW-e. In LGMS, there is almost no difference between climatology of model years 4600-4700 and 4500-5000. To better compare with the

outputs from the 27ka simulation (see details in Section 1.3), thus we define the climatology mean between model years 4600-4700 as LGMS-e to represent the quasi-equilibrium state in LGMS.

Note that the ocean state between model years 2500-3000 in LGMS also meets PMIP criteria, although the trend in its deep ocean properties is significant (Fig. 3.4). Accordingly, to better compare with LGMW-e, model years 2900-3000 in LGMS are averaged to represent this ocean state and named as LGMS-t_{deep} here.

A comparison among the ocean states LGMS-t_{deep}, LGMS-e and LGMW-e was made with respect to the corresponding climatology (Figs. 3.5-3.7) and surface and deep ocean trends (Figs. 3.2-3.4). It suggests that due to their similarity LGMS-e and LGMW-e can represent the final equilibrium LGM state in our model, however LGMS-t_{deep} is the state in the transient phase of bottom water properties. In this study, we will mainly focus on the contrast between LGMS-t_{deep} and LGMW-e (Figs. 3.2-3.4).

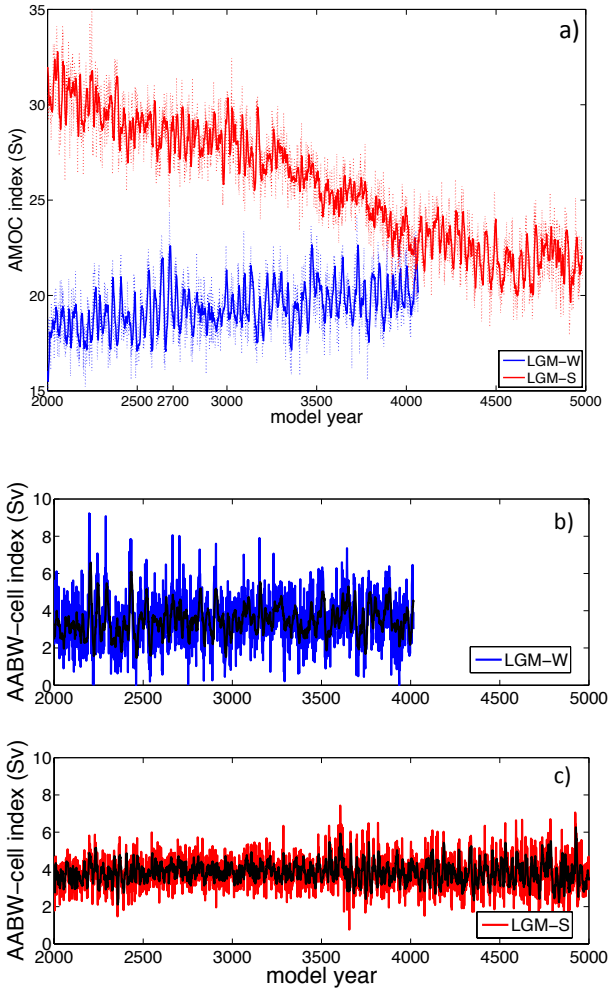

Fig. 3.2 AMOC indices with respect to a) NADW-cell (defined as the maximum value of stream function below 500m in the North Atlantic) and b-c) AABW-cell (defined as the maximum of absolute value of stream function below 2500m along 30°S) for LGMS (red) and LGMW (blue). The bold solid lines are the 10-year running mean. Units: Sv.

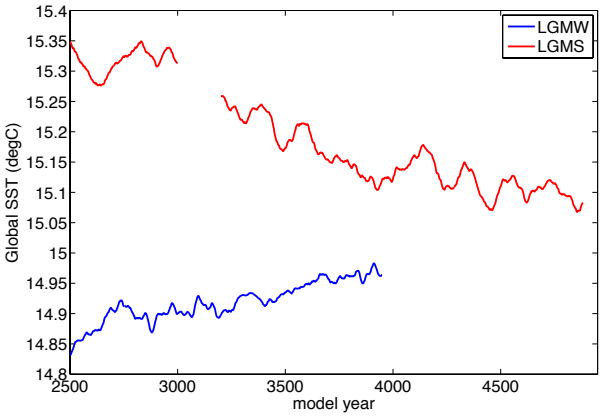

Fig. 3.3 100-year running mean for global mean SST in LGMW (blue) and LGMS (red). The gap between the model year 3000-3200 in LGMS is due to missed dataset. Units: °C.

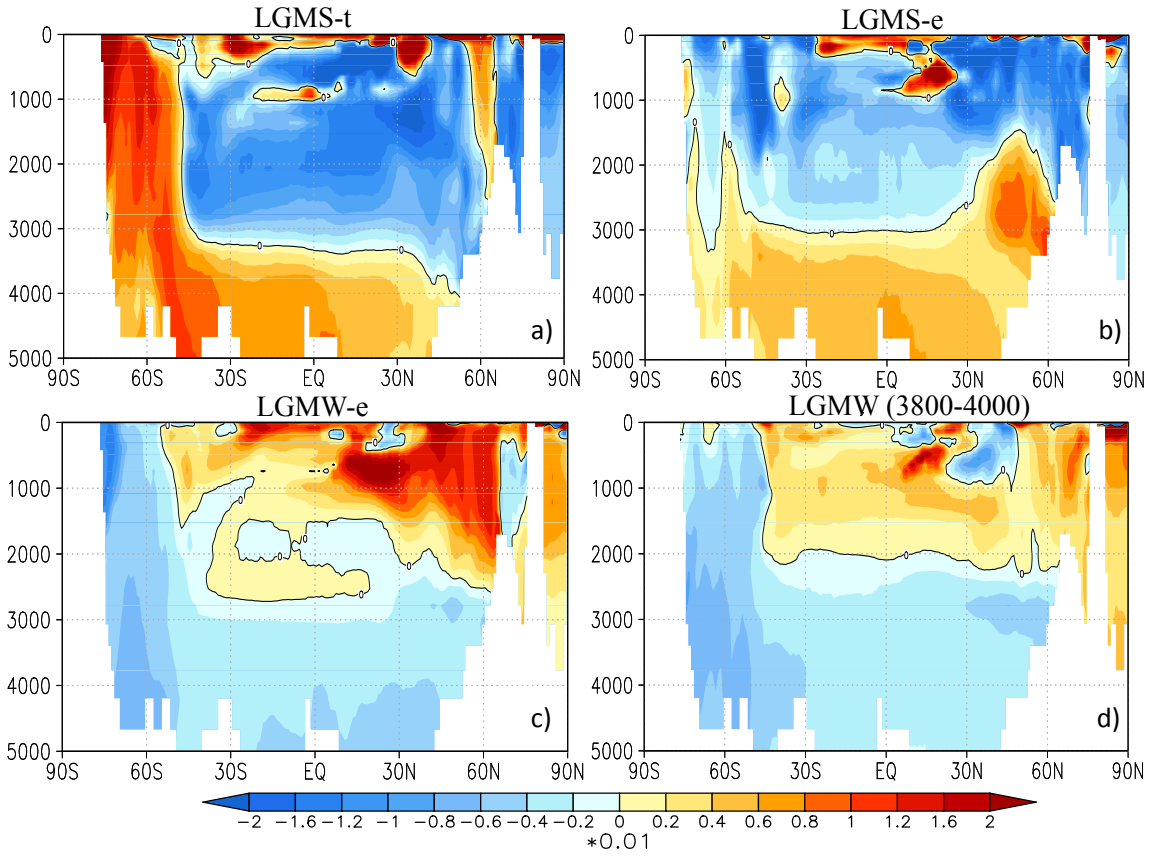

Fig. 3.4 Salinity trend in Atlantic Ocean for model year 2800-3000 in LGMS-t_{deep} (A) and LGMW-e (C) and model year 4500-4700 in LGMS-e (B) and model year 3800-4000 in LGMW (D). Units: psu/century.

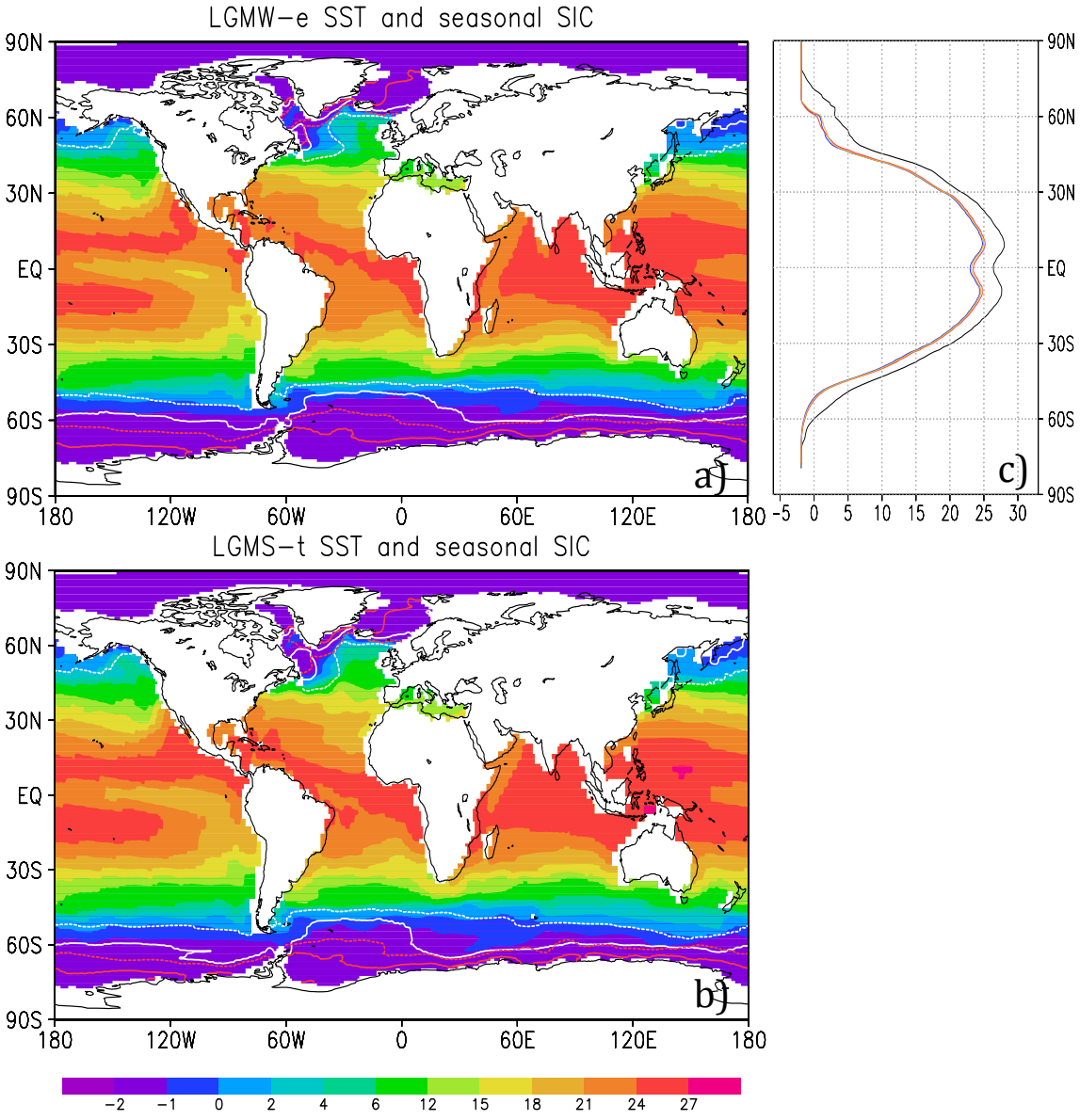

Fig. 3.5 Annual mean of sea surface temperature (SST, unit: °C, shaded) and seasonal sea ice concentration (SIC, unit: %, contour) in the LGMW-e (a) and LGMS-t_{deep} (b). The white lines represent winter for each hemisphere, while the red line represents summer. The dashed lines indicate 15% SIC, and solid lines 90% SIC. (c) Zonal mean of global SST in PI (black), LGMW-e (blue) and LGMS-t_{deep} (red). Units: °C.

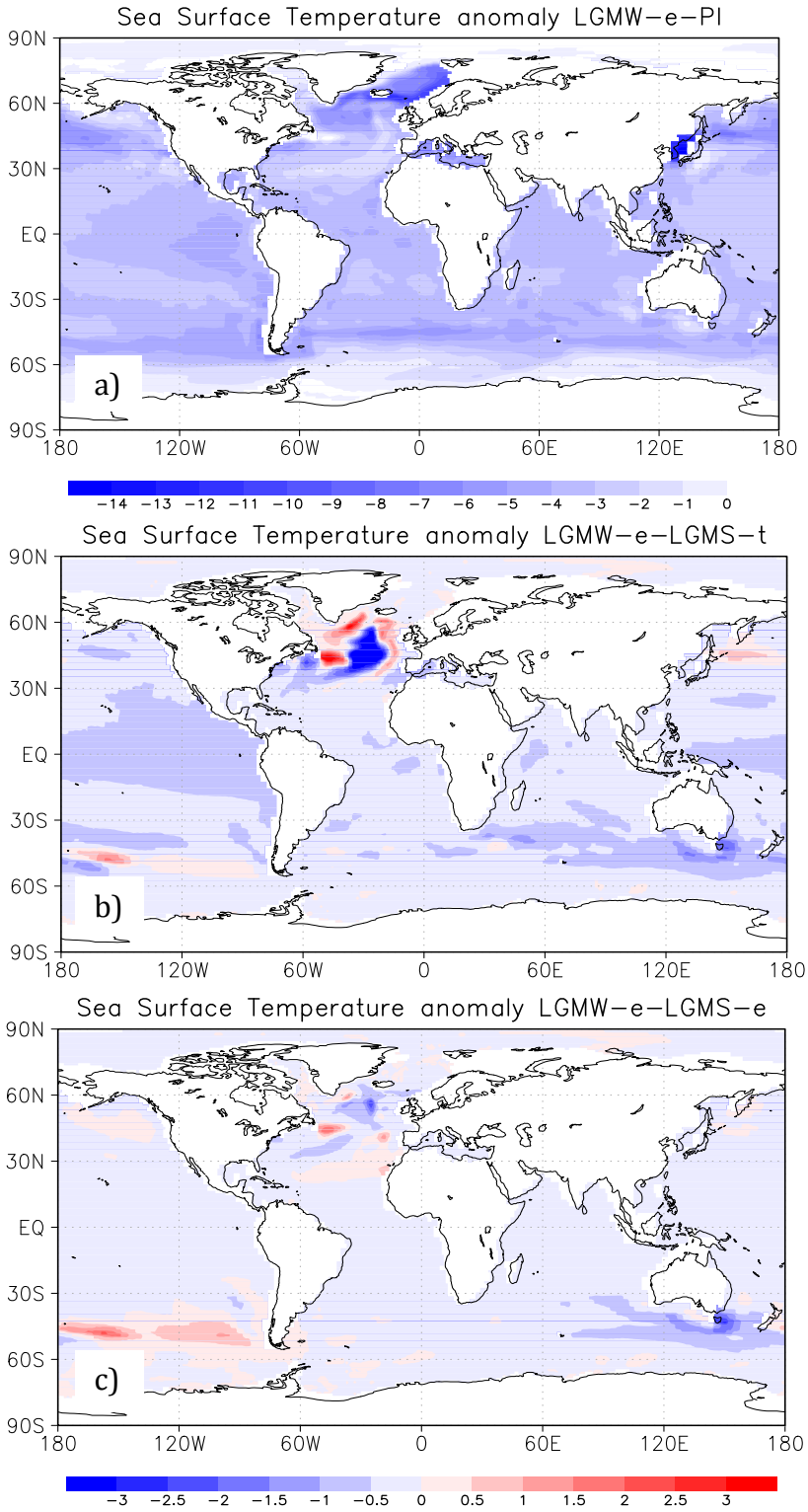

Fig. 3.6 Anomaly of annual mean SST for a) LGMW-e minus PI, b) LGMW-e minus LGMS-t_{deep} and c) LGMW-e minus LGMS-e. Units: degC.

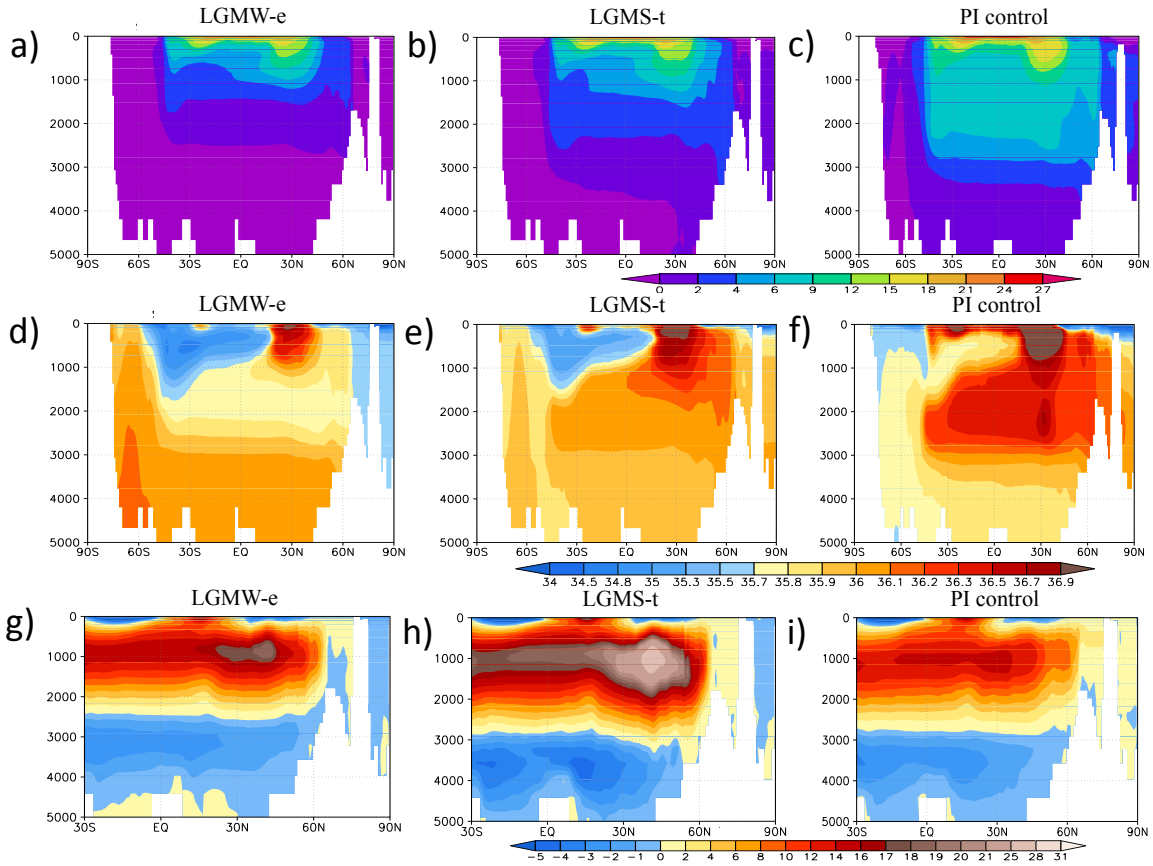

Fig. 3.7 Meridional section of zonal mean temperature (A-C, units: °C), salinity (D-F, units: psu) and stream function (G-I, units: Sv (10^6 m^3/s)) in the Atlantic Ocean. For panel (F), we added 1 psu to the salinity field for a better comparison with the glacial salinity structure.

3.1.2 Pre-industrial Simulations

To examine whether the feature of time-dependency on initial ocean states in glacial simulations is also present in a warm climate, we conducted two pre-industrial (PI) simulations in this study. One was initialized from the same present-day ocean state as LGMS, which is referred to as PI control run and has been analyzed by Wei et al. [2012]. The other one, LGM2PI, was initialised from the glacial ocean state of LGMW. Both PI simulations were integrated for 3000 years (Table 1) using identical PI boundary conditions as in previous studies in PMIP. The average of the model years 2900-3000 is considered to represent the climatology in both simulations.

3.1.3 The 27ka BP simulation

Previous studies suggest that additional cooling in the Southern Ocean will benefit the formation of AABW during the LGM [*Shin et al.*, 2003; *Butzin et al.*, 2005; *Liu et al.*,

2005; *Otto-Bliesner et al.*, 2007]. Given the long term equilibrium time scale of LGM simulation initialized from present-day ocean, it is of great interest that whether changes in the insolation is capable to promote formation of dense AABW. Thus, we performed the simulation LGMS27ka in which orbital parameters of 27ka BP (precession: 196.532°, obliquity: 22.2514°, eccentricity: 0.017451) [*Laskar et al.*, 2004] are imposed on LGM boundary conditions. This simulation was initialized from model year 4000 of LGMS and is integrated for 700 years (Table 1). The last 100-year average was considered to represent the corresponding 27ka BP climatology.

3.2 Results and Discussions

3.2.1 Surface Properties

The global climatological mean SST are 14.9°C and 15.3°C in LGMW-e and LGMS-tdeep, i.e. 2.8°C and 2.4°C lower than the PI control run, respectively. The SST differences relative to PI are similar in the quasi-equilibrium ocean states (Figs. 3.5 and 3.6). In the high latitudes of the Southern Hemisphere, our model simulates a pronounced annual mean cooling of SST around Antarctica (Figs. 3.5 and 3.6), in line with proxy data [*Gersonde et al.*, 2005]. In the Northern Hemisphere, a robust meridional thermal gradient is well simulated around 40~45°N, and the most pronounced cooling is found off the eastern coast of Iceland to eastern part of Nordic Sea (Figs. 3.5 and 3.6). Both features are comparable to reconstructions [*Kucera et al.*, 2005; *de Vernal et al.*, 2006]. In contrast to the MARGO data [*Waelbroeck et al.*, 2009], our model as well as PMIP2 models underestimate the pronounced east-west SST anomaly gradient in the northern North Atlantic.

Despite the different initial conditions in LGMW and LGMS, there is also a reasonable agreement between the sea ice concentrations (SIC) in both ocean states and proxy data (Fig. 3.5a, b), such as the austral winter sea ice extent in the Atlantic sector and the austral summer sea ice extent in the Indian ocean sector [*Gersonde et al.*, 2005]. But the simulations underestimate the large extent of summer sea ice between 5°E and 5°W in the Southern Ocean. During boreal winter, sea ice increases, especially along the coast of Newfoundland, extending far into the western Atlantic [*Pflaumann*, 2003; *Kucera et al.*, 2005; *de Vernal et al.*, 2006]. Sea ice extent is underestimated in the north-eastern

Atlantic Ocean in our model [*Paul and Schäfer-Neth*, 2003; *Pflaumann*, 2003] due to an active North Atlantic current maintains relatively warm conditions at the sea surface (Fig. 3.5). During boreal summer the eastern part of the Nordic Seas is partly sea-ice free (Fig. 3.5a, b), which is spatially coherent with sea ice free conditions as indicated in the GLAMAP reconstruction of the LGM [*Paul and Schäfer-Neth*, 2003; *Pflaumann*, 2003]. In addition, there is perennial summer sea-ice extent in the west of the Nordic Sea along the eastern coast of Greenland and Labrador Sea (Fig. 3.5), in agreement with the reconstructions [*Pflaumann*, 2003; *Kucera et al.*, 2005; *de Vernal et al.*, 2006]. In summary, the similar surface properties generated in both LGM ocean states LGMS-tdeep and LGMW-e are consistent with the reconstructions, representing the climatological surface patterns during the LGM.

3.2.2 Distinct Deep Ocean Properties

Figure 3.7 shows the meridional sections of zonal mean sea salinity and temperature along the Atlantic Ocean and the spatial patterns of the AMOC. In terms of the water mass properties of ocean interior there are pronounced differences between LGMW-e and LGMS-t_{deep} (Fig. 3.7). Only LGMW-e possesses an important key feature of the glacial ocean, i.e. the saltier and colder AABW at the bottom of the Southern Ocean compared to LGMS-t_{deep}. This is consistent with a reconstruction of Adkins et al. [2002], while the water mass of LGMS-t_{deep} is more similar to the present-day ocean state (Fig. 3.7e, f). According to water mass configuration reconstructed from nutrient tracers [*Duplessy et al.*, 1988; *Curry and Oppo*, 2005; *Marchitto and Broecker*, 2006; *Lynch-Stieglitz et al.*, 2007; *Hesse et al.*, 2011], the North Atlantic Deep Water (NADW) shoals to about 2000-2500 m as Glacial North Atlantic Intermediate Water (GNAIW) due to the enhanced northward invasion of Antarctic Bottom Water (AABW) at the LGM. The AMOC associated with the sinking of NADW (hereafter NADW-cell) in LGMW-e shoals by ~500 m relative to present day to 2500 m. This is indicative of a shallow NADW-cell and an abyssal ocean occupied by the AABW (hereafter AABW-cell) (Fig. 3.7a, d, g). A similar pattern is also found in the quasi-equilibrium state LGMS-e. However, in LGMS-t_{deep} the NADW-cell penetrates to ~3100 m, even deeper than today (Fig. 3.7b, e, h).

Besides the evident contrast in the deep ocean properties, differences in the AMOC strength between LGMW-e and LGMS-t_{deep} are also pronounced, although both are

stronger than present day (Fig. 3.7g, h, i). In our LGM simulations, enhanced southern westerlies relative to the PI control run (Fig. 3.8) result in a stronger NADW-cell due to a stronger "Drake Passage Effect" via the enhanced Ekman upwelling of the deep water [*Toggweiler and Samuels*, 1995; *Wei et al.*, 2012]. Furthermore, stronger net evaporation in the Atlantic catchment area (Fig. 3.9) combined with more heat loss to the atmosphere from the convection sites over the North Atlantic (Fig. 3.10) also result in an enhanced NADW-cell [*Weber et al.,* 2007]. In addition, the formation of AABW as a result of brine rejection during sea-ice formation is enhanced due to extensive sea-ice formation and increased sea-ice export during the LGM (Fig. 3.11) [*Shin et al.*, 2003]. As a consequence, the expected stronger AMOC states in LGMW-e and LGMS-t_{deep} should be distinct from today. Note that the overturning circulation is evidently reduced due to the stronger vertical stratification that weakens the AMOC from ~27 Sv in LGMS-t_{deep} (Fig. 3.7h) to ~18 Sv in LGMW-e (Fig. 3.7g). Furthermore, the resulting AMOC in LGMW-e is also supported by reconstructions, suggesting that the glacial AMOC is shallower [*Duplessy et al.*, 1988; *Curry and Oppo*, 2005; *Marchitto and Broecker*, 2006; *Lynch-Stieglitz et al.*, 2007; *Hesse et al.*, 2011] but as strong as in the subsequent warm periods within data uncertainties [*Lippold et al.*, 2012; *Ritz et al.*, 2013]. Although proxy data for the LGM are actually consistent with a range of Atlantic circulation states [*McCave et al.*, 1995; *Yu et al.*, 1996; *McManus et al.*, 2004; *Lynch-Stieglitz et al.*, 2007; *Praetorius et al.*, 2008; *Gherardi et al.*, 2009; *Huybers and Wunsch*, 2010], even including the modern state [e.g., *LeGrand and Wunsch*, 1995], the ocean state LGMS-t_{deep} can be ruled out due to its large inconsistency with the proxy data.

The different ocean states found in our model are in quasi-equilibrium according to the PMIP criteria but possess distinct features with respect to ocean structure and overturning circulation, which can be also found in PMIP2 models (Fig. 3.1). Accordingly, one can classify the simulated ocean states in PMIP2 models into two classes, "glacial-like" ocean state as LGMW-e and "present day-like" glacial ocean state as LGMS-t_{deep}.

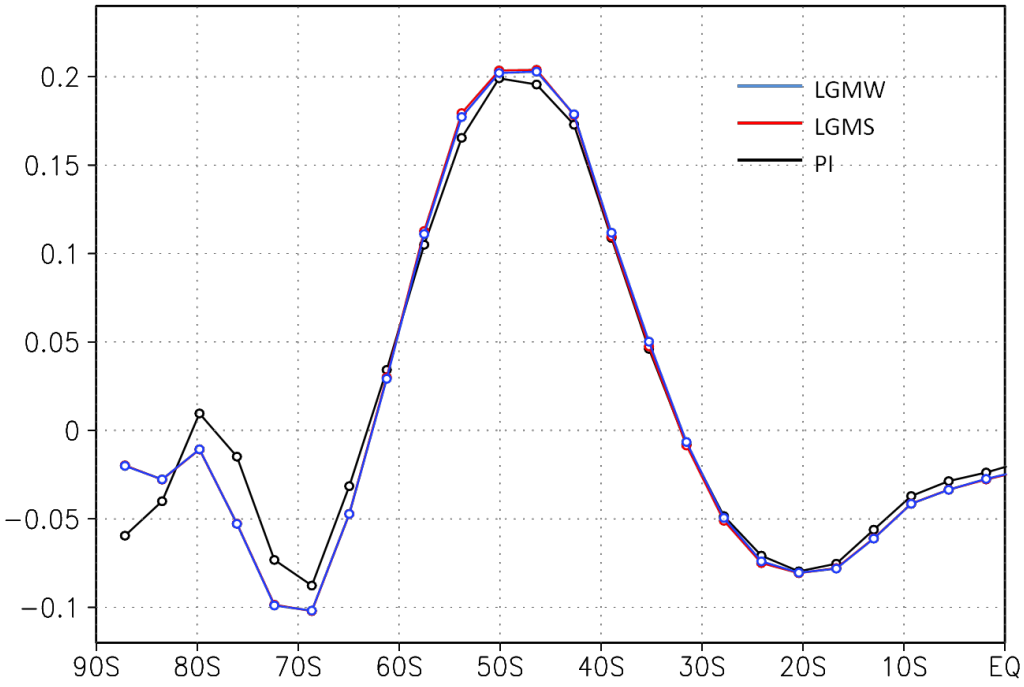

Fig. 3.8 Zonal mean of wind stress in Southern Hemisphere (unit: Pa). PI: preindustrial run; LGMW-e: the LGM simulation is initialized from the glacial Ocean; LGMS-t_{deep}: the LGM simulation is initialized from the Present Day Ocean.

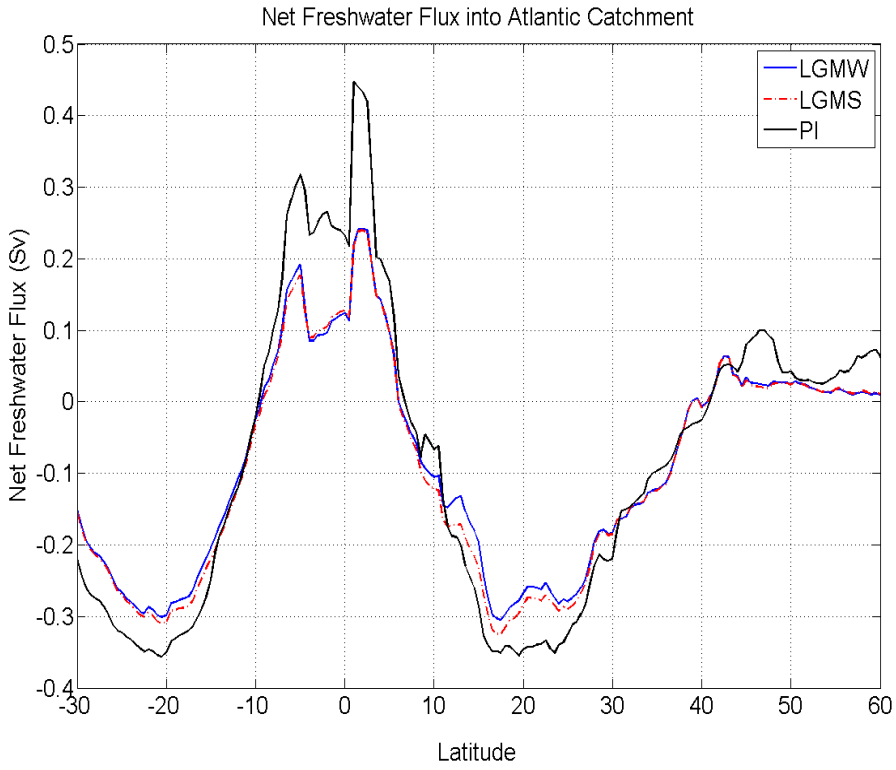

Fig. 3.9 Zonal mean of net freshwater flux (FWF, unit: Sv, $10^6 m^3/s$) in the Atlantic catchment area. Blue line represents LGMW-e, red LGMS-t_{deep} and black PI.

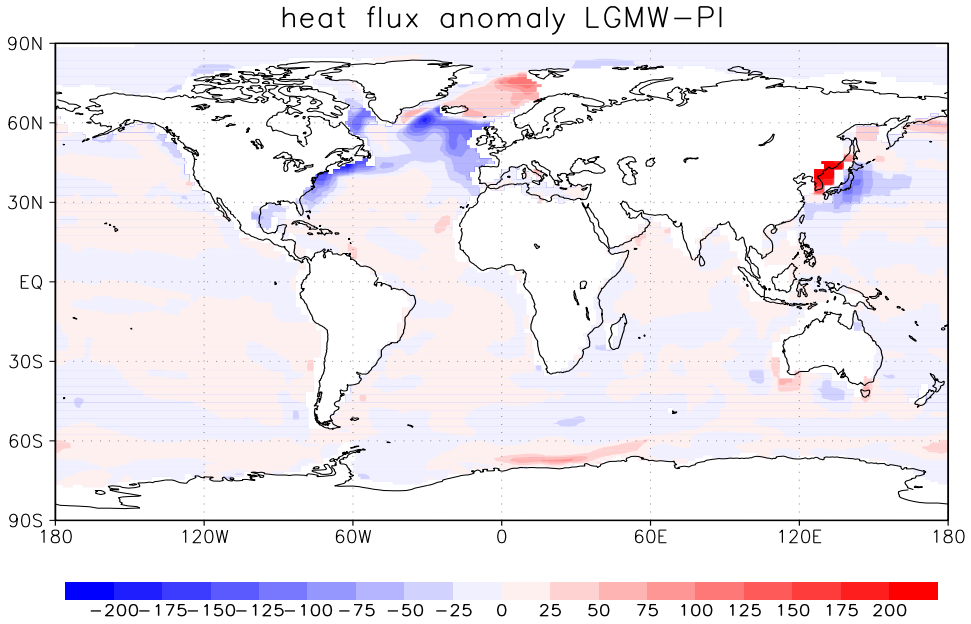

A

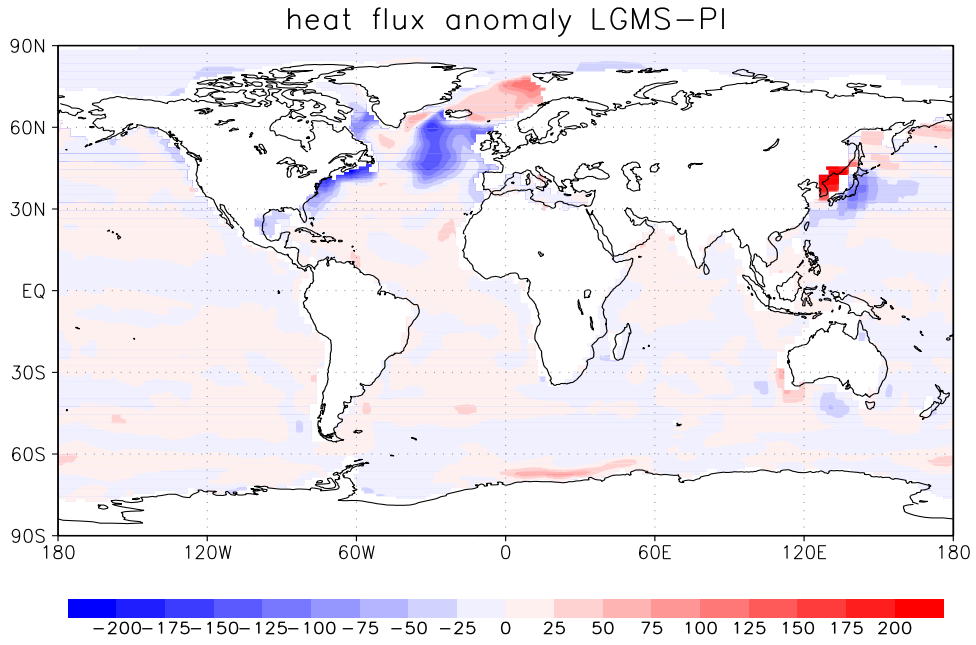

B

Fig. 3.10 Anomaly of heat flux (unit: W/m^2) between A) LGMW-e and PI, B) LGMS-t_{deep} and PI. Negative values indicate heat loss from the ocean. The reduced heat loss from the ocean in Nordic sea and in the Japan Sea is attributed to the enhanced sea ice cover (Fig. 3.5)

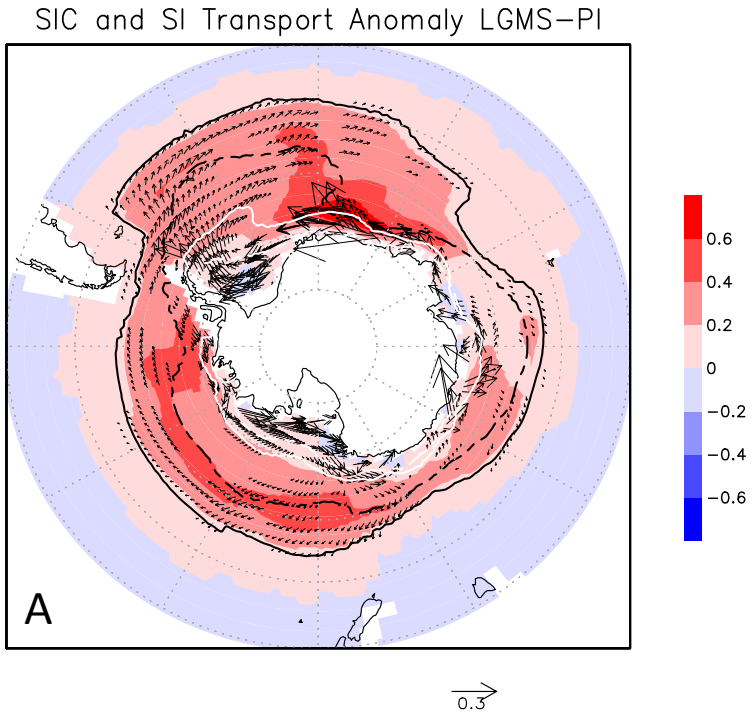

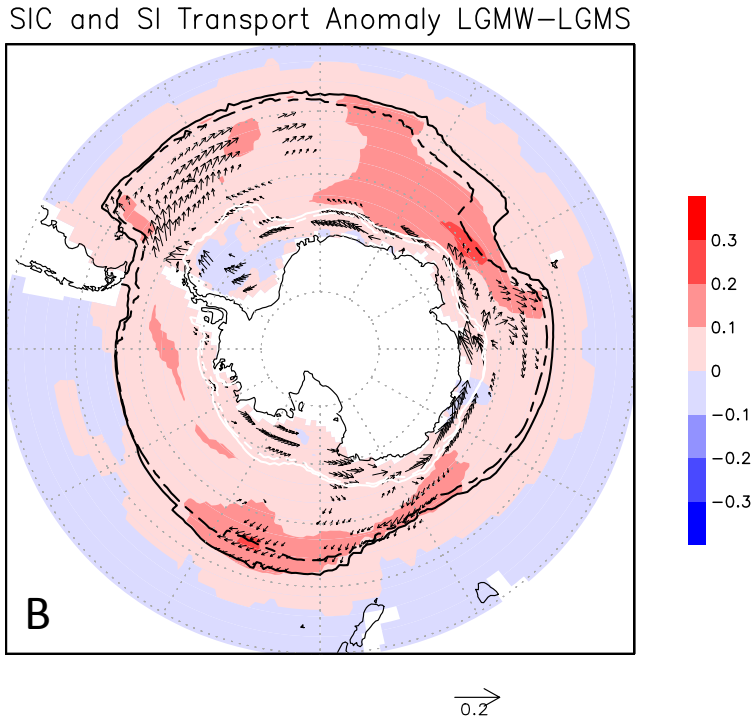

Fig 3.11 A. Anomaly of climatological SIC (%, shaded) and Sea Ice Transport (m^2/s, vector, the scale is indicated by the black arrow below the panels) between LGMS-t_{deep} and PI. Black contour represent 15% SIC, while blue for 90% SIC. Solid line indicates SIC in LGMS-tdeep, and the dashed is for PI. B) Same as A), but for LGMW-e and LGMS-t_{deep}. In our LGM runs, the extensive SIC and SIC export contribute to enhanced brine rejection, which is of great importance to maintain the AABW formation during the LGM.

3.2.3 Reconciling the discrepancies in simulated LGM ocean states

A significant feature in our LGM simulations is the different equilibrium time scales depending on the initial ocean states. When the present-day ocean serves as the initialization (e.g. LGMS), the simulated ocean state after 2500 model years reaches a temporary quasi-equilibrium state identified by the PMIP protocol, in which the trends in the deep ocean are significant. (Figs. 3.2-3.4). The simulated surface properties are consistent with reconstructions (Figs. 3.5 and 3.6), further masking the transient deep ocean characteristics. This feature is not identified in the simulation initialized from a glacial ocean state (LGMW). Due to the lack of a specification regarding the initial ocean state for simulating the LGM, all the PMIP2 models (except CCSM3 and HadCM) were initialized from the present-day ocean [*Braconnot et al.,* 2007*; Weber et al.,* 2007]. As a consequence, CCSM3 and HadCM eventually generate a glacial-like ocean (e.g. LGMW-e), whereas other simulations generate a present day-like ocean (e.g. LGMS-t_{deep}), emphasizing the important role played by initial ocean states on LGM simulations (Figs. 3.1). Furthermore, our results could be interpreted in the sense that the large spread of simulated LGM ocean state among the PMIP2 models can be attributed to different (or insufficient) deep ocean equilibration or initialization.

3.2.4 Deep Ocean Quasi-equilibrium criteria

It is noteworthy that the fundamental difference between LGM ocean states LGMW-e and LGMS-t_{deep} is their distinct vertical stratification associated with the AABW-cell, which is relatively stable compared with the NADW-cell in the LGM simulations (Fig. 3.2). This is supposed to be the main cause for a weaker NADW-cell associated with a pronounced vertical stratification, owing to continuous transportation of the dense AABW to the abyssal Atlantic basin in LGMS. To explicitly diagnose the transient characteristics of the deep ocean in LGMS and qualify the possibility that the deep ocean in some of the PMIP2 models were not in quasi-equilibrium, an equilibrium criteria for deep ocean properties should be well specified for future model inter-comparisons.

Shown in Fig. 3.4 are the salinity trends in the Atlantic Ocean in LGMS-t_{deep}, LGMS-e, LGMW-e and model years 3800-4000 of LGMW. In the quasi-equilibrium ocean states in LGMW and LGMS-e (Fig. 3.4b-d), salinity varies at a rate of no more than 0.006 psu/century at a water depth lower than 3000 m, whereas up to or even more than 0.01

psu/century in LGMS-t_{deep} (Fig. 3.4a). In addition, the deep ocean salinity trend is relatively larger in the Atlantic section of the Southern Ocean that is one of main formation sites of AABW. Therefore, we propose that the glacial deep ocean can be diagnosed as quasi-equilibrium at least when basin-wide average salinity at depths larger than 3000 m varies at a rate less than 0.006 psu/century in Atlantic Ocean and less than 0.008 psu/century in Atlantic section of Southern Ocean.

Previous model studies suggested that the strengthened sea ice formation and export under a cold climate could enhance brine rejection in the Southern Ocean, leading to a strengthened AABW [*Shin et al.*, 2003; *Butzin et al.*, 2005; *Liu et al.*, 2005; *Otto-Bliesner et al.*, 2007]. This suggests that the colder the simulated Southern Ocean is, the more efficient the AABW formation.

Figure 3.12 shows the zonal mean SST bias of the PMIP2 models with observation data at present day. It is evident that only CCSM3 in the PMIP2 models and the model used in this study (COSMOS) have a general cooling bias south of 50°S that is close to the northern edge of winter sea ice cover during the LGM [*Gersonde et al.,* 2005]. This surface cooling bias may accelerate the formation of AABW and thus shorten the equilibrium time scale for the deep ocean. Considering the integration time of 5000 years in the simulation LGMS, we suggest that the equilibrium time scale for the PMIP2 models initialized from present-day ocean state could be no less than 5000 years. Given the equilibrium time scale of ~2500 years in LGMW, it is of utmost importance to specify one standard glacial ocean state to initialize the glacial simulations in the new phase of PMIP for the improvement of LGM simulations and future inter-model and model-data comparison.

In addition, a time interval with decreased obliquity that reduces the annual mean insolation over the high latitudes of both hemispheres can be characterized by enhanced sea-ice formation, promoting the formation of dense AABW. Shown in Figure 3.13 is the salinity anomaly of global meridional section between LGMS27ka and LGMS. It is evident that 27ka BP orbital configuration is more efficient to form the dense AABW than the LGM. This result provides one potential, regardless of the model uncertainty, to explain the origin of the reconstructed LGM ocean structure.

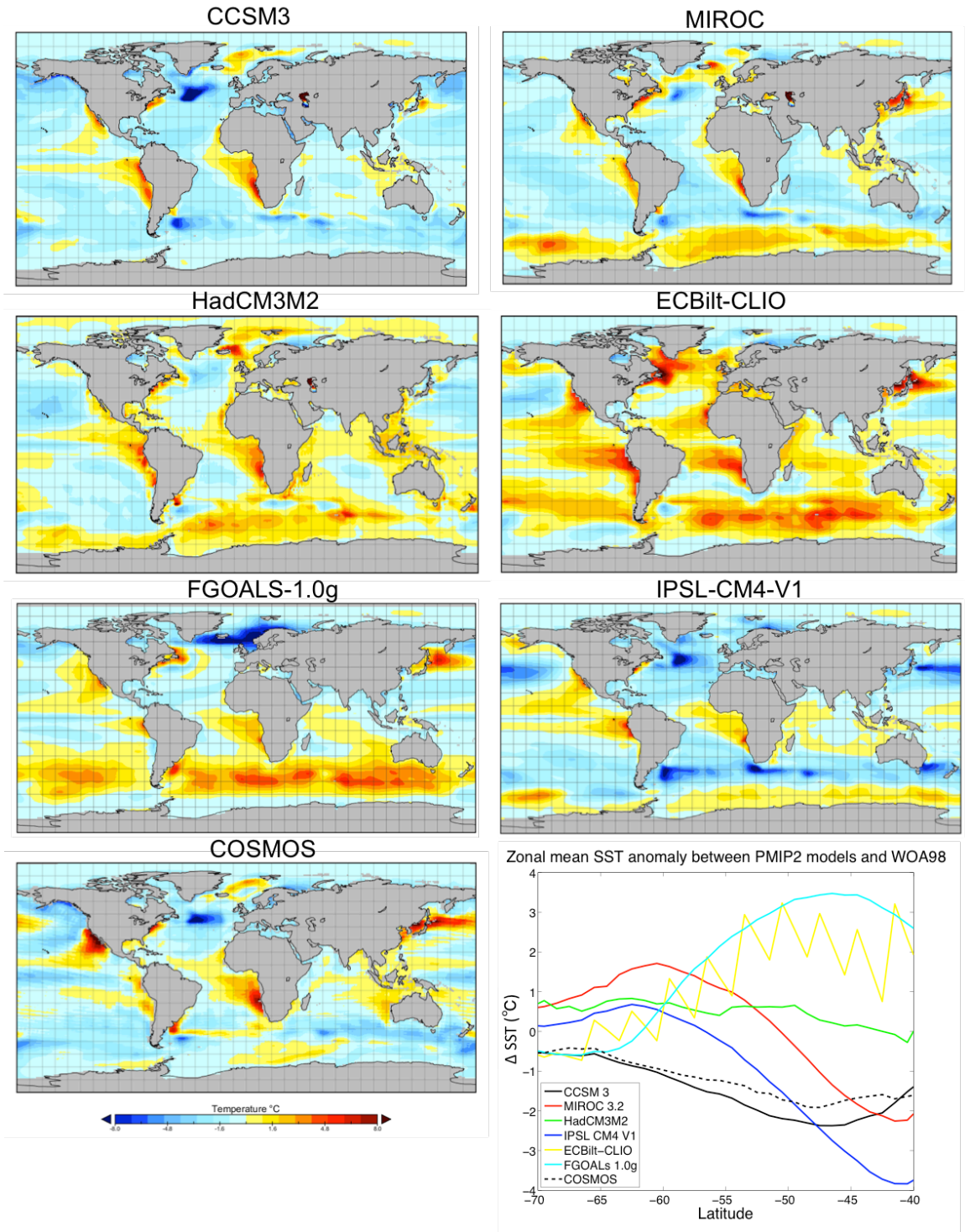

Figure 3.12 Spatial SST anomaly between respective PI control runs of the models participating in PMIP2 and observational data (World Ocean Atlas 98). Panel in lower right is the zonal mean SST anomaly, i.e. CCSM3 (black solid), MIROC 3.2 (red solid), HadCM3M2 (green solid), IPSL-CM4-V1-MR (blue solid), ECBilt-CLIO (yellow solid), FGOALS-1.0g (cyan solid)), as well as the model used in this study (COSMOS, black dashed).

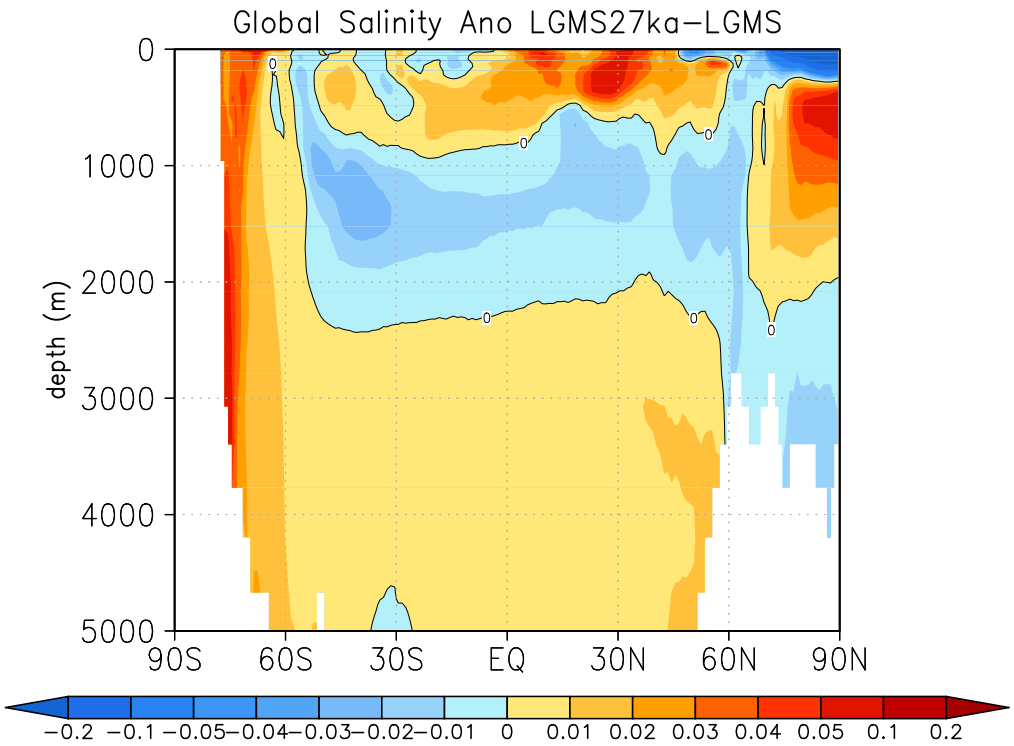

Fig. 3.13 Meridional section of zonal mean salinity anomalies (shaded) in global ocean between LGMS27ka and LGMS-e. For the comparison, we averaged the corresponding model year 4600-4700 in both experiments.

3.2.5 Differences of deep ocean equilibrium time scales between PI and LGM conditions

In the following we investigate whether the dependence of equilibrium time scales on initial ocean states is also present in PI simulations. Figure 3.14 shows the meridional sections of zonal mean sea salinity and temperature along Atlantic Ocean in simulation LGM2PI. The resulting deep ocean properties are similar to our PI control run (Fig. 3.14), implying that equilibrium time scale of the deep ocean under PI boundary conditions is shorter than under LGM conditions.

Shown in Fig. 3.15 are the changes of sea temperature and salinity with time during the spin-up of LGM2PI and LGMS. In the spin-up of the LGM2PI, the upper layers of the ocean are warmed due to the warm boundary conditions, reducing the AMOC and NADW formation (Fig. 3.15a). In this case the way that the bottom water mass interacts with the surface is mainly through the AABW formation in the Southern Ocean. In our

climate model the major regions of AABW formation in PI are Antarctic on-shore areas where brine rejection occurs (Fig. 3.15a, b) due to sea ice formation and export. Given this, the warm upper-layer water mass can be transported to the bottom in the Southern Ocean (Fig. 3.15a) and destabilizes the ocean stratification. Under LGM boundary conditions, the equatorward-extended permanent sea ice edge (Fig. 3.5) will shift the major AABW formation regions to the open ocean (Fig. 3.15c, d) where the dilution of the brines released by sea ice is more important and the effect of the brine-generated dense water is much more reduced than in on-shore regions [*Bouttes et al.*, 2012]. In addition, the cooled upper-layer water mass favors a strengthened AMOC during the spin-up of LGMS, decelerating the northward extension of glacial AABW. Thus, the difference of the equilibrium time scale of deep ocean water mass between PI and LGM boundary conditions can be attributed to the shift of AABW formation sites and different responses of the AMOC to the boundary conditions during the spin-up.

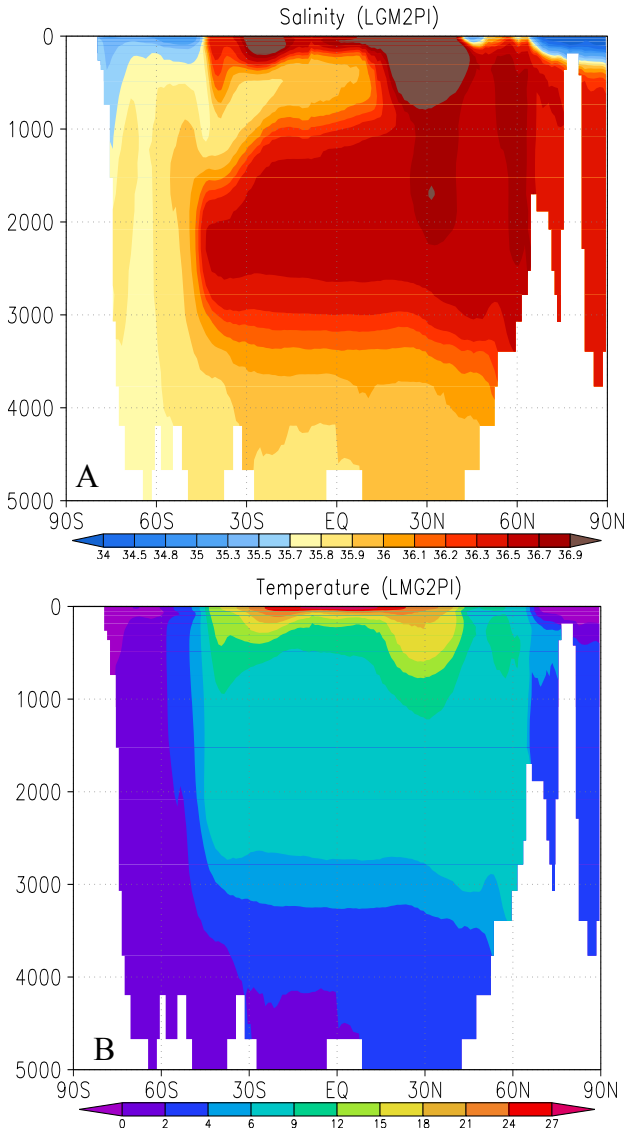

Fig. 3.14 Meridional section of zonal mean temperature (A) and salinity (B) in the Atlantic Ocean in LGM2PI. The deep ocean structure is similar to PI control run, indicating that the Pre-industrial simulation is insensitive to the initial ocean condition.

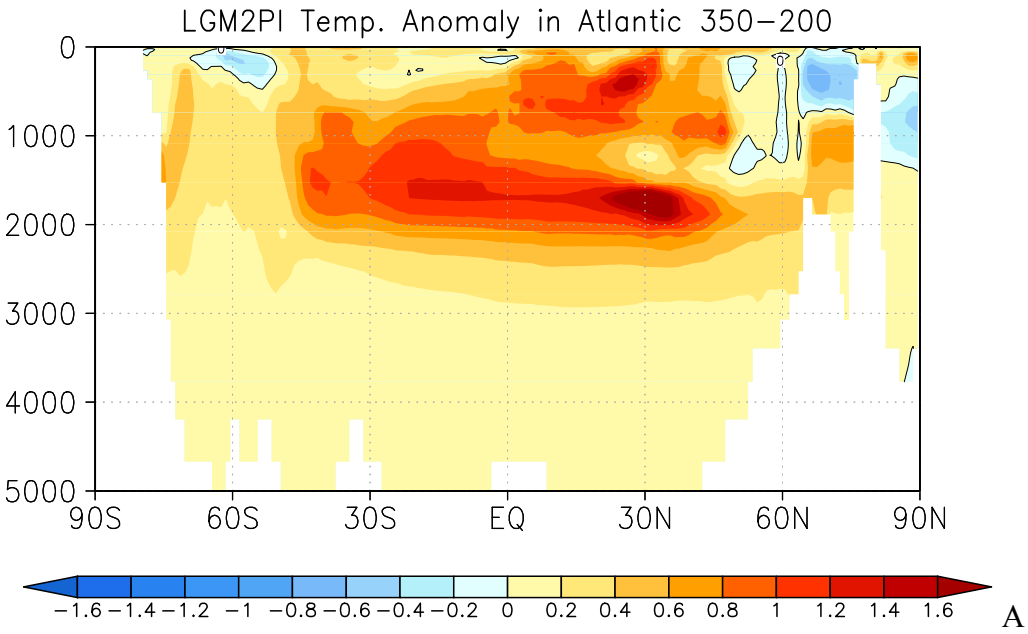
LGM2PI Temp. Anomaly in Atlantic 350−200
0
1000
2000
3000
4000
5000
90S
60S
30S
EQ
30N
60N
90N
−1.6 −1.4 −1.2 −1 −0.8 −0.6 −0.4 −0.2 0 0.2 0.4 0.6 0.8 1 1.2 1.4 1.6

A

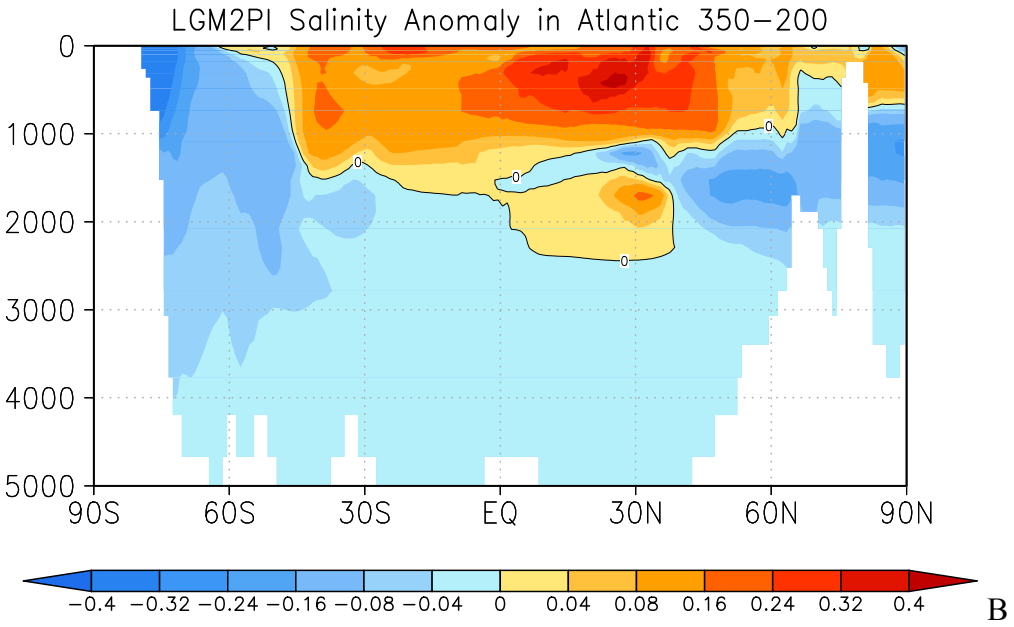
LGM2PI Salinity Anomaly in Atlantic 350−200
0
1000
2000
3000
4000
5000
90S
60S
30S
EQ
30N
60N
90N
−0.4 −0.32 −0.24 −0.16 −0.08 −0.04 0 0.04 0.08 0.16 0.24 0.32 0.4

B

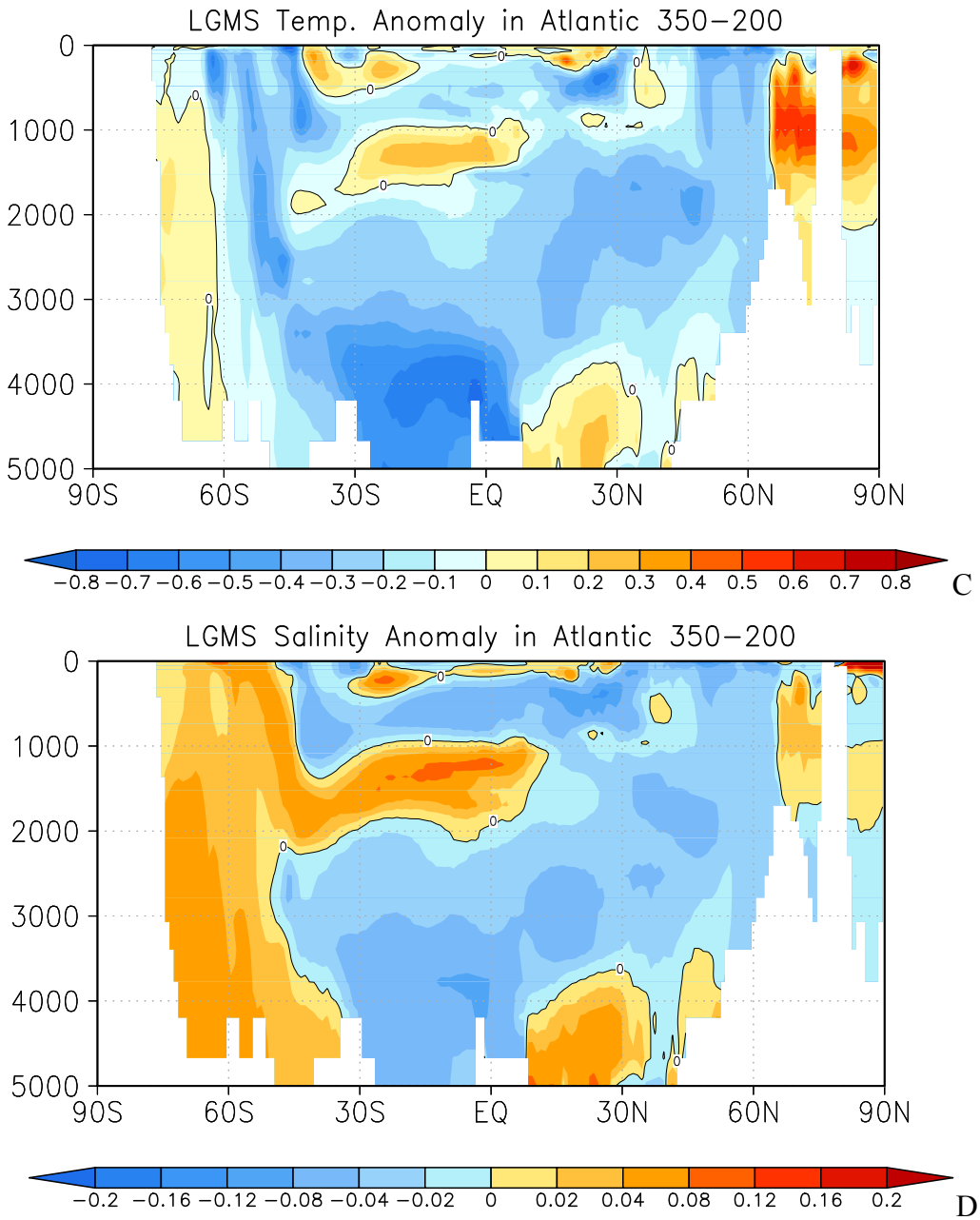

Fig. 3.15 Zonal mean temperature (A, C) and salinity (B, D) anomalies between the 350th and 200th model year in LGM2PI (A, B) and LGMS (C, D). Note that the range of color bar in LGM2PI is twice as large as in LGMS.

3.3 Conclusions of Chapter 3

Based on our investigations of transient and quasi-equilibrium integrations of the glacial climate we find a suite of key findings and conclusions that can be summarized as follows.

- Climatological surface characteristics can be similar and quasi-stationary, even

when a significant trend in deep ocean properties still exists.

- The equilibrium time scale of the deep ocean in the LGM simulation initialized from present-day ocean might be in the order of ~ 5000 years, whereas only around 2500 years in the ocean initialized from a glacial ocean state. Orbital configuration of 27ka BP can shorten the equilibrium time scale in the former case by accelerating the AABW formation due to the corresponding weak insolation over the Southern Ocean.

- The equilibrium time-scale under LGM boundary conditions (~5000 years) is much longer than under pre-industrial boundary conditions, most likely due to a less effective transfer of temperature and salinity changes to the abyssal ocean and different responses of the AMOC to boundary conditions during the spin-up.

- According to the PMIP criteria [*Braconnot et al.,* 2007], such quasi-stationary states can be classified as equilibrium states, based on surface temperature trend analysis. Hence, caution on deep ocean must be taken when these allegedly quasi-equilibrium states on the basis of surface properties are used as a reference for both model inter-comparison and data/model comparison.

- Differences in the AMOC strength and deep ocean properties between quasi-equilibrium states suggest that the large spread among the modeled LGM ocean states and the apparent discrepancies in comparison to proxy data could be partly due to the dependency of equilibrium time scale of the deep ocean on the initial ocean states under glacial conditions. Thus, future protocols of PMIP might benefit from a detailed description of initialization procedures to warrant a sensible model inter-comparison, as well as data/model comparison

Chapter 4. Control of rapid glacial climate shifts by variations in intermediate ice-sheet volume*

A common explanation for DO cycles involves changes in the AMOC [*Clark et al.*, 2002b; *Rahmstorf*, 2002], perhaps triggered by freshwater forcing [*Ganopolski and Rahmstorf*, 2001; *Schmittner et al.*, 2002]. However, the representation of freshwater origin, history and magnitude, used to force abrupt ocean circulation changes, varies among models [*Ganopolski and Rahmstorf*, 2001; *Schmittner et al.*, 2002; *Roche et al.*, 2004; *Stouffer et al.*, 2006; *Liu et al.*, 2009; *Menviel et al.*, 2011; *Carlson and Clark*, 2012; *Roberts et al.*, 2014] *and* paleoceanographic evidence for these ocean circulation changes and their linkage to freshwater perturbation remains elusive [*Dansgaard et al.*, 1993; *McManus et al.*, 1999; *Elliot et al.*, 2002; *Hemming*, 2004; *Ahn and Brook*, 2008; *Piotrowski et al.*, 2008; *Barker et al.*, 2011]. One fundamental characteristic, proposing a profound clue in the mystery, is that almost all of the DO-type events occurred during glacial periods when global ice volume was of varying intermediate levels [*Dansgaard et al.*, 1993; *McManus et al.*, 1999; *Schulz et al.*, 1999; *Barker et al.*, 2011], suggesting a potential relationship between the intermediate ice sheets and the existence of millennial scale variability [*Wunsch*, 2006].

4.1 Nonlinear responses of glacial ocean to changes in global ice volume

To test how changes in Northern Hemisphere ice-sheets affect global climate during glacial periods, we initialize the simulations by the LGMctl ocean state (i.e. LGMW-e mentioned in the Chapter 3) with imposing different NHIS heights (Table 1). The corresponding NHIS heights are achieved by multiplying the height anomaly between LGM and present day (PD) ice sheet orography with a variable height scaling factor (Hsf). Hsf = 1 corresponds to LGM default orography; Hsf = 0 corresponds to PD default orography. All other model parameters and forcings are identical to LGMctl and the area out of the NHIS is fixed to the LGM orography. The ice volume anomaly between Hsf=1 and Hsf=0 is equivalent to about 90m global sea level change (Fig. 4.1). In addition, the Antarctic Ice Sheet (AIS) contributes around 30m equivalent sea level

* This work was *in revision* in *Nature* now.

drops, which is fixed in our simulations. Noteworthy is that the change in the NHIS by multiplying the factor Hsf also change the ice-sheet shape and volume (Fig. 4.1). Regarding this issue, we refer the combined NHIS height, volume and size changes as 'NHIS height' in this study. It is evident that the higher NHIS leads to a relatively stronger AMOC and a nonlinear behaviour of the AMOC exists at intermediate ice-sheet levels of which the equivalent sea level drop is around 66 m (Fig. 4.2).

Furthermore, to evaluate the different contributions of the Fennoscandian Ice Sheet (FIS) and the Laurentide Ice Sheet (LIS) to the glacial ocean circulation, we conducted two more sensitivity simulations (FIS_0.4 and LIS_0.4); one fixing the FIS at Hsf = 1 and setting the LIS to Hsf=0.4, and the other fixing the LIS at Hsf = 1, and setting the FIS to 0.4, respectively (Table 1). Based on these two experiments it is shown that the role played by the LIS is more important than the FIS on controlling the glacial ocean circulation (Fig. 4.2).

4.2 Tempo-spatial variation of internal climate variability in the northern North Atlantic and Nordic Sea

To further investigate the transient characteristics of the abrupt climate shift, we conduct a simulation (ISTran45) by gradually increasing the NHIS volume from an intermediate ice-sheet level at a rate of 1.8 cm/year equivalent sea level drop (Fig. 4.3a). In response to a linear ice-sheet increase, surface air temperature (SAT) in the northeastern North Atlantic is characterized by a gradual warming, rather than the two-step resumption process as demonstrated by AMOC strength (Fig. 4.3a). Initially, over the first 70 years, SAT in the northern North Atlantic gradually warms up by 4 °C, coincident with a 3 Sv increase in AMOC strength (Fig. 4.3a). Once the surface warming passes a thermal threshold (~ -2.5 °C), the weak AMOC increases abruptly by ~10 Sv within half a century, resuming the strong mode, along with a further warming of about ~3 °C in the North (Figs. 4.3a and 4.4a, b).

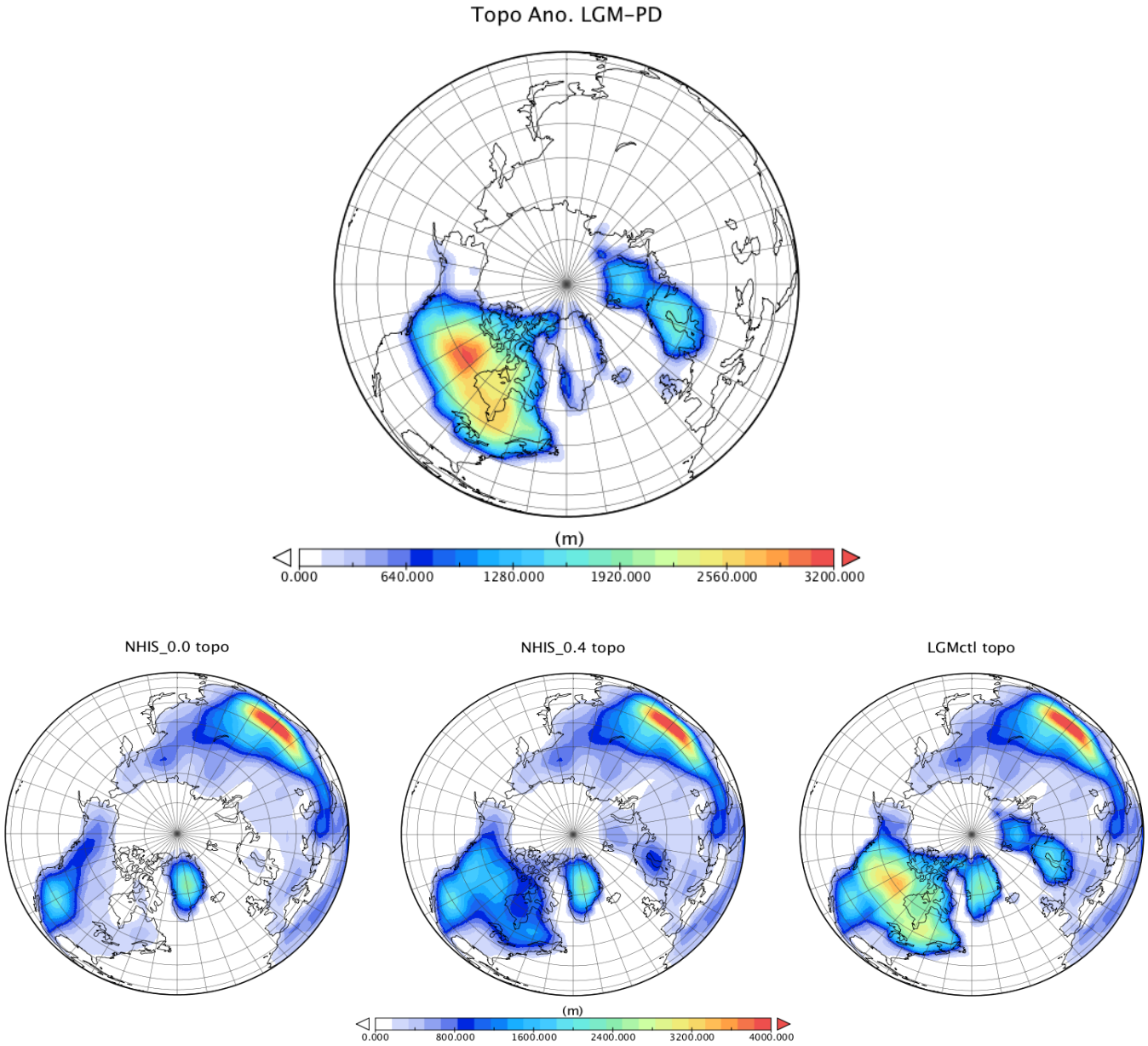

Fig. 4.1 Topography anomaly between Hsf=1 (LGMctl) and Hsf=0 (NHIS_0.0) and topography in LGMctl, NHIS_0.4 and NHIS_0.0. The ice-sheet imposed in LGMctl is derived from the PIMP3 protocol (https://pmip3.lsce.ipsl.fr/), referring to LGMW in chapter 3. The Northern Hemisphere ice-sheet anomaly between LGM (Hsf=1) and PI (Hsf=0) contributes to equivalent sea level change of ~90 meters.

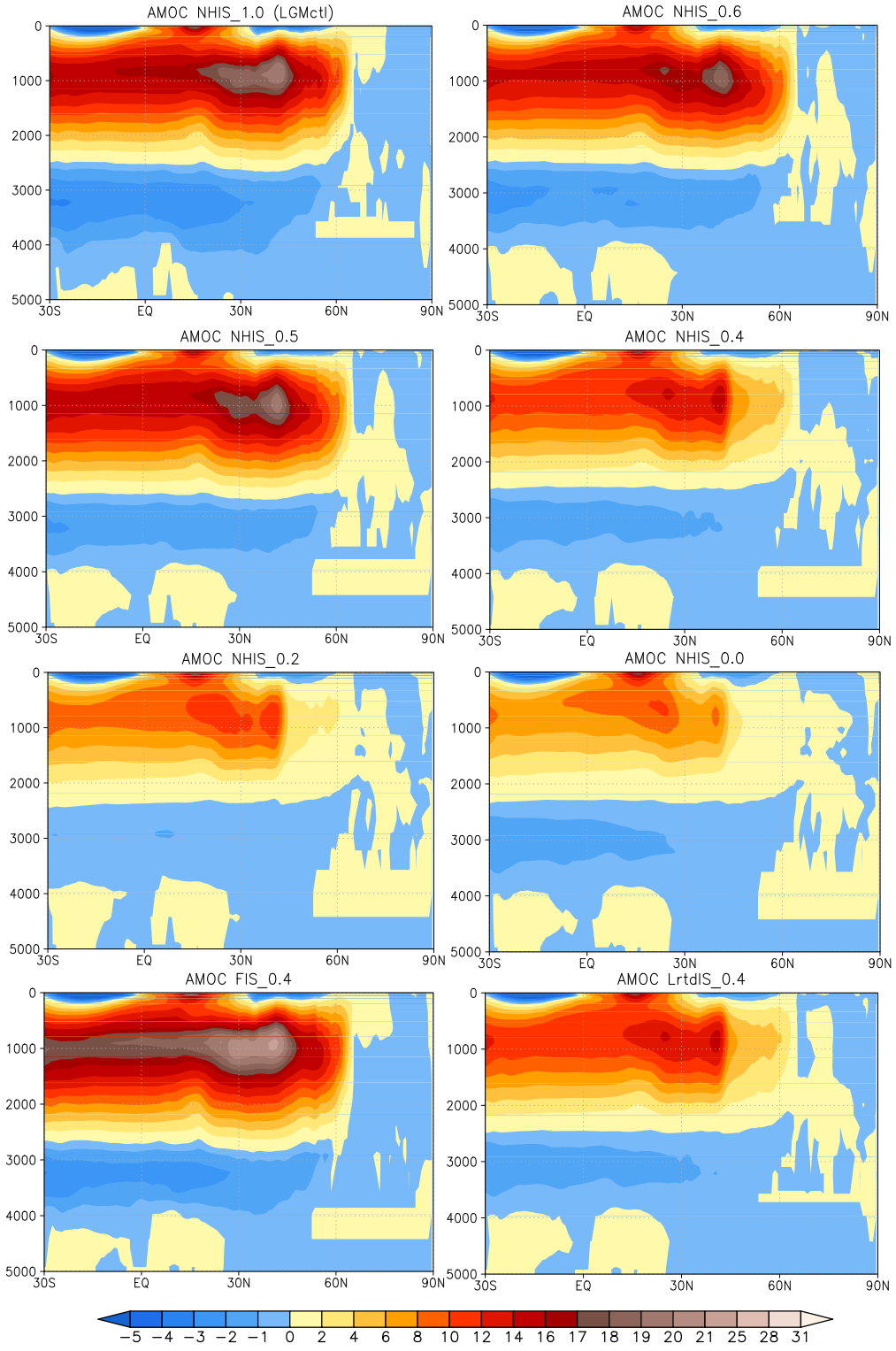

Fig. 4.2 Spatial patterns of simulated AMOC under the different ice-sheet configurations prescribed in Table 1.

	Initial ocean	NHIS (Hsf)	Other forcing	Integrated years
LGMctl	LGM	1	LGM	4000
NHIS_0.8	LGM	0.8	LGM	300
NHIS_0.7	LGM	0.7	LGM	300
NHIS_0.6	LGM	0.6	LGM	800
NHIS_0.5	LGM	0.5	LGM	600
NHIS_0.4	LGM	0.4	LGM	1400
NHIS_0.2	LGM	0.2	LGM	600
NHIS_0.0	LGM	0	LGM	2000
FIS_0.4	NHIS_0.4	0.4 (FIS)	LGM	700
LrtdIS_0.4	NHIS_0.4	0.4 (LIS)	LGM	700
ISTran45	NHIS_0.4w	0.4-0.45	LGM	250
TrGHG04	NHIS_0.4w	0.4	185-205ppm CO_2	500
NHIS_0.45	NHIS_0.4	0.45	LGM	600
NHIS_0.4s	NHIS_0.45	0.4	LGM	600
NHIS_0.35s	NHIS_0.4s	0.35	LGM	600
NHIS_0.3s	NHIS_0.35s	0.3	LGM	600
NHIS_0.25	NHIS_0.3s	0.25	LGM	600
NHIS_0.3w	NHIS_0.25	0.3	LGM	600
NHIS_0.35w	NHIS_0.3w	0.35	LGM	600
NHIS_0.4w	NHIS_0.35w	0.4	LGM	500

Table 1 Model simulations used in Chapter 4. The simulation LGMctl is identical to LGMW in the Chapter 3.

The SAT in the northern North Atlantic is characterized by strong variability during the weak AMOC mode as well as the SIC and subsurface temperature (SubST) (Figs. 4.3a and 4.4c). In fact the characteristics in the warm climate state with strong AMOC mode

are already within the range of variability in the cold climate state with weak AMOC mode (Figs. 4.3a and 4.5-4.9). We attribute the strong variability to the active interplay between the sea-ice change and the subsurface warming in the northern North Atlantic. Indeed, cold background climate (weak AMOC mode) supports sea-ice formation and build-up of a strong halocline in the northern North Atlantic. However, under the intermediate ice-sheet volume the accumulated warm subsurface water mass can gradually destabilize the water column, triggering the release of subsurface heat, and resuming a warm sea surface temporally [*Rasmussen and Thomsen*, 2004; *Rühlemann et al.*, 2004; *Kim et al.*, 2012] (Figs. 4.3a and 4.10). Once the gradual surface warming in the northern North Atlantic passes a thermal threshold, the reduced SIC and the weakened stratification undermine the interaction between the sea-ice change and subsurface warming, lowering the internal climate variability (e.g. SAT, SIC and SubST) (Figs. 4.3a, 4.4c-d). Thus, the warming background climate acts to increase air-sea heat flux and promotes a fast resumption of deep convection, further warming the northern North Atlantic and completing the abrupt transition to a warm climate state (Fig. 4.3a). In parallel, the robust variability in the northern North Atlantic actually shifts, along with the mode transitions, to the Nordic Sea, causing a fluctuation of SIC and resulting in large temperature variations there (Figs 4.4c, d).

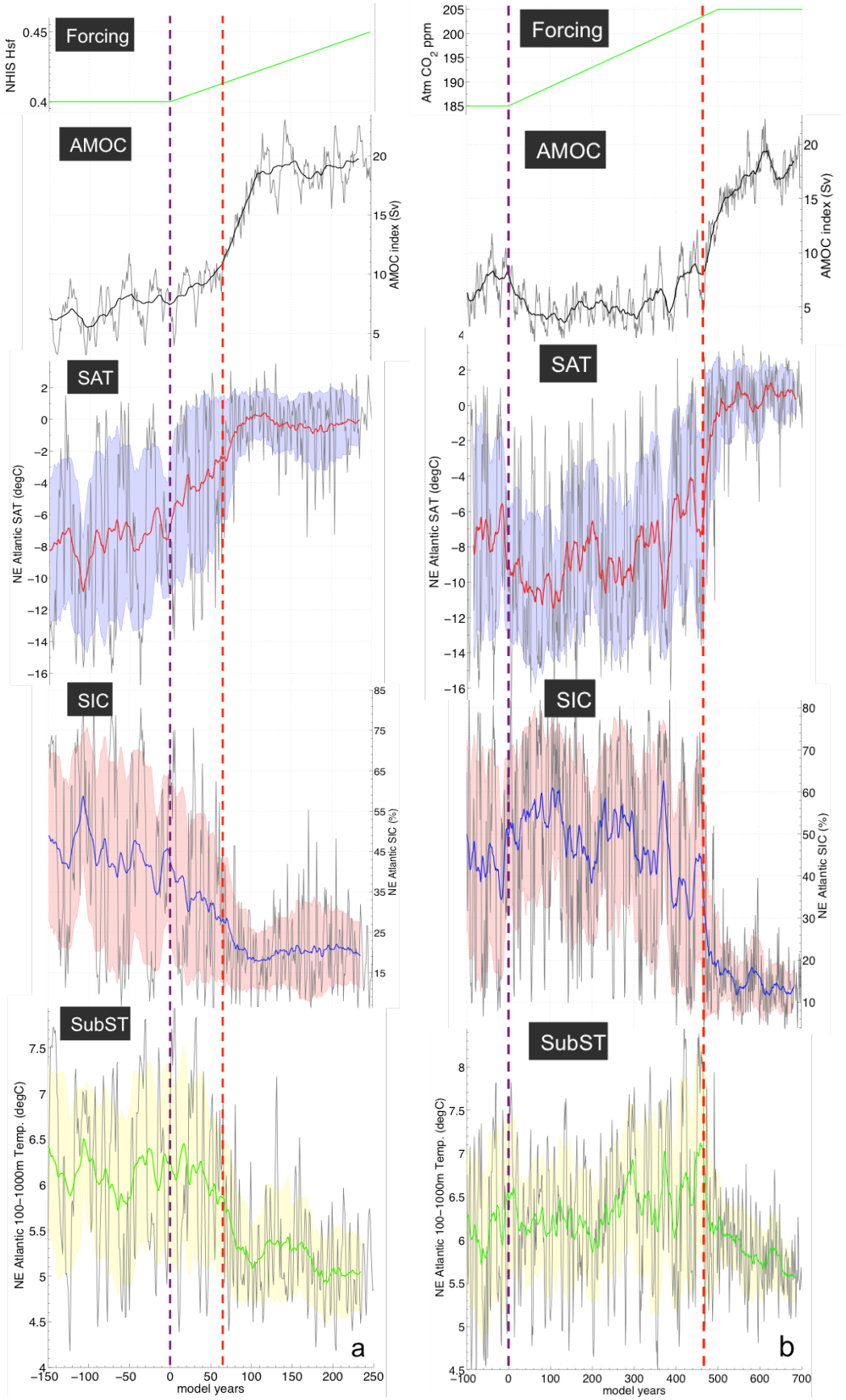
Forcing
NHIS Hsf
AMOC
AMOC index (Sv)
SAT
NE Atlantic SAT (degC)
SIC
NE Atlantic SIC (%)
SubST
NE Atlantic 100–1000m Temp. (degC)
model years
a
Forcing
Atm CO2 ppm
AMOC
AMOC index (Sv)
SAT
NE Atlantic SAT (degC)
SIC
NE Atlantic SIC (%)
SubST
NE Atlantic 100–1000m Temp. (degC)
model years
b

Fig. 4.3 Transient simulations with gradually increasing NHIS height (ISTran45) and CO_2 level (TrGHG04). The variables in each subplot, respectively, are the forcing, NHIS volume in (a) and CO_2 concentration (units: ppm) in (b)), AMOC index (AMOC maximum in the north of 45°N, units: Sv), SAT index (average in 56-65°N, 5°W-30°W units: °C), SIC index (same regional mean as SAT index, units: %) and SubST index (same regional mean as SAT index, units: °C) in the northern North Atlantic. Bold lines for 30-year running mean of original data (gray lines). Shadings indicate one standard deviation of the indices. The vertical purple and red dashed lines represent the starting point for the transient simulations and abrupt AMOC transitions. Negative model years indicate the control simulation of NHIS_0.4.

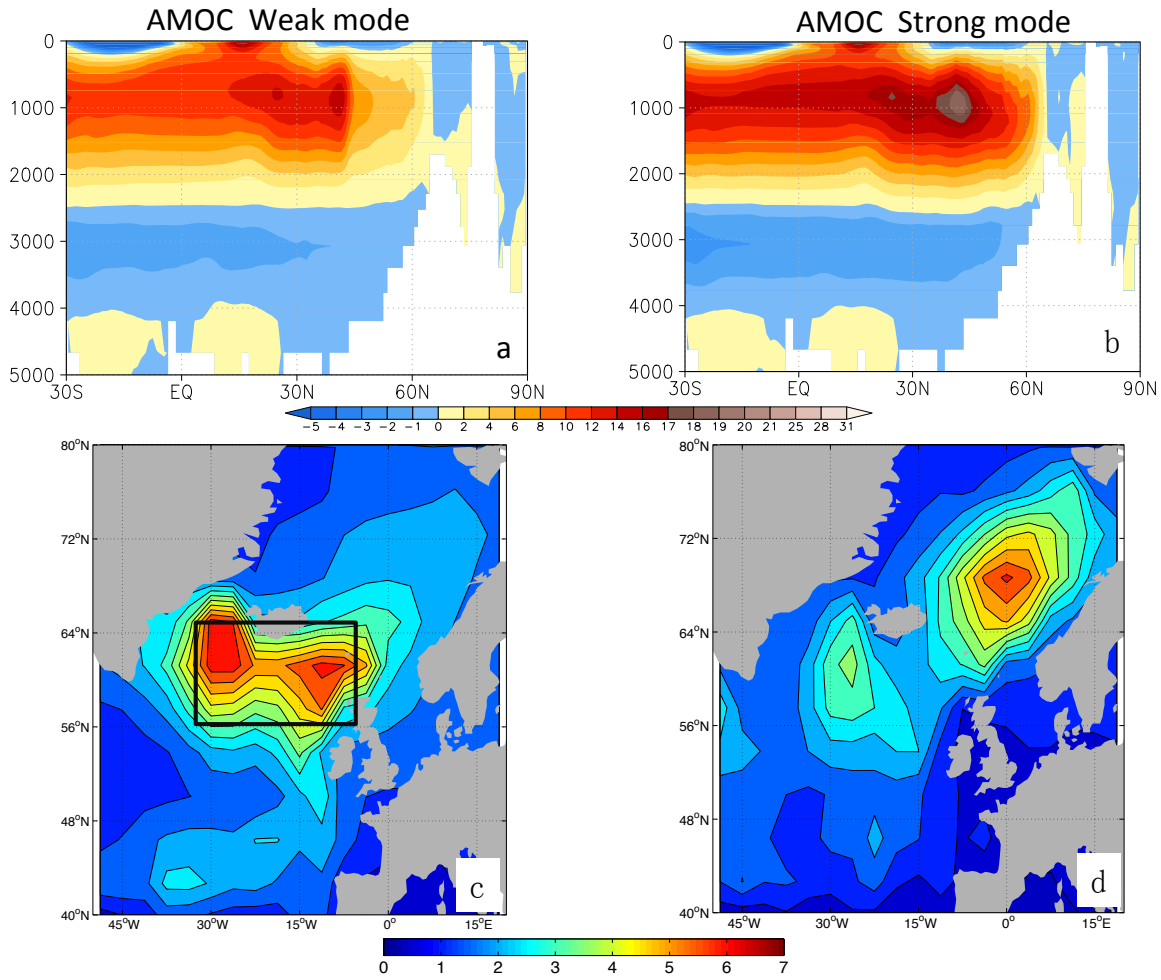

Fig. 4.4 Ocean circulation and internal SAT variability in experiment IStran45 under both cold and warm climate states. Cold and warm climate defined as model year -200 to 0 and 150-250 in Fig 1a. (a) and (c) represent the AMOC and standard deviation of surface air temperature in the cold climate, and (b) and (d) for the warm climate. AMOC plots indicate zonally integrated meridional transport in the Atlantic Basin from 30°S. Noteworthy is the increased strength and northward shift of the deep-water convection sites in (b) compared to (a).

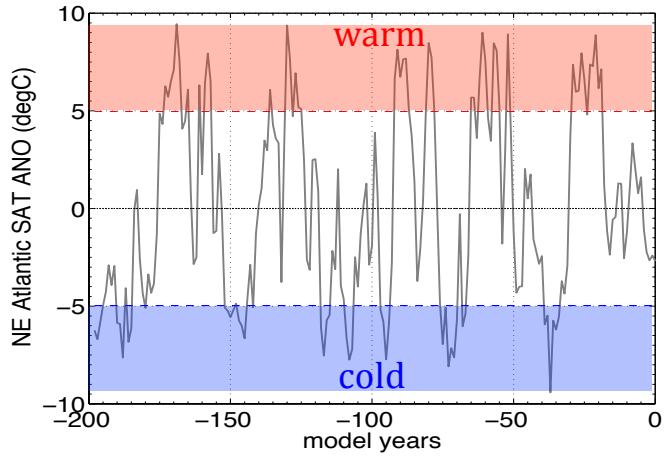

a)

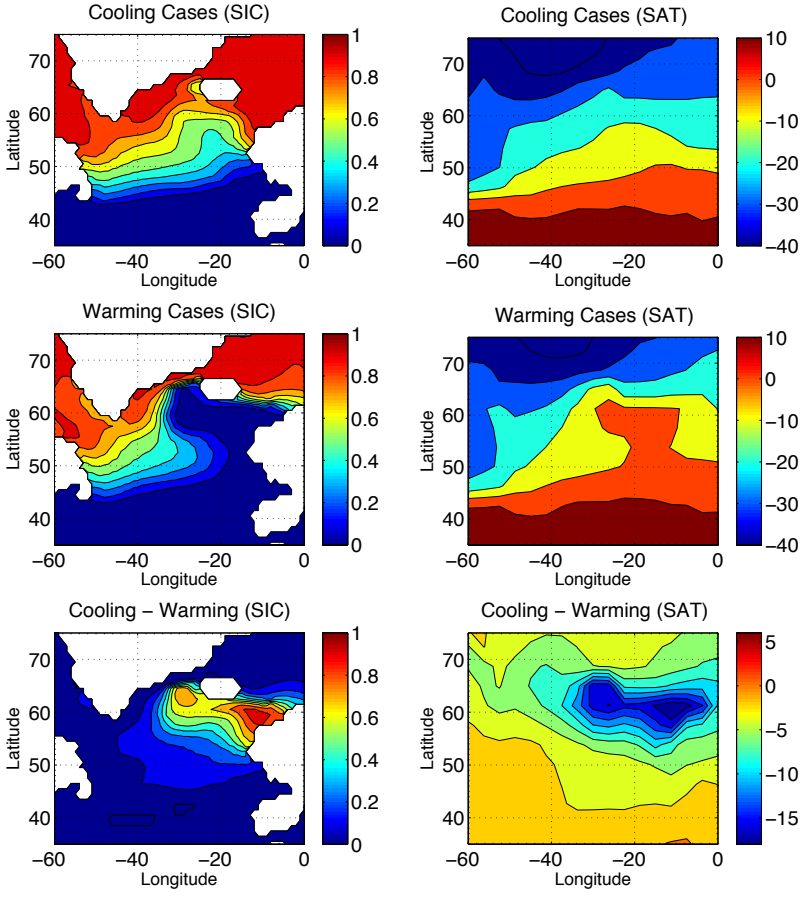

b)

Fig. 4.5 a) time series of SAT index in northern North Atlantic (average in 56°-65°N, 5°W-30°W units: °C) and b) composite maps of sea-ice cover in warming and cooling cases in the weak AMOC mode of ISTran45 (the model year -200-0). Dashed lines in a) represent $\pm 1\sigma$ of the SAT index. The warm (cold) cases are defined as above (below) one standard deviation.

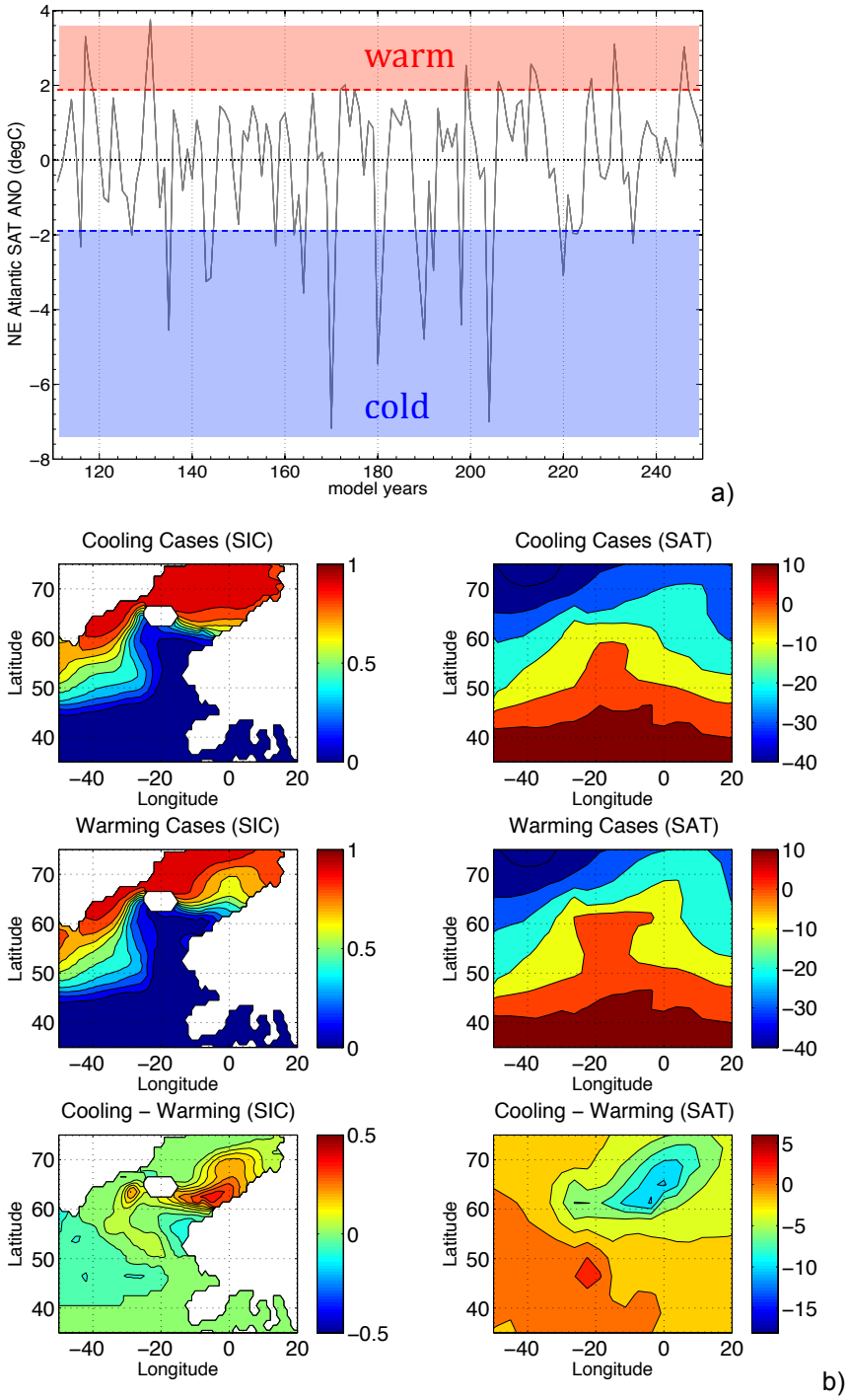

Fig. 4.6 Same as Fig. 4.5 but for the strong mode (the model year 150-250) in ISTran45.

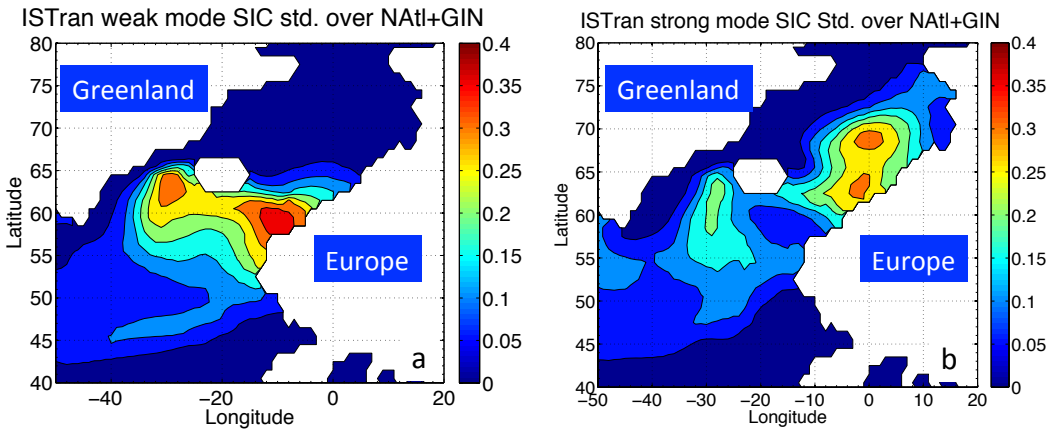

Fig. 4.7 Spatial pattern of SIC variability in weak (a) and strong (b) AMOC modes of ISTran45. The weak and strong mode are define as the model year -200 to 0 and 150 to 250 in the Fig 4.3a, respectively.

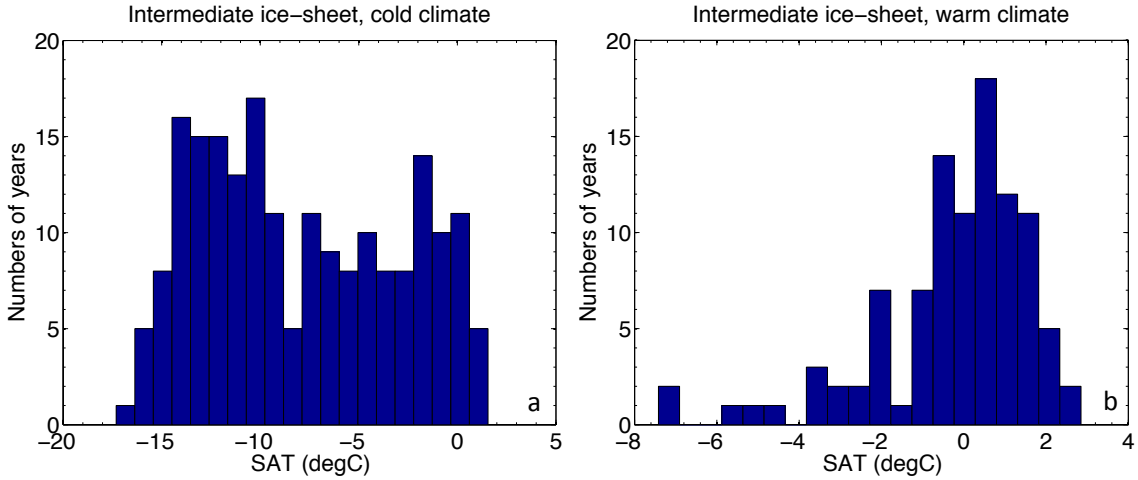

Fig. 4.8 Histogram of the SAT index in the weak (model year -200 to 0) and strong mode (model year 150 to 250) of ISTran45.

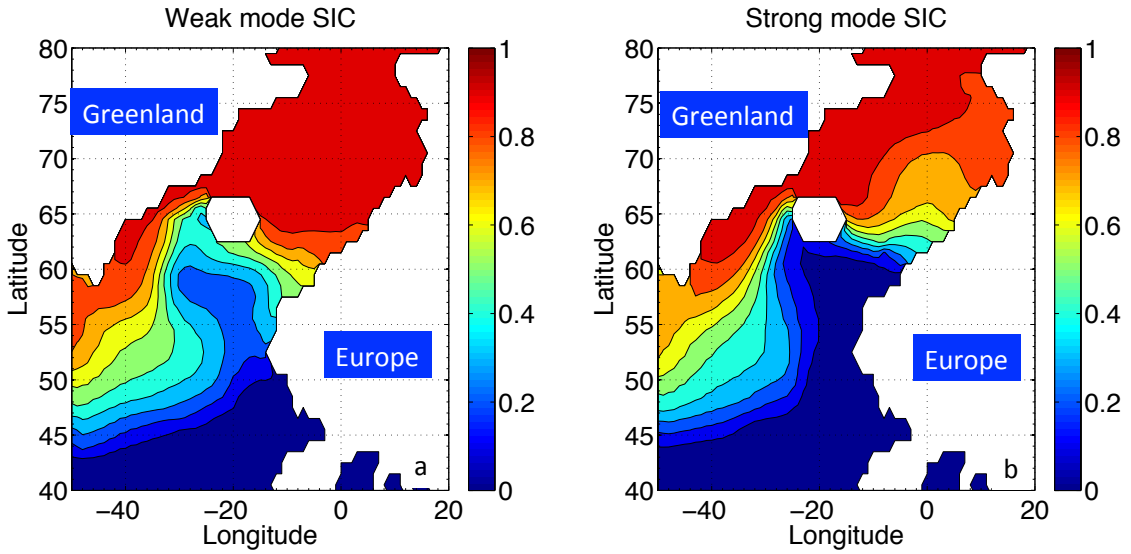

Fig. 4.9 Climatology mean of sea-ice concentration in the weak (model year -200 to 0) and strong mode (model year 150 to 250) of ISTran45

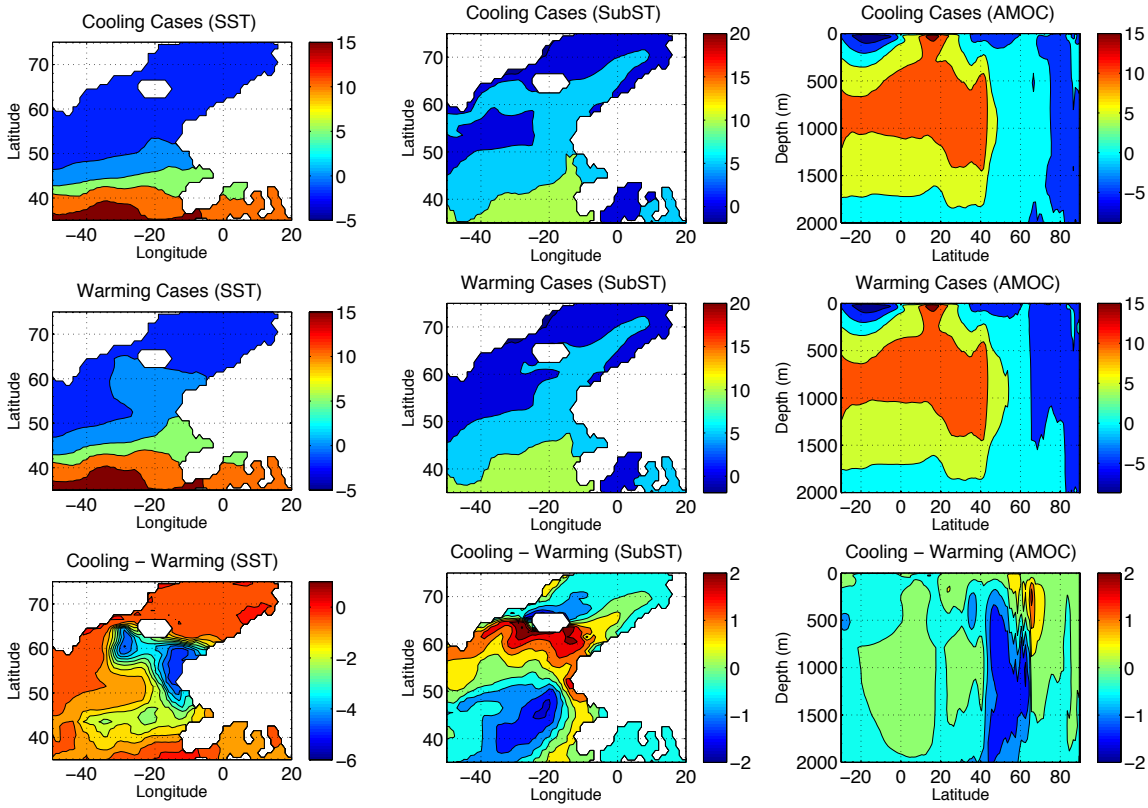

Fig. 4.10 Same as Fig. 4.5, but for sea surface temperature (units: degC), 100-1000m subsurface sea temperature (units: degC) and AMOC (units: Sv).

4.3 Hysteresis of Glacial Ocean with respect to Ice-sheets variations

Further towards a full understanding on the effect of ice-sheet height variation on glacial climate and the governing mechanism, the hysteresis behavior of the glacial ocean is also tested in our model and shown in Figure 4.11. In this case, the NHIS height was adjusted in a Hsf sequence of 0.45, 0.4, 0.35, 0.3, 0.25, 0.3, 0.35 and 0.4, initializing each new run with the previous ocean state (Table 1). Every simulation was integrated for no less than 500 years, ensuring that the ocean is close to a quasi-equilibrium state.

Following the hysteresis, branch 1 (points a-b in Fig 4.11a, b) demonstrates the abrupt AMOC resumption, branches 2 (points b-e in Fig 4.11a, b) and 3 (points e-f in Fig 4.11a, b) respectively represent the gradual and rapid Northern Hemisphere cooling and the return to cold conditions, indicated here by hysteresis branch 4 (points f-h in Fig 4.11a, b). Indeed, the associated AMOC change following this hysteresis curve is remarkably similar to the general shape of the DO cycle [*Dansgaard et al.*, 1993] (Fig. 4.11b). Most notably, the hysteresis curve demonstrates a glacial ocean characterized by a classical bistable regime, in the range between 30% and 40% of full glacial NHIS volume (Fig. 4.11a). This is equivalent to a 57-66m global sea-level drop (Fig. 4.1). Within the bistable range, two distinct glacial ocean modes with strong and weak AMOC (not "off" mode) coexist under identical boundary conditions, and are characterized by spatial patterns generally consistent with proxy data outlining interstadial and stadial conditions, respectively [*Voelker*, 2002] (Figs. 4.12-4.15).

Given the same ice-sheet configuration, the strong AMOC mode, in comparison to the weak circulation, is characterized by reduced sea-ice cover in the northeastern North Atlantic, allowing heat loss to the atmosphere and enhancing the AMOC via the formation of North Atlantic Deep Water (Fig. 4.16a). In parallel, the warmer surface associated with this reduced sea ice acts to enhance the local atmospheric low pressure system (Fig. 4.16b), thereafter boosting the Gulf Stream water mass and heat transport via the altered wind system over the North Atlantic ocean (Figs. 4.16c and 4.17). This contribution provides an atmosphere-ocean positive feedback mechanism stimulating further sea-ice melting and thus heat flux from the ocean, maintaining convection in the

North Atlantic.

In addition to the positive atmosphere-ocean feedback, two mechanisms with respect to the varying NHIS involve to account for this hysteresis behaviour of the glacial climate. Firstly, changes in the sea-ice export to the North Atlantic, and secondly, adjustments of the gyre systems, both of which occur in response to wind changes forced via variations in the NHIS height, especially the LIS (Fig. 4.2). Our model simulations show that changes in the height of the LIS splits the northern and southern branch of the westerly winds in different directions, leading to changes in the Atlantic circulation and sea-ice coverage. Associated with a gradual increase of the NHIS, the maximum westerly wind-stress shifts northwards to ~57°N (Fig. 4.17). Consequently, the zonal wind stress over the South Labrador Sea decreases, effectively weakening the sea ice export to the North Atlantic. This reduces the sea-ice concentration and results in a surface warming over the region, permitting open ocean convection and the reformation of North Atlantic Deep Water (Figs. 4.16 and 4.17). In parallel, a strengthened wind-stress curl accelerates the North Atlantic gyre systems, encouraging both the advection of heat via the Gulf Stream *and* vertical mixing in the sub-polar North Atlantic, the latter acting to increase ventilation of subsurface warm waters, resulting in large-scale heat loss and further open ocean convection (Figs. 4.16-4.18).

In combination with the positive atmosphere-ocean feedback, therefore, a slight variation in the intermediate ice-sheet height (i.e. less than 2m equivalent sea-level change) is capable of instigating the abrupt mode transitions via an adjustment of the heat distribution and sea ice cover in the North Atlantic (Figs. 4.3a and 4.11). Although the hydrological compensation due to the global ice volume changes is not considered here, salinification/dilution in the North Atlantic are characterized by the similar effect as the increasing/decreasing NHIS on triggering the climate mode shifts. It is important to note that the existence of this bistable regime is attributed to the local atmosphere-ocean positive feedback mechanism rather than the hydrological balance in the Atlantic basin as suggested by numerous other studies (see details in Chapter 5).

In addition to millennial-scale sea level fluctuation [*Hemming*, 2004; *Siddall et al.*, 2008], it is known that some large DO events are accompanied by global increases of

atmospheric CO_2 concentration [*Ahn and Brook*, 2008]. We therefore performed a transient experiment (TrGHG04) in which a linear increase of atmospheric CO_2 concentration ranging from 185 to 205 ppm is imposed over 500 years (under constant ice-sheet size of 40% maximum glacial level). In this simulation, a similar, yet even more abrupt Northern Hemisphere warming is simulated (Fig. 4.3b). This is due to a release of additional subsurface heat (resulting from a weakened overturning circulation which exists in response to the increasing CO_2 level) [*Gregory et al.*, 2005] to the atmosphere, thereafter triggering an abrupt warming of ~ 7°C in the North-East Atlantic within 20 years. The timing and magnitude of this warming is consistent with proxy data revealing DO-events to be simultaneous with increased global CO_2 [*Dansgaard et al.*, 1993; *Ahn and Brook*, 2008], indicating that only increases in atmospheric CO_2 can trigger [*Banderas et al.*, 2012] and even amplify the abrupt Northern Hemisphere warming under the intermediate ice-sheet volume.

4.4 Conclusions of Chapter 4

In summary, the model results discussed here demonstrate for the first time the role of NHIS on the hysteresis behavior of the glacial ocean, corroborating a previous hypothesis that the millennial-scale variability during glacial periods is dependent on the existence of continental ice sheets [*Wunsch*, 2006]. The bistable ocean regime accounting for the glacial abrupt climate switches is related to intermediate ice-sheet volumes, consistent with the fundamental characteristic of the millennial-scale variability in the records [*Dansgaard et al.*, 1993; *McManus et al.*, 1999; *Schulz et al.*, 1999; *Barker et al.*, 2011]. The simulated global responses are also supported by a host of proxy data associated with DO-type variability [*Voelker*, 2002]. In conclusion our results provide a novel and broad framework for understanding the occurrence of rapid climate changes during glacials, indicating that only minor changes in global sea level and/or carbon dioxide may induce abrupt ocean circulation change under intermediate ice-sheet volume.

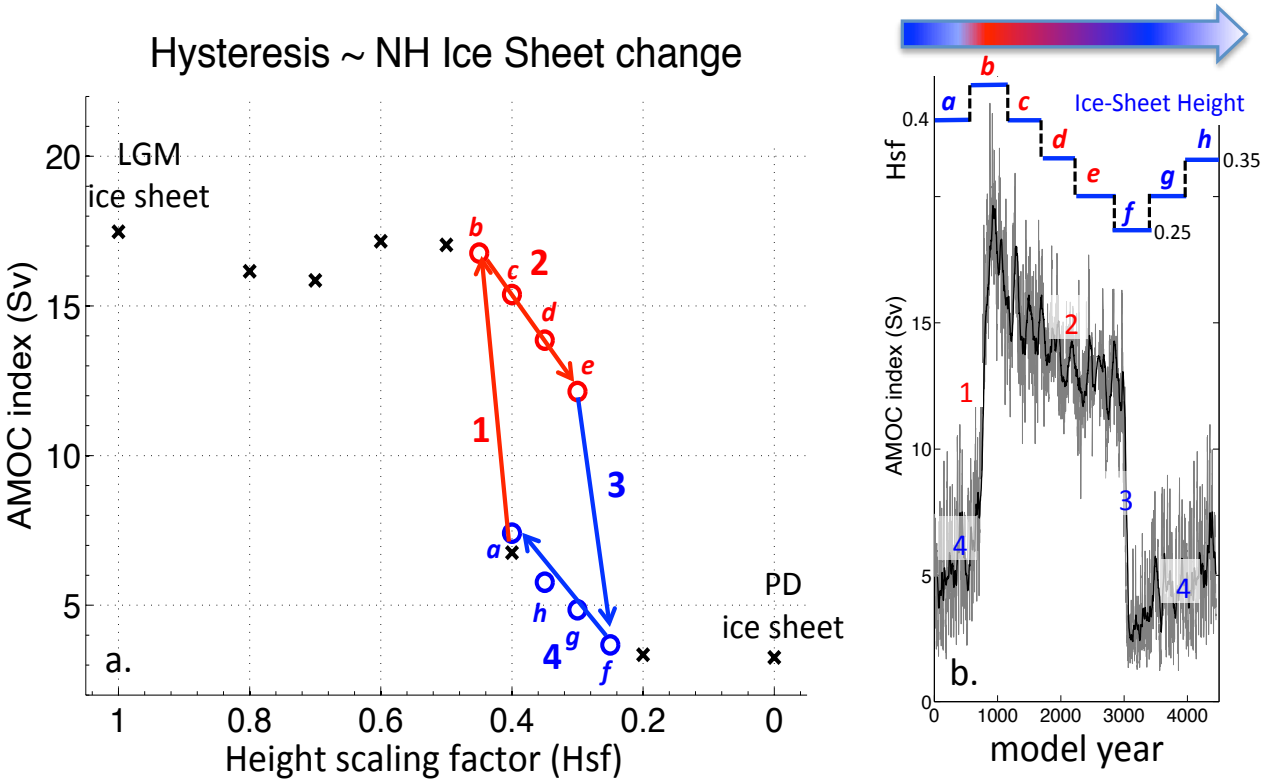

Fig. 4.11 Hysteresis of glacial ocean associated with ice-sheet height and its relationship to abrupt climate variability. (a) Response of glacial ocean to variations in the NHIS heights and (b) AMOC index for the experiments associated with the Hysteresis of glacial ocean (Table 1). Numbers in (b) correspond to the hysteresis branches defined in (a). Crosses in (a) represent the experiments performed to analyze the response of the glacial ocean to NHIS change, while circles indicate the simulations related to hysteresis behavior of glacial ocean (Table 1). Two bifurcation points at 40% and 30% of NHIS heights, are revealed respectively in the increasing and decreasing phases of the NHIS, responsible for the abrupt climate shifts. The equivalent sea level change for a 10% increase/decrease NHIS height is approximately 9m, indicating a narrow window for the bistable regime during glacials. The strong (weak) mode in Fig. 4.16 consists of the model results from NHIS_0.4s (point c), NHIS_0.35s (point d) and NHIS_0.3s (point e) (NHIS_0.4w (point a), NHIS_0.35w (point h) and NHIS_0.3w (point g)).

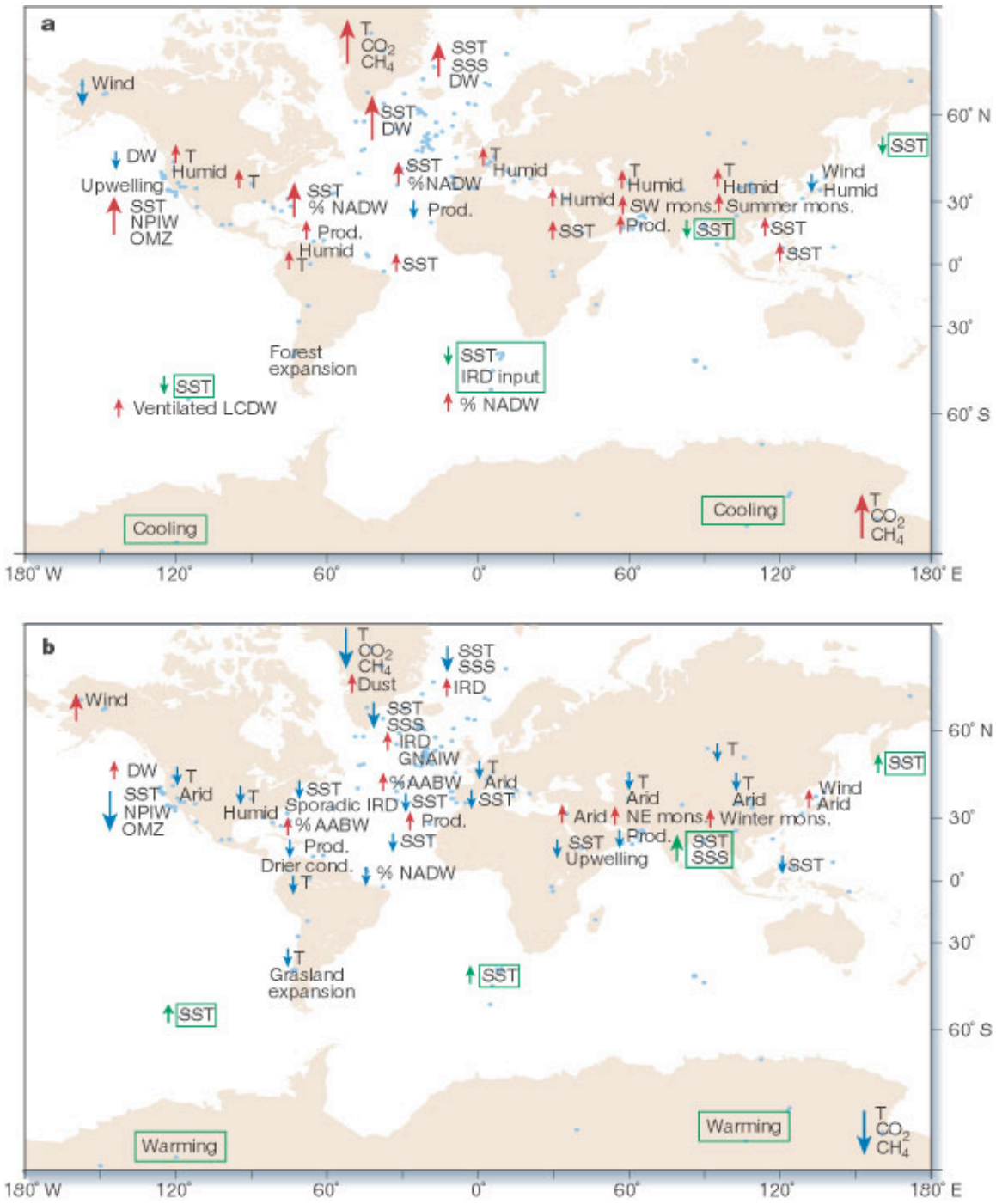

Fig. 4.12 Overview of palaeoclimatic proxy data characterizing warm phases (top) and cold phases (bottom) during MIS 3. Red arrows (blue arrows) indicate trends, that is, warmer (colder), more (less) or increased (lowered). Green text and arrows indicate trends opposite to the general climate conditions. Abbreviations: T, temperature; SST, sea surface temperature; SSS, sea surface salinity; mons., monsoon; prod., productivity; cond., conditions; IRD, ice-rafted debris; OMZ, oxygen minimum zone. Water masses are labelled as follows: DW, Deep Water; NADW, North Atlantic Deep Water; AABW, Antarctic Bottom Water; Ventilated LCDW NPIW, North Pacific Intermediate Water; LCDW, Lower Circumpolar Deep Water; GNAIW, Glacial North Atlantic Intermediate Water. (Figures are adapted from Rahmstorf 2002, originally from Voelker 2002)

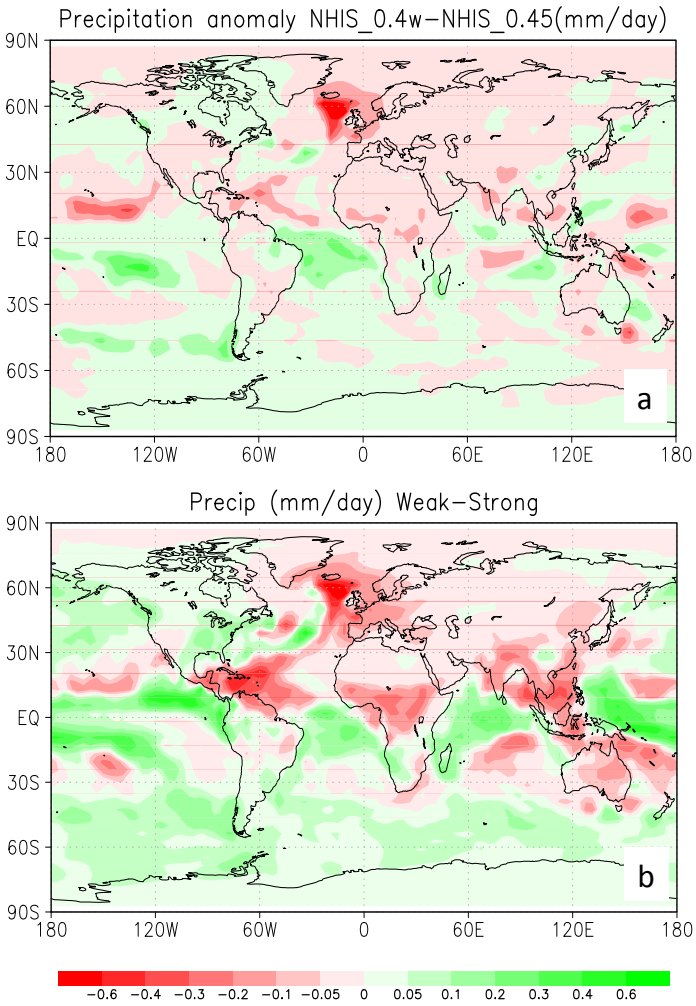
Precipitation anomaly NHIS_0.4w−NHIS_0.45(mm/day)
90N
60N
30N
EQ
30S
60S
90S
180
120W
60W
0
60E
120E
180
a
Precip (mm/day) Weak−Strong
b
−0.6 −0.4 −0.3 −0.2 −0.1 −0.05 0 0.05 0.1 0.2 0.3 0.4 0.6

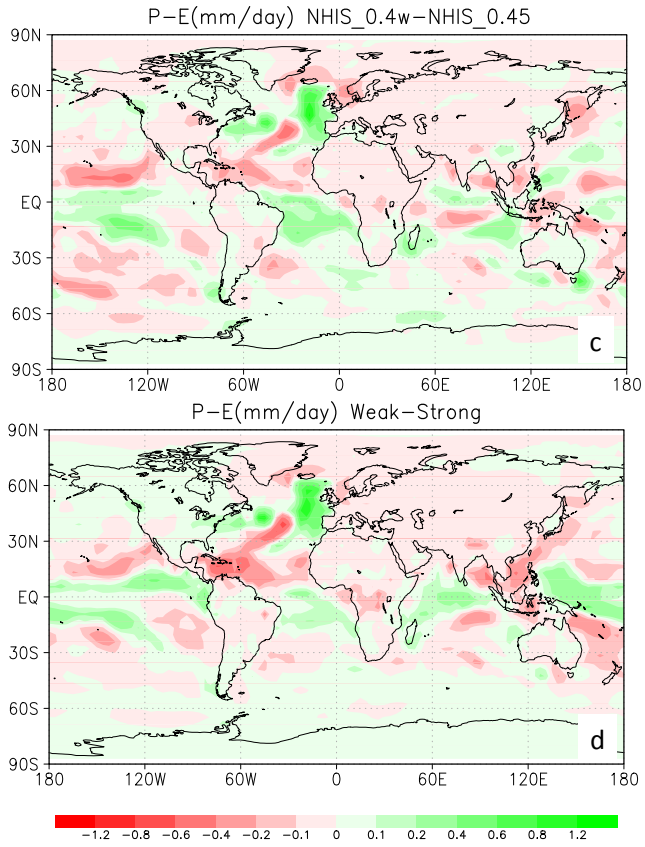

Fig. 4.13 Precipitation (a-b) and P-E (c-d) anomaly (units: mm/day) between NHIS_0.4w and NHIS_0.45 (a,c) and the weak (ensemble mean of NHIS_0.4s, NHIS_0.35w and NHIS_0.3w) and strong (ensemble mean of NHIS_0.4s, NHIS_0.35s and NHIS_0.3s) AMOC modes (b, d). The response of the Intertropical Convergence Zone (ITCZ) to changes in glacial ocean circulation is consistent with proxy data [*Peterson et al.*, 2000].

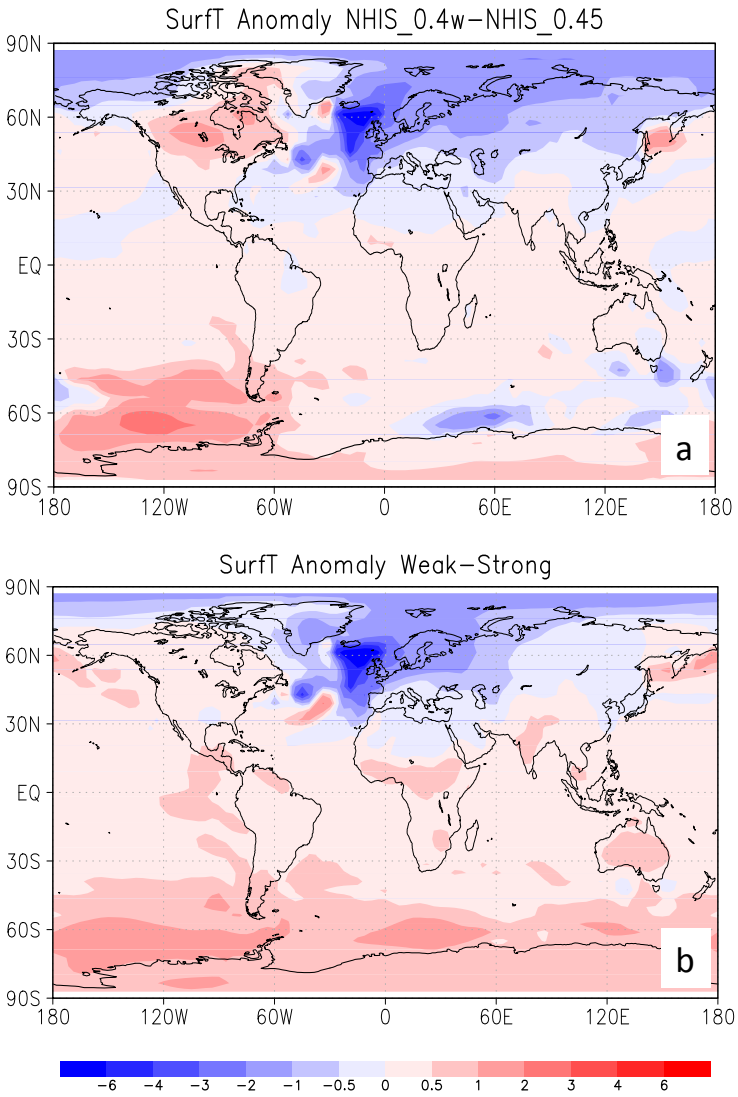

Fig 4.14. Same as Fig 4.13, except for surface air temperature (SAT).

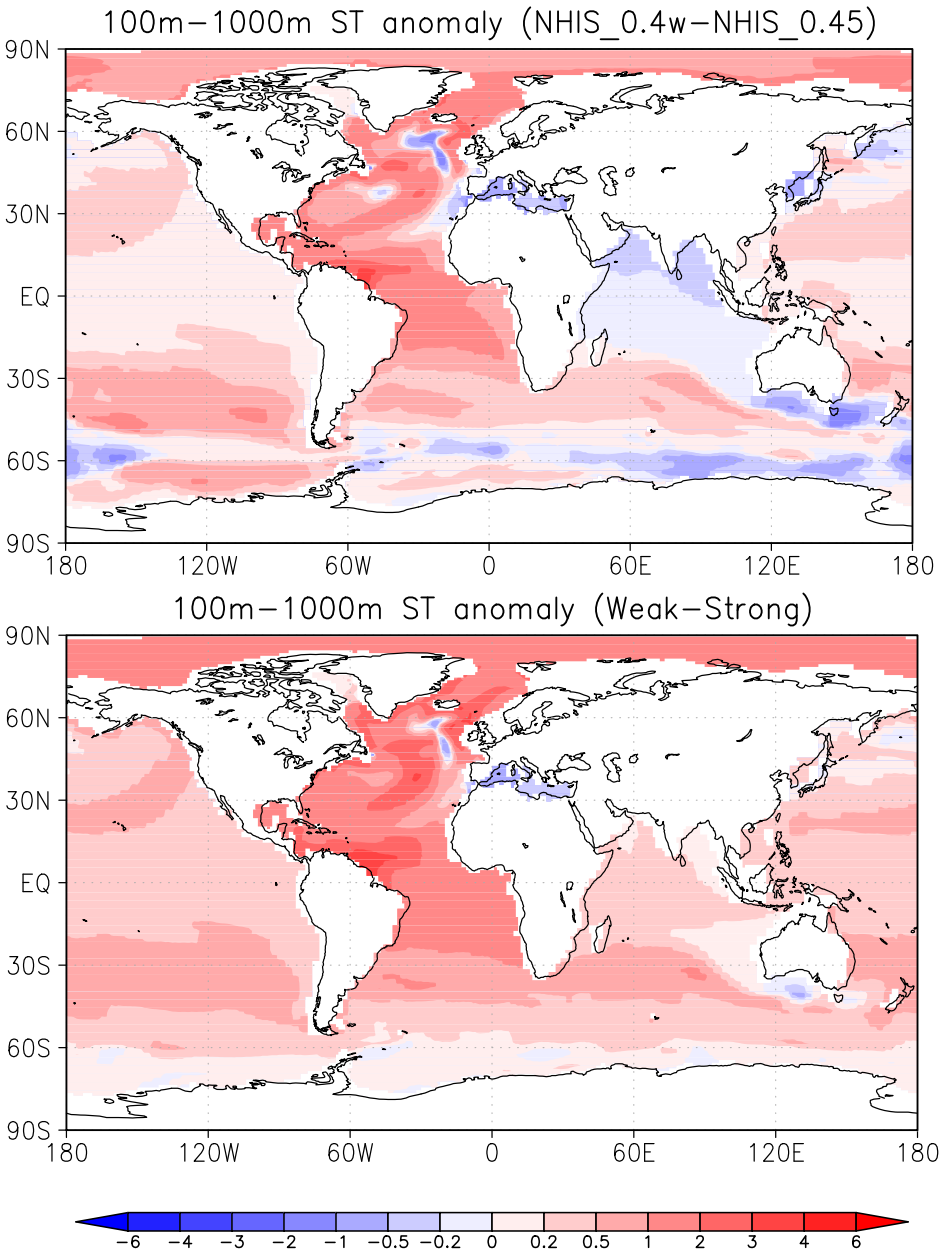

Fig. 4.15 Same as Fig 4.13, except for subsurface sea temperature that is consistent with reconstructions suggesting a significant warming during the stadials [*Rasmussen and Thomsen*, 2004].

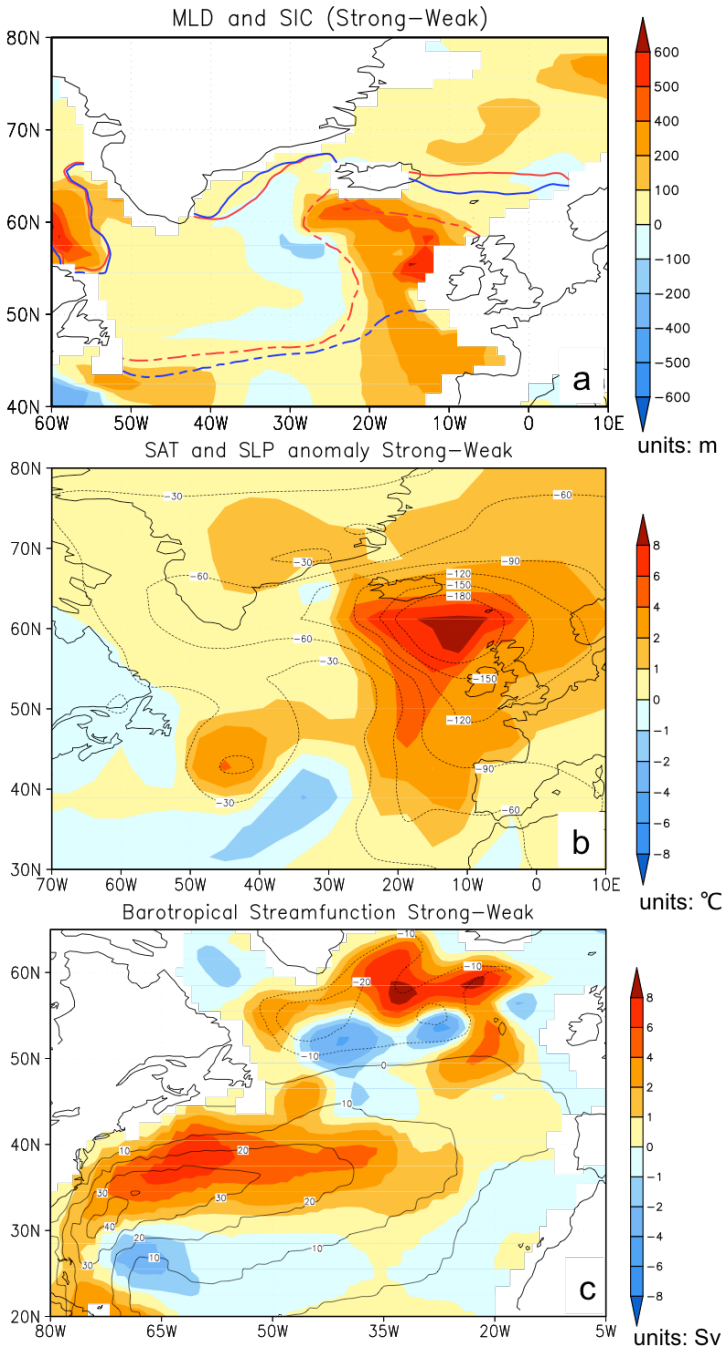

Fig. 4.16 Anomaly maps between strong and weak AMOC modes. a) Mixed layer depth anomaly (shaded, units: m) and absolute values for 15% (dashed) and 90% (solid) sea-ice concentration in the strong (red line) and weak (blue line) modes, b) anomalies of surface air temperature (SAT, shaded, units: °C) and sea-level pressure (contour, units: Pa), and c) anomaly of barotropic horizontal stream function (shaded, units: Sv) and its absolute value in the strong AMOC mode (contour).

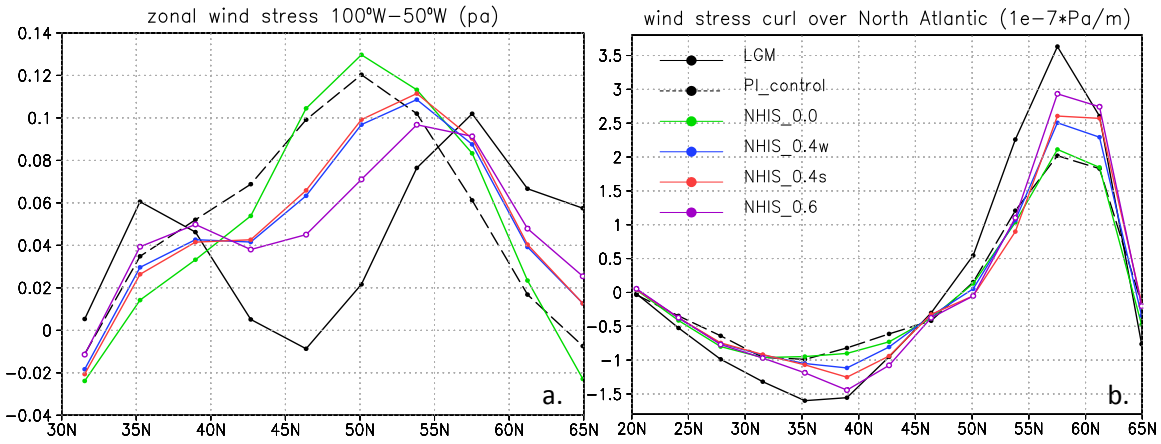

Fig. 4.17 Zonal mean u-wind stress (Pa) along 100°W-40°W (a) and wind stress curl over the North Atlantic Ocean (b). It can be observed that the core of Northern Westerlies shifts northward as the NHIS height increases, meanwhile strengthening wind stress curl over the North Atlantic basin. Under identical NHIS configurations (NHIS_0.4w and NHIS_0.4s), the wind stress curl over the North Atlantic can also be modified as a consequence of wind system changes occurring in response to the atmosphere-ocean-sea ice feedback in the northeastern North Atlantic.

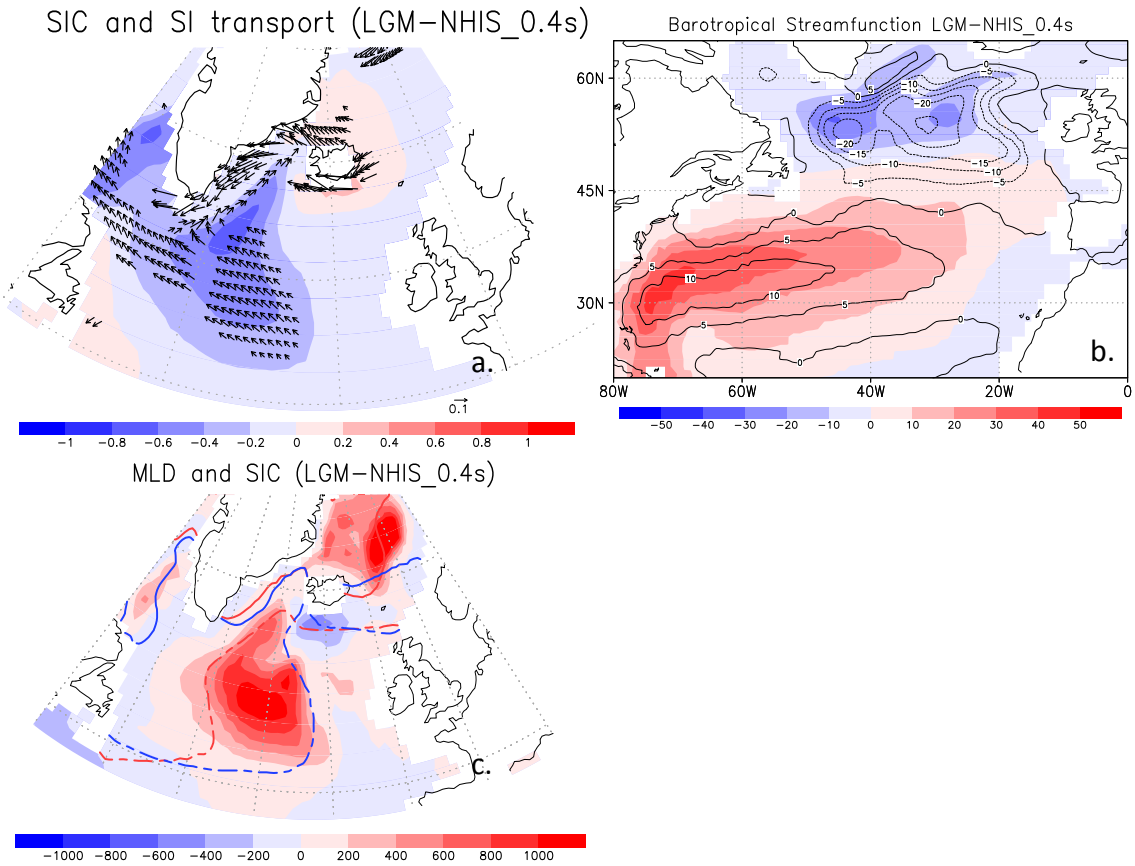

Fig. 4.18 Anomalies between two strong AMOC modes (LGM minus NHIS_0.4s). a) anomalies of sea ice concentration (shaded) and sea ice transport (vector), b) absolute (shaded) and anomalous (contour) values of horizontal barotropic stream function, and c) mixed layer depth anomaly (shaded) and absolute values for 15% (dashed) and 90% (solid) SIC in LGMctl (red line) and NHIS_0.4s (blue line).

Chapter 5. Responses of the glacial ocean to freshwater perturbation

Evidence from paleoclimate proxy records suggests the AMOC has undergone large fluctuations during MIS3 and LDG, many of them abrupt [e.g. *Kissel et al.*, 1999; *McManus et al.*, 2004]. Freshwater discharge to the North Atlantic from the melting ice sheets is assumed to be linked to the significant slowdowns indicated by the records, representative of HEs [e.g. *Clark et al.,* 2001; *Clark et al.,* 2002; *Rahmstorf,* 2002; *McManus et al.,* 2004]. The weakened AMOC reduces the northwards heat transport [*Broecker et al.*, 1985; *Crowley*, 1992], and thus warms the Southern Hemisphere as a consequence of bipolar thermal seesaw [*Broecker*, 1998; *Stocker and Johnsen*, 2003; *Knutti et al.*, 2004]. Although there remain some controversies concerning the relationship between HEs and AMOC changes (as discussed in Chapter 1, hypothesis 2), freshwater hosing experiments are still useful numerical experiments for understanding the mechanisms of global climate change relating to variations in AMOC [e.g. *Ganopolski and Rahmstorf*, 2001; *Stouffer et al.*, 2006; *Clement and Peterson*, 2008].

In this chapter, climate responses to different freshwater perturbation schemes under glacial boundary conditions are systematically investigated in the fully coupled climate model COSMOS. It is noteworthy that the work in this chapter involves several studies that are either already published (e.g. section 5.1.1. is referred to Kageyama et al. [2013] and Zhang et al. [2013]), or accepted (e.g. section 5.1.2 Weber et al. (*accepted*)) and in revision (section 5.2 Zhang et al. (*in revision*)).

5.1 Freshwater perturbation under maximum glacial ice sheet conditions

5.1.1 FWP in the North Atlantic

Most perturbation experiments are related to FW forcing in the North Atlantic due to its direct effects on the main NADW formation sites that are crucial to variations in the AMOC. In terms of the reduced/shut-down AMOC phase, a multi-model comparison of hosing experiments under LGM boundary conditions [*Kageyama et al.*, 2013] was conducted to quantitatively evaluating consistent/inconsistent features amongst different

models. In this study, 11 sets of hosing simulation by six different models are collected from six different modeling groups (Table 1, more model details see [*Kageyama et al.*, 2013]). There was no common protocol decided in advance by all the groups, but an attempt was made to gather experiments that were as close to each other as possible. For more details about individual model setups, please refer to Kageyama et al. [2013] and the corresponding reference for each model (Table 1).

Experiment Abbreviation	Hosing experiment	Years taken for average	Reference for hosing experiment
CCSM-NCAR	0.1Sv (imposed as negative salinity flux) for 500year in North Atlantic, 50-70°N	250-299	*Otto-Bliesner and Brady*, 2010
CCSM-MARUM	0.2 Sv (imposed as negative salinity flux) in Greenland-Iceland-Norwegian Seas for 360 year	261-360 for the AMOC, 341-360 for the climate variables	*Merkel et al.*, 2010
MIROC-S	0.1 Sv (freshwater flux) in North Atlantic (50-70N) for 500 year	370-419	
MIROC-W	0.1 Sv (freshwater flux) in North Atlantic (50-70N) for 500 year	370-419	
IPSL	0.1 Sv (freshwater flux) in North Atlantic (50-70N) for 419 year	370-419	*Kageyama et al.*, 2009
LCM10-0.15	0.15 Sv in "Ruddiman Belt" (i.e. North Atlantic, 40-50N) (freshwater flux)	350-400	*Roche et al.*, 2010
LCM10-0.30	0.3 Sv in "Ruddiman Belt" (i.e. North Atlantic, 40-50N) (freshwater flux)	220-240	*Roche et al.*, 2010
HadCM3-0.1	0.1Sv in North Atlantic (50-70N), imposed as a negative salinity flux, for 1000year, reference experiment: 24 ka BP	270-299	*Singarayer and Valdes* (2010) for similar 1Sv hosing experiments and full description of reference for 24ka BP
HadCM3-0.1	0.4Sv in North Atlantic (50-70N), imposed as a negative salinity flux, for 1000year, reference experiment: 24 ka BP	270-299	*Singarayer and Valdes*, 2010
COSMOS-S	0.2Sv (freshwater flux) in North Atlantic (Ruddiman Belt) for 150 year	140-150	*Zhang et al.*, 2013
COSMOS-W	0.2Sv (freshwater flux) in North Atlantic (Ruddiman Belt) for 250 year	200-250	*Zhang et al.*, 2013

Table 1 Brief description of the experiments in the multi-model comparison study (from Kageyama et al., 2013).

Responses of SAT and precipitation to FWP in different models are shown in Figures 5.1 and 5.2. Some regions, i.e. the North Atlantic, the tropical Atlantic and the African and Indian monsoon regions share consistent features with paleoclimate records of abrupt events occurring during HEs. For instance, all models produce their strongest cooling over the high latitude North Atlantic Ocean (Fig. 5.1), which is accompanied by decreased precipitation (Fig. 5.2). In parallel, the African monsoon consistently weakens in all models, although it is difficult to relate the amount of precipitation decrease to SAT changes over the adjacent tropical Atlantic or to North Atlantic SST changes as suggested from the data presented by Niedermeyer et al. [2009]. In addition, the weakened Indian monsoon appears to be correlated both with North Atlantic and South Tropical Atlantic cooling. In conclusion, the common features among models are qualitatively consistent with those obtained from the pre-industrial base state by Stouffer et al. [2006] with the exception of the behaviour over the northern Nordic Seas and the Arctic for which no model simulates a warming for the glacial base state. Regions like the Northeast Pacific, the Southern Ocean and especially Southeast Pacific and Antarctic are characterized by inconsistent behaviour in response to FWP. One distinction in the model responses can be attributed to the different extents of AMOC reduction. Models with a weak AMOC decrease appear to transport the northern cooling signature to the Southern Ocean (e.g. HadCM3.0.1 and LCM10-0.15). In contrast, models with a strong AMOC decrease simulate a bipolar seesaw that generates a zonally symmetric or a zonally asymmetric form, confirming the classification proposed by Clement and Peterson [2008]. For more results and discussions in this study, please refer to Kageyama et al., [2013].

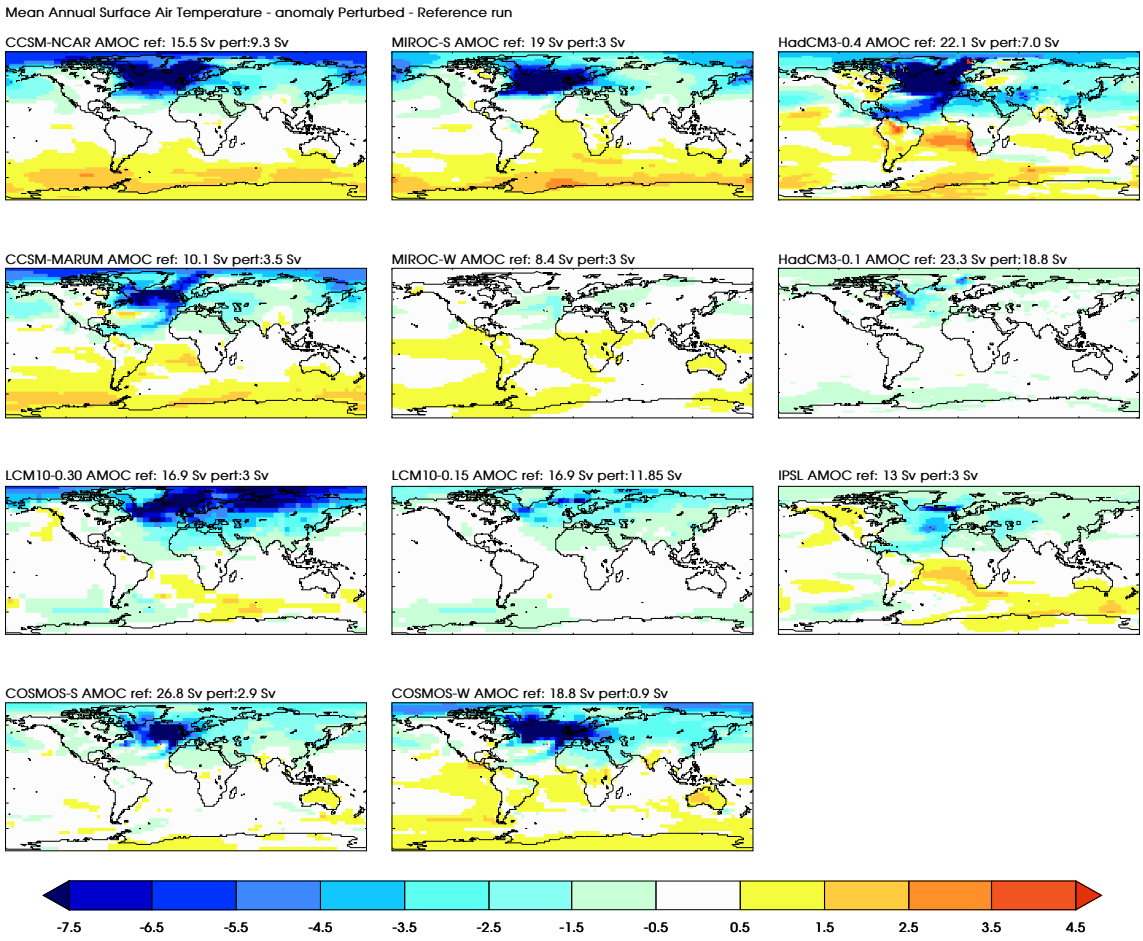

Fig. 5.1 Mean annual surface air temperature response (hosing experiment – reference experiments, in K) to freshwater hosing in the 11 hosing experiments. (from Kageyama et al., 2013)

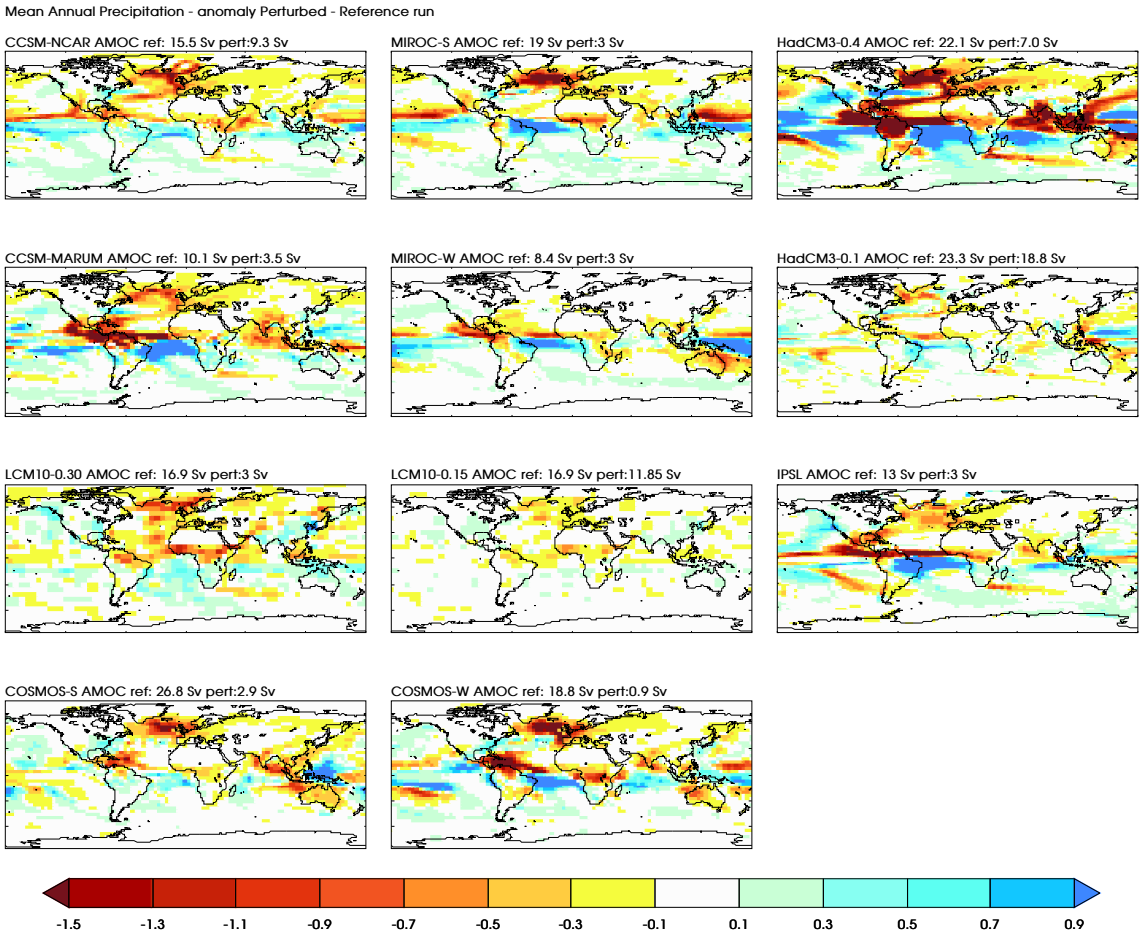

Fig. 5.2 Same as Fig. 5.1 but for the mean annual precipitation, in mm/day. (from Kageyama et al., 2013)

Among these six different models, only the COSMOS model is characterized by two distinct quasi-equilibrium ocean states under the identical LGM boundary condition [*Zhang et al.,* 2013] (for more details, please refer to Chapter 3). Previous model studies show that under present climate conditions [e.g. *Rahmstorf et al.*, 2005] or glacial conditions [e.g. *Ganopolski and Rahmstorf*, 2001], a bistable regime of the AMOC in its parameter space, whereby North Atlantic deep-water formation can be "on" (as in the present climate) or "off". As a consequence different AMOC states can exist within the same boundary conditions, depending on the initial conditions in the ocean. In this case, transitions between different ocean states can be fulfilled by modifying the hydrological balance in the Atlantic basin [e.g. *Ganopolski and Rahmstorf*, 2001; *Rahmstorf et al.*, 2005]. After imposing constant freshwater perturbations (FWP) of +0.2 Sv and +1 Sv over the IRD belt (around 40°N-55°N, 45°W-20°W) [*Hemming*, 2004] in the North

Atlantic respectively for 150 and 100 years (Table 2), we continue to run the simulations for another several hundreds years in order to evaluate the potential bistability and recovery features.

	Boundary conditions	Initial conditions	Integrated years
LGMW-0.2Sv	21ka	LGMW-e (model year 2900 in LGMW)	150
LGMW-1Sv	21ka	As above	100
LGMS-0.2Sv	21ka	LGMS-t_{deep} (model year 2900 in LGMS)	150
LGMS-1Sv	21ka	As above	100
LGMS-e-0.2Sv	21ka	LGMS-e (model year 4600 in LGMS)	150

Table 2 Hosing experiment in two glacial ocean states in COSMOS. For the detailed information about the base ocean states (LGMW-e, LGMS-e and LGMS-t_{deep}), please refer to Chapter 3.

Figures 5.3 and 5.4 shows the time series of AMOC indices for the respective hosing experiments. It is notable that neither of these is able to trigger the transition from one ocean state to the other (Figs. 5.3 and 5.4). The simulated LGM ocean circulation is characterized by a monostable AMOC, in contract to the results from models with intermediate level of complex [e.g. *Ganopolski and Rahmstorf*, 2001] but consistent with one fully-coupled climate model [*Liu et al.,* 2009]. Thus, we propose that the cause for the different LGM ocean states is not related to the hydrological balance in the North Atlantic. After the FWP, the overshoot of the AMOC in LGMW-e (see LGMS-e case in Fig. 5.4) results in an abrupt warming over Greenland for several decades, but not in the LGMS-t_{deep} case (Figs. 5.5). Given the distinct ocean structures during and after the FWP, we propose that the stratified glacial ocean plays an important role in the AMOC recovery by influencing the subsurface warming in the convection sites (especially in the northern North Atlantic, Fig. 5.6), northward transport of tropical warmer and saltier water and basin-wide salinity adjustment (Figs. 5.7 and 5.8) [cf. *Mignot et al.*, 2007; *Liu et al.*, 2009; *Cheng et al.,* 2011]. This may explain the abrupt warming events over Greenland following the HEs during glacial periods (e.g. the abrupt warming after Heinrich Event 2) [*Dansgaard et al.*, 1993; *Blunier and Brook*, 2001].

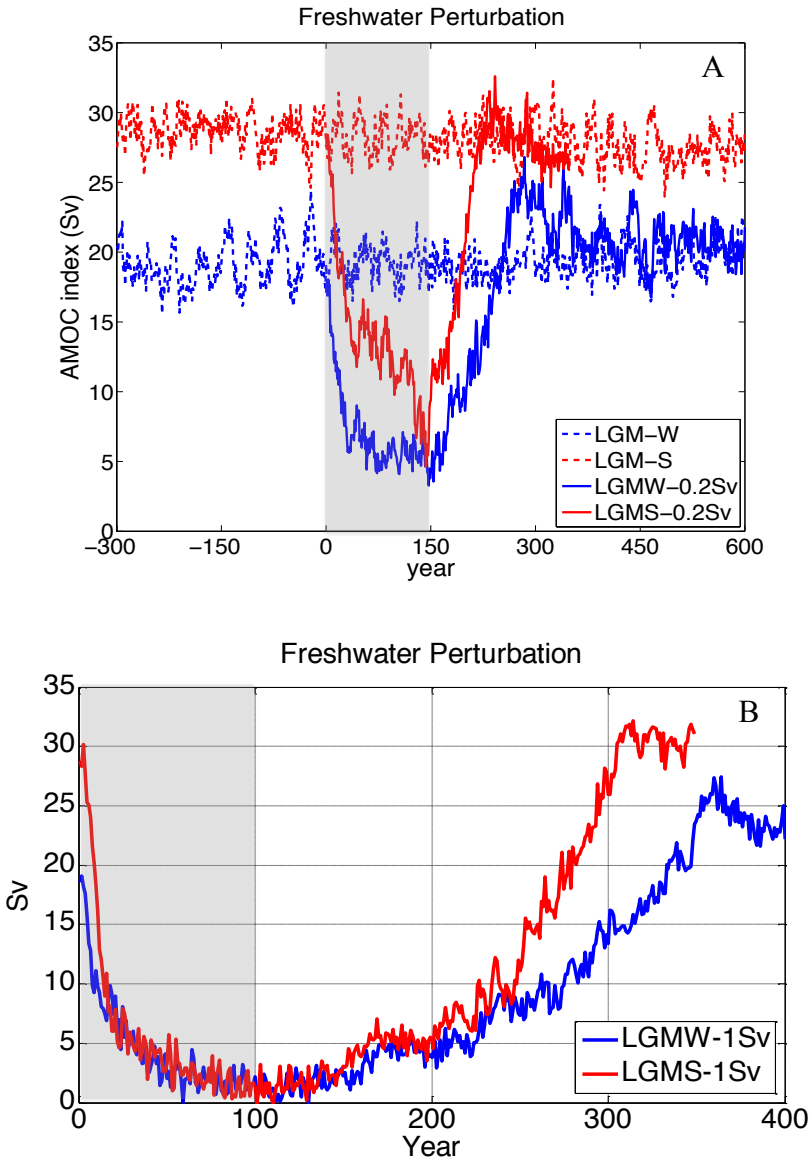

Fig. 5.3 Time series of AMOC in the 0.2Sv (A: FWP lasts for 150 years) and the 1Sv (B: FWP lasts for 100 years) hosing experiments LGMW-e (blue) and LGMS-t_{deep} (red), respectively. The hosing experiments started from the model year 2700 in each LGM simulation. Dashed lines represent the LGM control runs (A), and solid lines the hosing experiments (A, B). Despite the different amount of FWP, a transition between the states LGMW-e and LGMS-t_{deep} is not triggered. A robust overshoot of the AMOC is only detected in quasi-equilibrium ocean states with respect to the deep ocean properties.

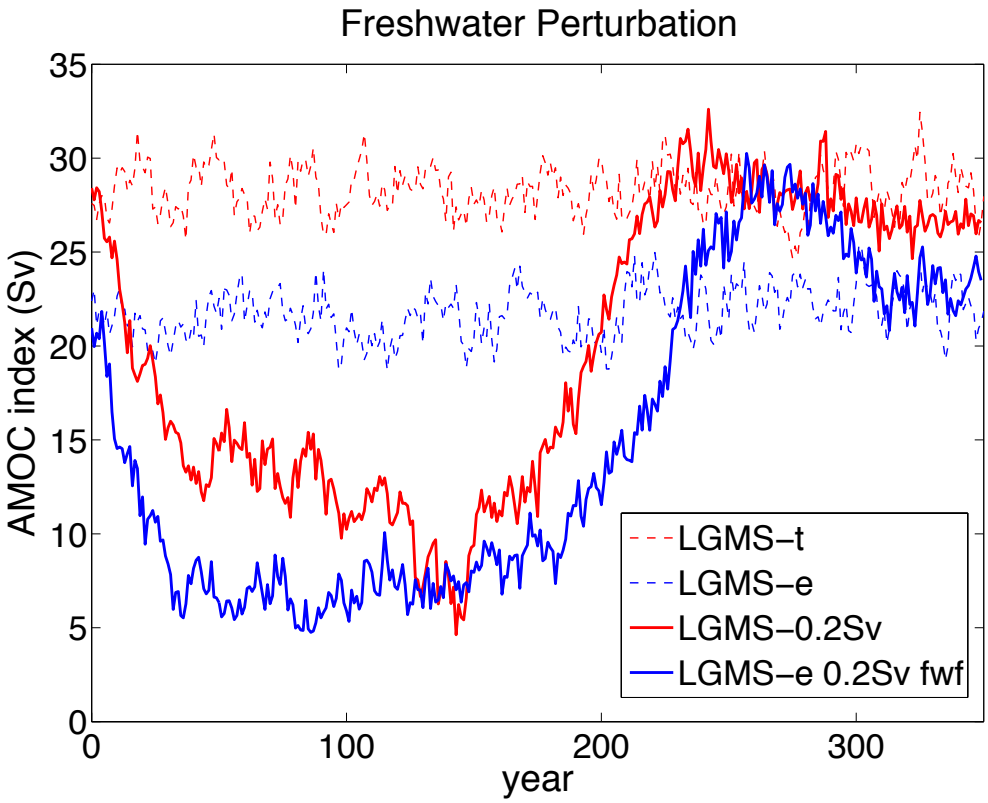

Fig. 5.4 Time series of AMOC in the 0.2Sv (FWP lasts for 150 years) hosing experiments of LGMS-t_{deep} (red) and LGMS-e (blue). The hosing experiments started from the model year 2700 and 4500 in the LGMS simulation for LGMS-t_{deep} and LGMS-e, respectively. The dashed lines represent the LGMS control runs, and solid line for hosing experiments. It is shown that after the FWP an AMOC overshoot was found in LGMS-e as LGMW-e, while no overshoot in LGMS-t_{deep}.

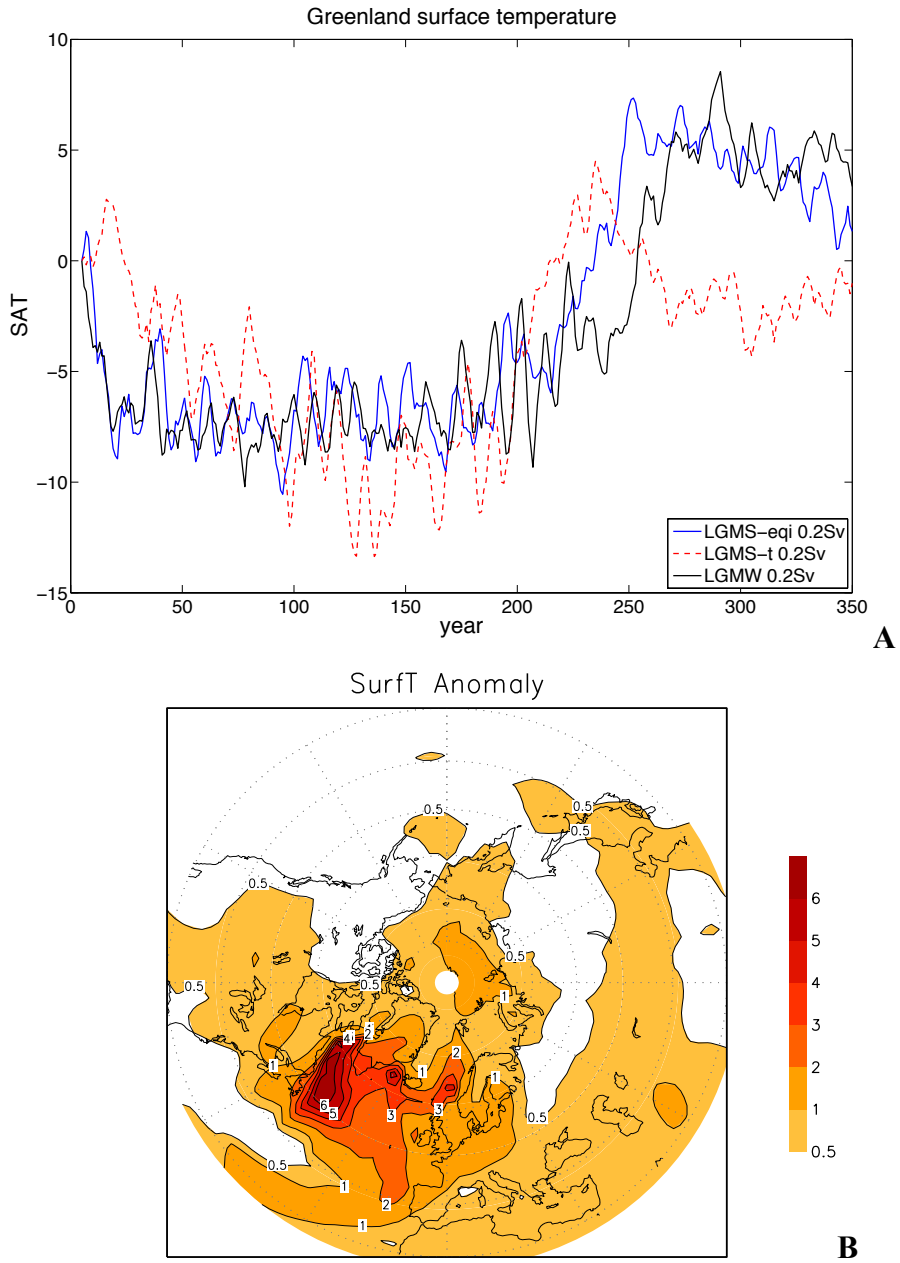

Fig. 5.5 A) Surface air temperature (SAT) in the latitude belt of 60-70°N in the North Atlantic in LGMW-0.2Sv (black), LGMS-0.2Sv (red) and LGMS-e-0.2Sv (blue). 5-year running mean was used to filter out the high frequency signals of the SAT. B) Excess surface temperature increase related to the overshoot of the AMOC (270th-300th years) in LGMW-0.2Sv. The pronounced temperature increase relative to LGMW in the North Hemisphere is up to 6.8°C at convection sites in the North Atlantic.

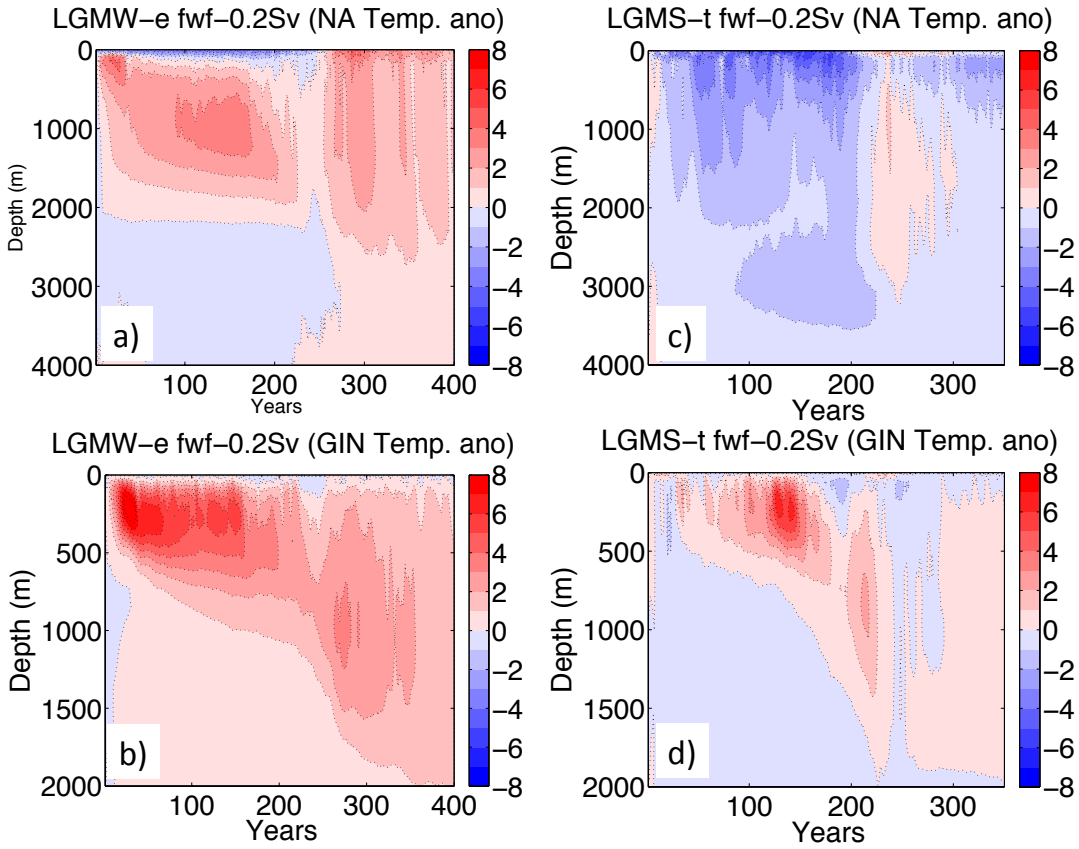

Fig. 5.6 The vertical structure of the temperature anomaly between 0.2Sv hosing and corresponding control runs in the convection sites of the North Atlantic (20°W-40°W, 50-60°N) (a, c) and the Nordic Sea (20°W-10°E, 65-75°N) (b, d) for the 0.2Sv hosing experiments of LGMW-e (a, b) and LGMS-t_{deep} (c, d). It is shown that the subsurface warming in quasi-equilibrium ocean state is much more pronounced than the transient ocean state LGMS- t_{deep} in response to the FWP, especially in the convection sites of the North Atlantic. This will benefit a rapid destabilization of water column and finally the AMOC overshoot [*Mignot et al.,* 2007].

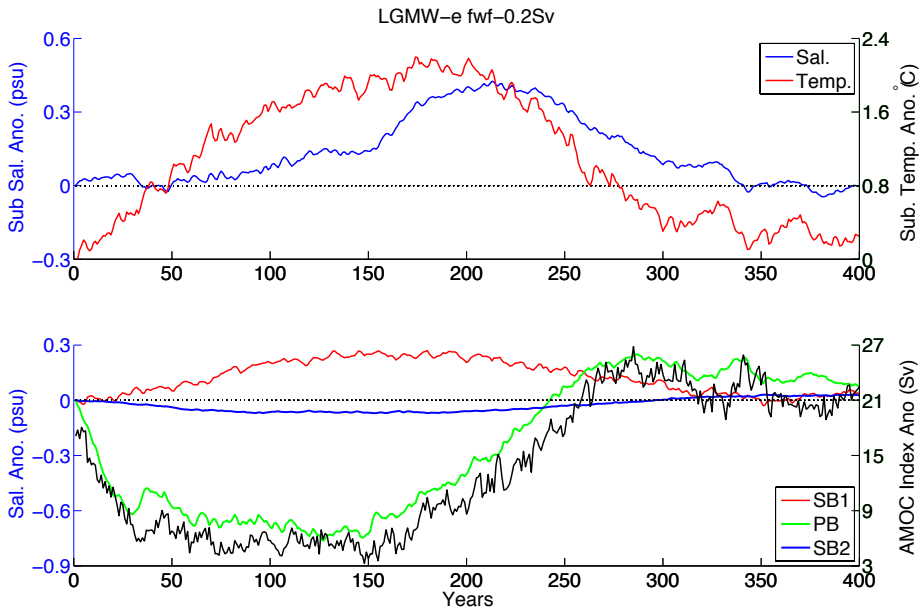

Fig. 5.7 Upper panel: Subsurface temperature (red, right y-axis) and salinity (blue, left y-axis) in Tropical regions (20°S-30°N, 100-500 m). Lower panel: Time series for AMOC transport (black, right y-axis) and box salinities (red, green and blue, left y-axis) for the 0.2 Sv hosing experiments in the simulation LGMW-e. The Atlantic basin is partitioned into box SB1 (45°S-20°S, 0-500 m), PB (35°N-80°N, 0-2000 m) and SB2 (45°S-20°S, 500-2000 m). Combined with Fig. 5.8, we propose that the AMOC overshoot in quasi-equilibrium ocean states can also be attributed to the basin-wide salinity adjustment [Liu et al., 2009], while the tropical contribution might also play a role on restoring the AMOC by transportation of warmer and saltier subsurface water to the convection sites [*Cheng et al.*, 2010].

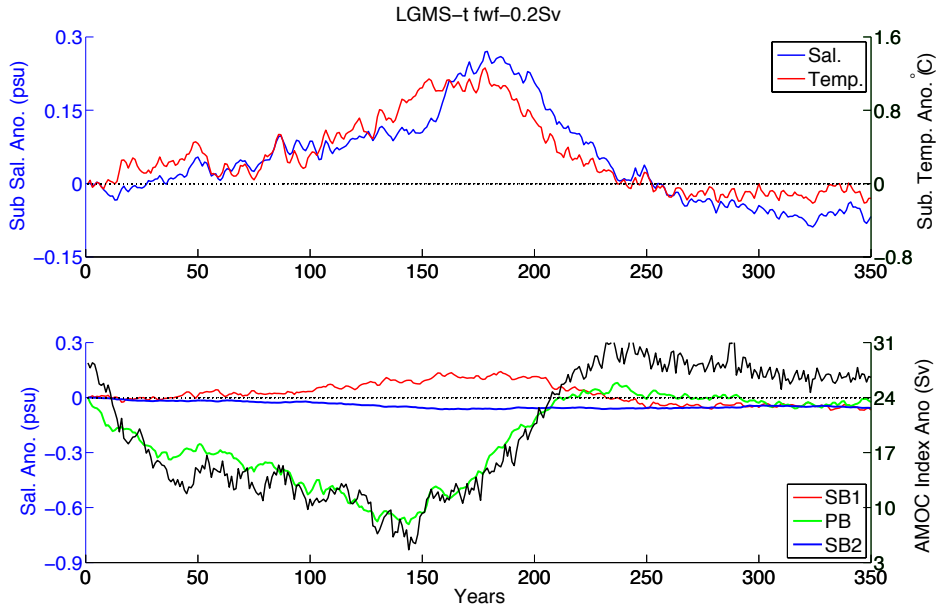

Fig. 5.8 Same as Fig. 5.7 but for 0.2 Sv hosing experiment in LGMS-t_{deep}.

It is worth noting that the subsurface temperature response to the FWP is also dependent on the reference glacial ocean states (Figs. 5.9 and 5.10). An overall subsurface warming can be identified in the entire Atlantic basin from Nordic Sea to the South Atlantic in the hosing experiment based on the state with a stratified ocean structure (LGMW-e and LGMS-e). In contrast, a top-down cooling signature cuts off the basin-wide subsurface warming pattern in the convection sites of Northern North Atlantic in simulation LGMS-0.2Sv. This cooling can be attributed to the partially active convection during the hosing in the LGMS-t_{deep}, which continuously transports the surface cooling water down to the deep ocean.

In addition, based on a well-stratified ocean state, freshwater-induced subsurface warming can also be identified in the South Ocean adjacent to the Antarctica, in contrast to a cooling in LGMS-t_{deep}. According to bipolar thermal seesaw [*Broecker*, 1998; *Stocker and Johnsen*, 2003; *Knutti et al.*, 2004], there will be more heat stored in the Southern Hemisphere in response to the reduced AMOC, warming the Southern Ocean and facilitating the sea-ice melting there. This causes more freshwater injected into the ocean, forming a strong stratification due to the increased vertical density gradient. As a consequence, the vertical mixing in the Southern Ocean weakens, suppressing the air-sea heat exchange and promoting subsurface warming. However, surface warming in the Southern Hemisphere is limited in LGMS-0.2Sv, probably due to the intervention of subsurface cooling signature that is transported from the North Atlantic by the AMOC and is ventilated to the surface by wind-driven upwelling over the Antarctic Circumpolar Current (ACC) regions (Figs. 5.9 and 5.10). Therefore, this prohibits extensive sea-ice melting and the subsurface warming. As far as the bipolar seesaw is concerned, cautions should also be paid to this mechanism since the equilibrium time-scale of climatic response of the Southern Ocean to the northern cooling could be longer than the perturbed time [*Kageyama et al.*, 2010].

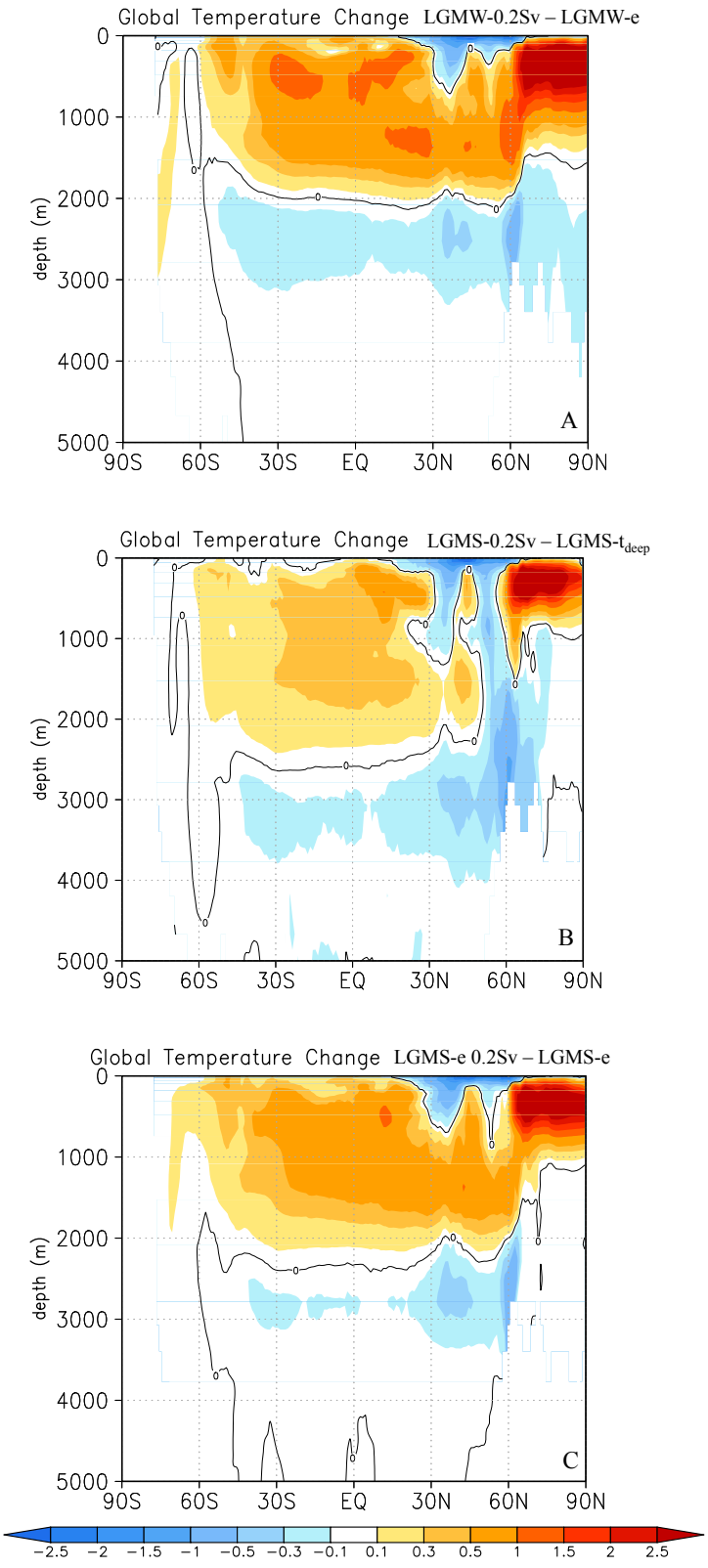

Fig 5.9 Meridional section of global sea temperature anomaly in the 0.2Sv hosing experiments for LGMW-e (a), LGMS-t_{deep} (b) and LGMS-e (c) (units: ℃).

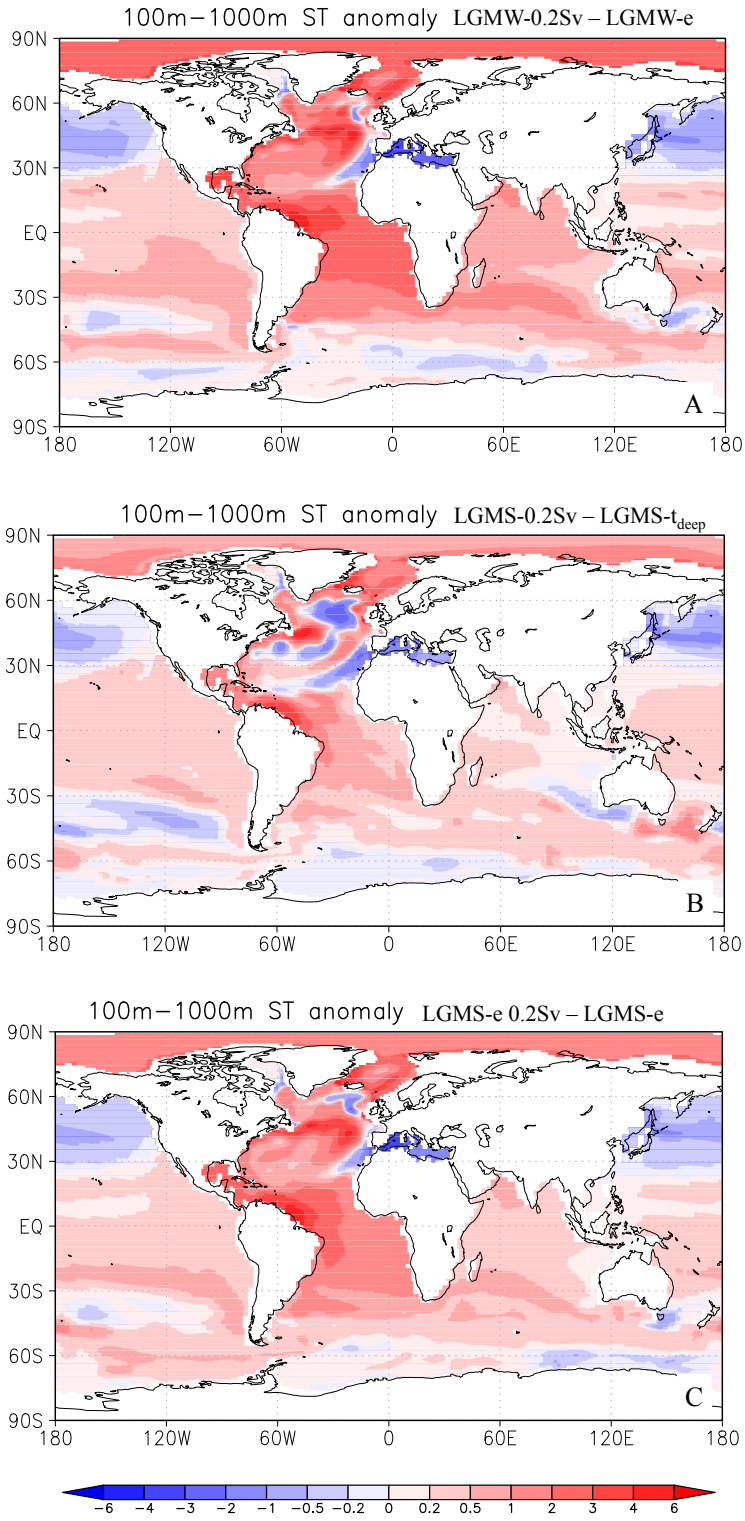

Fig 5.10 Subsurface (100-1000m) temperature anomaly in the 0.2Sv hosing experiments for LGMW-e (a), LGMS-t_{deep} (b) and LGMS-e (c) (units: ℃).

5.1.2 FWP in the Southern Ocean

Besides the Northern Hemisphere Ice Sheets as a major source of meltwater to the ocean, the Antarctic Ice Sheet also bears potential for contributionto sea level rise during the LDG, especially the BA [e.g. *Clark et al*., 2002; *Carlson and Clark* 2012; *Deschamps et al*., 2012], although some controversies remain [*Fairbanks*, 1989; *Peltier*, 1994]. To interpret the synchronization of sea level rise and abrupt northern warming during the BA, Weaver et al. [2003] simulated a rapid AMOC transition that causes abrupt northern warming, by imposing FWP to Southern Ocean in an AMOC 'off' mode. However, Stouffer et al. [2007] showed that a FWP in the Southern Ocean tended to slightly reduce the AMOC strength, owing to the invasion of fresh water to the North Atlantic via ocean circulation, in line with Seidov et al. [2005]. Although the latter case appears to be more realistic in the real world [*Stouffer et al.,* 2007], it is difficult to rule out the reliability of the former case due to the fact that different base ocean states are used in these two studies. Besides, it is important to note that all of them are based on the present-day boundary conditions which deviate largely from the glacial one. Therefore, the role played by the southern FWP on glacial climate change, e.g. BA warming, remains unclear.

Experiment ID	East AIS melting	West AIS melting	CO_2	Insolation
DGCMS1	21ka-14ka	/	/	/
DGCMS2	21ka-15ka	15ka-14ka	/	/
DGCMS3	21ka-16ka	16ka-14ka	/	/
DGCMS2C	21ka-15ka	15ka-14ka	18ka-14ka	/
DGCMS2CO	21ka-15ka	15ka-14ka	18ka-14ka	17ka-14ka

Table 3 Transient simulations in COSMOS (21 – 14ka BP). Freshwater flux is added to coastal areas of East AIS (0 – 180°E) and West AIS (120°W – 60°W) for different icebergs release scenarios (Fig. 5.12). Slash "/" indicates identical forcing to LGM simulations (see details in Chapter 3 [*Zhang et al.,* 2013]).

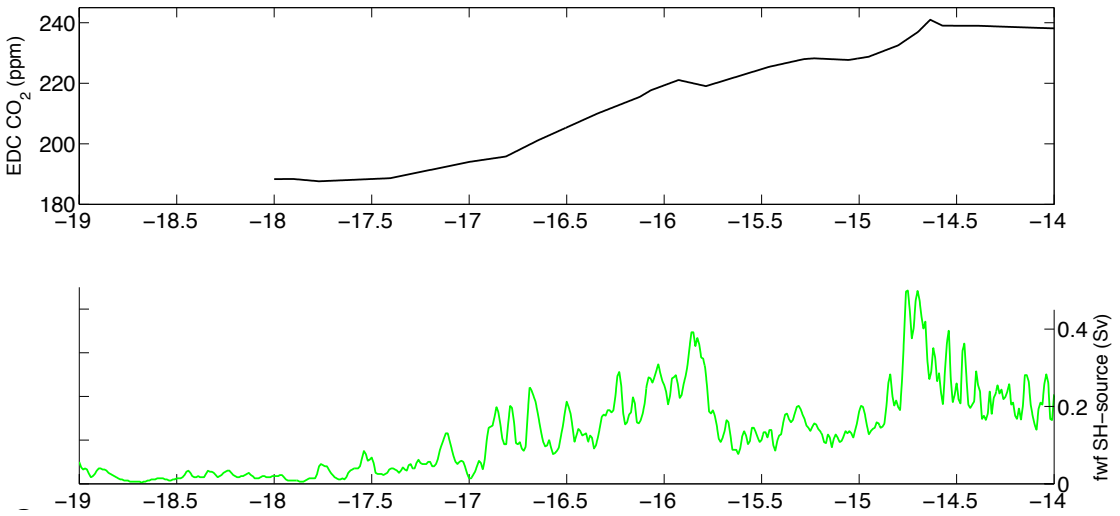

Fig 5.11 Time-series of CO_2 and freshwater forcing used in the transient simulation with respect to southern FWP.

In a recent study by Weber et al. (*accepted*), a continuous millennial-scale signal of AIS variability based on two high-resolution records of IRD from deep-sea core sites in the south-central Scotia Sea, is presented, providing direct evidence on the AIS contribution to sea-level rise during the BA. Here the converted freshwater amount from the IRD records (Fig. 5.11) is prescribed in our fully coupled model COSMOS to investigate how the southern FWP influences the global glacial climate as well as the potential local feedback promoting persistent IRD events since ~18ka BP. Due to the uncertainty regarding origin of the IRD, three different scenarios are designed to represent the collapse of the Eastern and Western Antarctic ice-shelves during the LDG (Table 3). In addition to the FWP, varying carbon dioxide (Fig. 5.11) [*Lourantou et al.*, 2010] and orbital parameters [*Laskar et al.*, 2004] are further prescribed to assess their contributions to climate changes (Table 3). All the other boundary conditions are fixed to the LGM (see details in Chapter 3 [*Zhang et al*., 2013]). Note that the transient simulations before and after the calendar year 17ka BP are respectively accelerated by a factor of 10 and 5, i.e. the FWP amounts prescribed in our simulations are 10 and 5 times larger than the original and 100 model years in these simulations represent 1000 and 500 calendar years, respectively.

The FWP-single forcing runs (DGCMS1-3) are characterized by a gradual weakening of AMOC strength in response to the southern FWP, but a rapid reduction of AABW

formation in the Southern Ocean (Fig. 5.12). This can be attributed to the delayed and instant responses of the remote and local ocean circulation to the FWP in the South. Surface cooling over Greenland and Antarctic is also identified, with the former associated with the AMOC change and the later related to the FWP history. These features are independent of the locations where the FWP are imposed in the Southern Ocean. However, SubST in the Southern Ocean appears to be controlled by the perturbed locations around the Antarctica. The injection of freshwater along Western Antarctica is capable of forcing the strongest subsurface warming, in contrast to the hosing scenarios in Eastern Antarctica. This is likely associated with the existence of major convection sites in the Weddell Sea, of which suppression will efficiently prohibit the air-sea heat exchange and thus promote the subsurface warming. As a consequence, Antarctic ice-shelf thinning is accelerated by the induced basal melting, acting as a positive feedback by causing grounding line retreat, calving, and subsequent release of more freshwater.

The effect of atmospheric CO_2 concentration exerts a more important role on the temperature variation in the transient simulations, in comparison to orbital forcing (Fig. 5.12, DGCMS2C and DGCMS2CO). As carbon dioxide change is involved, the cooling over the Antarctica is largely reduced and the subsurface warming in the Southern Ocean is enhanced. This also works on the Greenland SAT of which variation, nevertheless, is still related to the AMOC changes. One distinct feature in contrast to the FWP-single forcing runs is the robust warming at around ~14.6 ka BP when the recorded BA warming occurred. This simulated warming is assumed to be related to the delayed (~ 50 model years) response of the AMOC to the reduced southern FWP at 15.5~14.8ka BP. Given the acceleration technique used in our simulations and weakening effect of southern FWP on the AMOC, it is concluded that in reality a rapid reduction of FWP at 14.6ka BP can lead to the resumption of the AMOC as well as the warming in the Greenland. In addition, it is confirmed that the increased carbon dioxide does play a role on the Northern warming during the BA via its thermal effect.

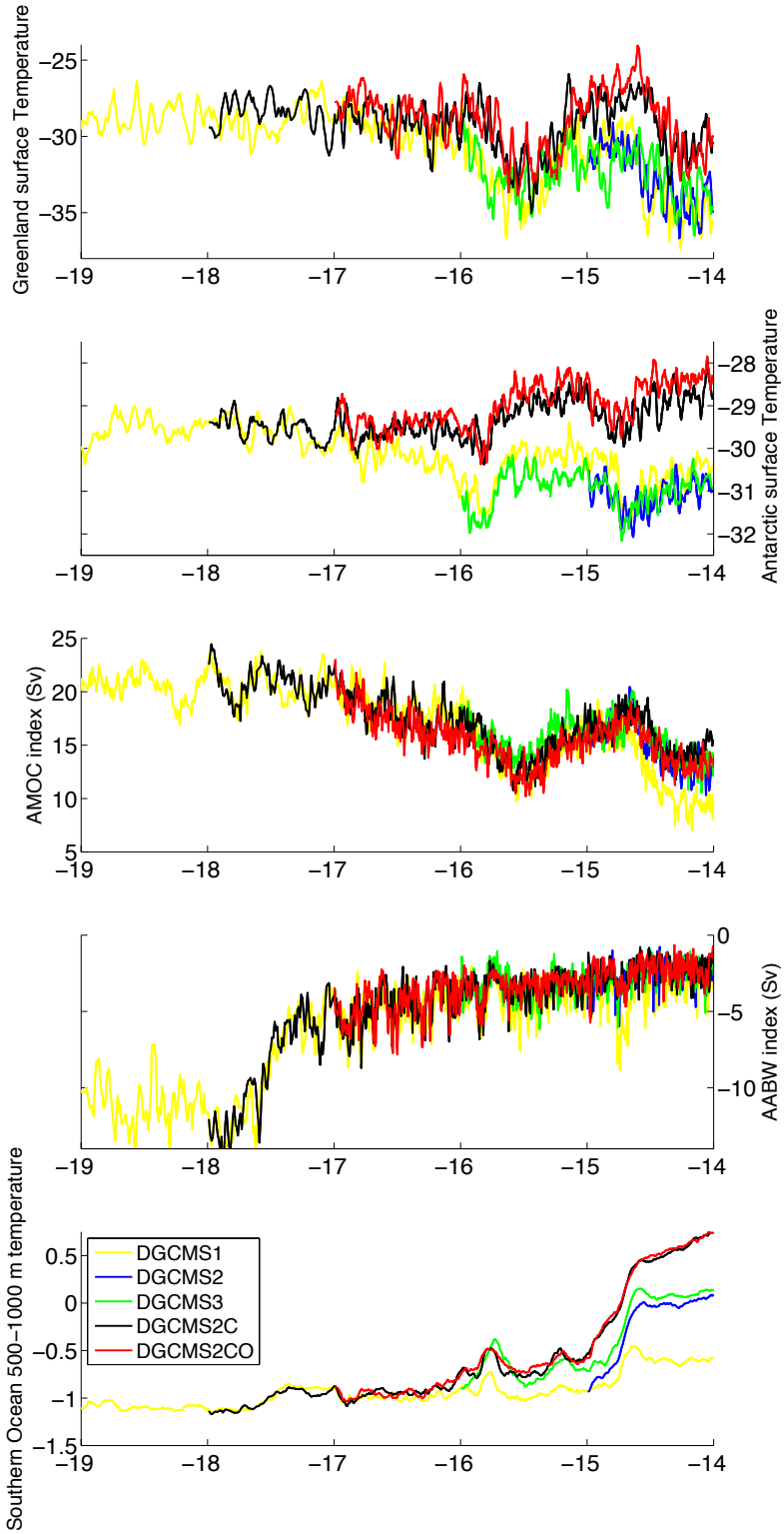

Fig. 5.12 Time-series of SAT over Greenland and Antarctica, AMOC index, AABW index and SubST (500-1000m) in the Southern Ocean for the period 18 – 14ka BP.

5.2 Freshwater perturbation under varying glacial ice sheet volumes

In Chapter 4, a hysteresis property of the glacial ocean with respect to NHIS changes was systematically demonstrated to explain the rapid glacial climate shifts [Zhang et al., *in revision*]. This is distinct to the one associated with hydrological cycle in the Atlantic basin [e.g. *Rahmstorf*, 1996]. Therefore the question is open as to whether the hysteresis with respect to NHIS changes is also related to the freshwater perturbation in the Atlantic basin. In addition, given evidence for the existence of IRD data during some DO-cycles, it remains important to investigate the role played by freshwater forcing on the millennial-scale climate variability during glacial times. Hence, here four sensitivity experiments are performed by imposing relatively small freshwater/saltwater perturbations (0.02Sv) over the northern North Atlantic (50-65°N, 5°W-30°W), testing whether the lower limit of estimated release of freshwater during HEs [*Roche et al.*, 2004; *Roberts et al.*, 2014] is sufficient to trigger significant changes in the glacial ocean circulation, under varying intermediate NHIS volumes (Table 4). Two of these experiments (N045_pfwp and N03_pfwp) involve freshwater perturbations performed on the strong AMOC state, while the other two (N04_nfwp and N025_nfwp) are salinification experiments conducted on the weak AMOC state. All experiments are performed on the climate states relating to NHIS heights at the boundaries, or just outside the boundaries, of the established bistable regime i.e. NHIS_0.45, NHIS_0.3w, NHIS_0.4w and NHIS_0.25, respectively.

	Initial ocean	**NHIS (Hsf)**	**Other forcing**	**Integrated years**
N045_pfwp	NHIS_0.45	0.45	+ 0.02 Sv freshwater	300
N04_nfwp	NHIS_0.4w	0.4	- 0.02 Sv freshwater	200
N03_pfwp	NHIS_0.3s	0.35	+0.02 Sv freshwater	200
N025_nfwp	NHIS_0.25	0.3	- 0.02 Sv freshwater	300

Table 4 Hosing experiments in varying intermediate NHIS configurations.

Figure 5.13 shows the time-series of AMOC indices of the four FWP experiments. It is evident that the slight change in hydrological cycle in the North Atlantic can cause significant responses of the glacial ocean circulation as the NHIS varies under

intermediate levels. This suggests a relatively more sensitive glacial climate compared with the maximum ice level under which only trivial reductions of AMOC are identified (not shown). Notably, only the glacial ocean existing within the bistable regime is characterized by two stable states, indicating that the ice volume is crucial for the glacial climate stability rather than the hydrological balance in Atlantic basin. These results further explain the inherent instability of glacial climate during the intermediate glacial levels [*Schulz et al.*, 1999] and its monostability under maximum glacial condition [*Prange et al.*, 2002].

It is noted that the recovery processes of the AMOC to the reference level are asymmetric between the cases when the NHIS volume is higher and lower than the boundaries of the established bistable regime (i.e. NHIS_0.45 pFWP and NHIS_0.25 nFWP) (Fig. 5.13). In NHIS_0.45 pFWP, the abrupt resumption to a vigorous circulation can be attributed to the nonlinear response of vertical mixing to the subsurface warming in the northern North Atlantic (see details in section 1.1 of this chapter [e.g. *Mignot et al.,* 2007]). The gradual decrease of AMOC in NHIS_0.25 nFWP, raises questions regarding the underlying mechanisms which are different from the abrupt resumption in NHIS_0.45 pFWP. We assume that the existence of ice sheets can be involved in this process via its dynamic effect on ocean circulation. Thus further studies are required to disentangle it in the future.

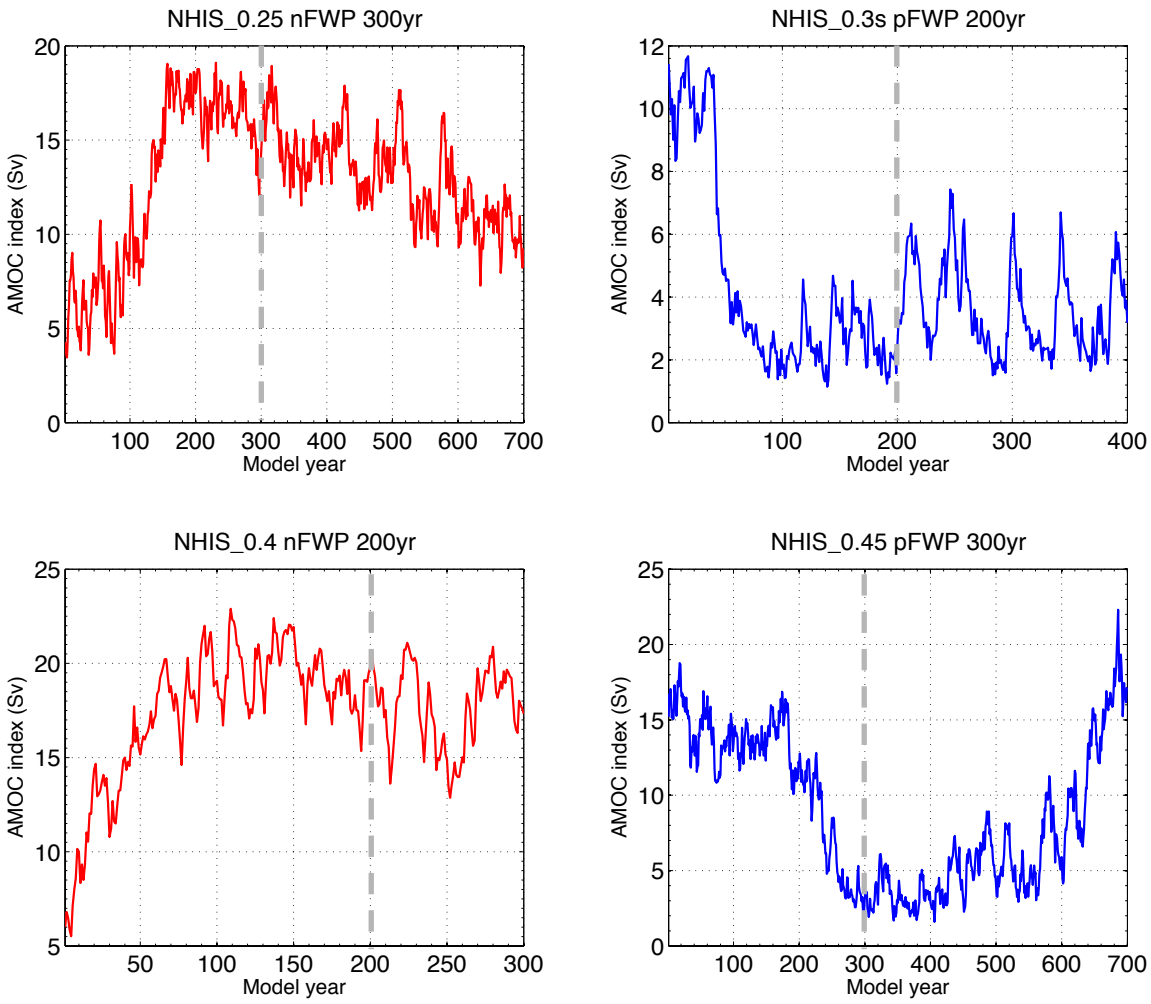

Fig. 5.13 AMOC indices from the hosing experiments prescribed in Table 4. The vertical dashed lines indicate the ending-time of the hosing experiment.

5.3 Conclusions of Chapter 5

Based on the hosing experiments provided in this Chapter, several key findings can be summarized as follows:

- In response to freshwater perturbation in the North Atlantic, different models under the LGM condition can simulate a consistent behaviour in some regions, such as the North Atlantic for temperature and precipitation which both decrease, the tropical Atlantic for southward shift of the ITCZ, the African and Indian monsoon regions (with a decrease in precipitation).

- Both quasi-equilibrium LGM ocean states in COSMOS are monostable with respect to hydrological balance in the Atlantic basin. The response of subsurface temperature in the Southern Ocean, especially the Weddell Sea, to northern FWP and recovery feature after the FWP, e.g. AMOC overshoot, are related to the stratification of the reference ocean states.
- Southern FWP can weaken the AMOC under glacial boundary conditions. Extent of subsurface warming in the Southern Ocean is dependent on the FWP locations along the Antarctic continent. The resulting subsurface warming can act as a positive feedback by causing grounding line retreat, calving, and subsequent release of more freshwater.
- Slight shifts in the hydrological balance in the Atlantic basin can cause significant response of the glacial ocean circulation under varying intermediate NHIS levels, but cannot change the stability of the glacial ocean circulation.

Chapter 6. Summary and Discussion

This Chapter briefly summarizes the conclusions of Chapters 3-5 and presents in-depth discussion on the broad implications for understanding the glacial ocean state and glacial abrupt climate shifts. At the end of each discussion paragraph there is a corresponding outlook on possible further research.

6.1 Reconstructing the LGM ocean state

The LGM represents the most recent interval when the global climate was substantially different to the present (e.g. low atmospheric CO_2 concentration, immense continental ice sheets etc.). With an abundance of available proxies, the LGM provides us with a test-bed for analyzing the response of climate models which are used for future projections under warming background climate states, due to large changes in associated radiative forcing. Therefore, reconstruction of the LGM surface temperature, a first-order diagnostic metric, became of great importance in evaluating the model performance in this regard. Coherent SST reconstructions have been uncovered in the tropical regions, but there is large disagreement over the northern North Atlantic and Nordic Sea [*de Vernal et al.*, 2006; *Waelbroeck et al.*, 2009]. In these regions, reconstructed SST ranges from -12 to 8 ℃, largely influencing the estimation of climate sensitivity as evaluated together with LGM model results [*Crucifix*, 2006; *Hargreaves et al.*, 2012]. One possible explanation is the failure of sediment cores with low sedimentation rate to record interannual and decal climate variability [*de Vernal et al*., 2006]. This is supported by model results in this thesis demonstrating that tempo-spatial changes in internal variability of sea-ice cover and surface temperature occurs between the northern North Atlantic and Nordic Sea during glacials. Further future research is required to uncover high-resolution proxy evidence appropriate for recording inter-annual to decadal signals in the paleocean.

It is well known that the reconstruction of the vertical structure of the LGM ocean is mainly based on the nutrient tracers, e.g. $\delta^{13}C$ [e.g. *Curry and Oppo*, 2005], Cd/Ca [*Marchitto and Broecker*, 2006] etc., indicating enhanced AABW dominant at the bottom of the Atlantic Ocean during the LGM. This is attributed to the enhanced AABW formation during the LGM when the cold climate promoted the sea-ice formation in the

Southern Ocean [e.g. *Shin et al.,* 2003; *Liu et al.,* 2005;]. However, to reconstruct comparable distribution of nutrient tracers in glacial Atlantic Ocean to proxy records, cooling anomaly or enhanced sea-ice export must be imposed to the glacial Southern Ocean [e.g. *Hesse et al.,* 2011; *Abe-Ouchi,* 2013]. This indicates that 1) the deep-ocean water mass distribution as inferred from reconstructions is sensitive to the sea-ice dynamics in the Southern Ocean and 2) pure LGM boundary forcing on ocean models cannot reproduce the glacial distribution of nutrient tracers. In fact, the distribution of nutrient tracers cannot rule out the possibility that the glacial ocean structure has been formed prior to the LGM. At the beginning of MIS 2 (~27 ka BP), a sharp decrease of atmospheric CO_2 concentration and benthic $\delta^{13}C$ occurred [e.g. *Hodell et al.*, 2003; *Ahn and Brook*, 2008], indicating abrupt formation of an abyssal carbon reservoir. Furthermore, *Schmitt et al.*, [2012] suggested that the carbon cycle in the climate system during the LGM was already in equilibrium and the net transfer of carbon to the deep ocean had occurred prior to the LGM. In our 27ka BP simulation, the reduced annual mean solar radiation to high latitudes, associated with the lowest obliquity in the last 30ka BP, promotes a relatively more extensive sea-ice formation, strengthening the brine rejection in the Southern ocean and thus enhancing the formation of dense AABW. Indeed, using a sea-ice reconstruction based on diatoms, *Allen et al.*, [2011] suggested that more extensive sea ice extent was found prior to the LGM. Furthermore, a northward invasion of enhanced AABW is identified in the western North Atlantic (Bermuda Rise), beginning at ~ 27ka BP [*Gutjahr and Lippold*, 2011]. In combination, it is most likely that the reconstructed water mass configuration during the LGM stems from the inception of MIS2 (~27ka BP). To further corroborate this hypothesis, fully coupled model complemented with isotope schemes is highly desirable in the future. Recently, a new version of COSMOS available with isotope components is well developed, capable to be as an effective means providing the direct modeling evidence on this issue.

In term of LGM modeling, simulated surface properties in different models are generally characterized by consistent patterns that are similar to the LGM reconstruction [*Braconnot et al.*, 2007]. However, there was a substantial difference in glacial ocean circulations among different models [*Otto-Bliesner et al.,* 2007]. In spite of model uncertainties among PMIP2 models, the two LGM simulations initialized from a previous

glacial ocean states were identified to yield AMOC states comparable to reconstructions [*Braconnot et al.,* 2007; *Otto-Bliesner et al*., 2007; *Weber et al.,* 2007]. In this thesis, it is shown that the initial ocean states significantly affect the transient characteristics and equilibrium time-scale of the LGM simulation. According to the long-term LGM simulations initialized from present-day ocean (LGMS in Chapter 3), it is proposed that the PMIP criteria cannot identify the transient characteristics in the deep ocean properties when only considering the surface trend. Climatological characteristics of surface properties in a transient phase (LGMS-t_{deep}) are quasi-stationary and similar to the equilibrated state (LGMS-e) and thus can be defined as "quasi-equilibrium" state by PMIP criteria. Nevertheless, a significant tendency is identified in its deep ocean properties that are similar to the present-day ocean configuration. These results provide a possible explanation for the large spread of simulated LGM ocean states among the PMIP2 models [*Otto-Bliesner et al*., 2007]. Accordingly, we suggest that a detailed prescription of deep ocean property and initialization procedure should be proposed to warrant a sensible and reliable inter-model comparison in the future.

As the starting point of deglacial simulation, choice of the correct LGM states is crucial for studies on the transient characteristics of the simulated LDG and underlying mechanism. In this thesis, two distinctions can be identified when the equilibrated glacial ocean (e.g. LGMS-e), in contrast to LGMS-t_{deep}, serves as the reference state for northern FWP experiments. The first difference is an evident subsurface warming associated with weakened AMOC phase in the regions where vertical mixing occurs in the high latitudes of both hemispheres. Another characteristic is the existence of AMOC overshoot in response to the cessation of freshwater hosing in the North Atlantic. These findings provides an potential interpretation to explain discrepancies amongst models on transient responses of glacial ocean to northern FWP [e.g. *Roche et al.,* 2010; *Cheng et al.*, 2011] and on mechanisms responsible for the rapid climate changes during the last termination [*Liu et al.*, 2009; *Menviel et al.*, 2011; *Bethke et al.*, 2012], perhaps as well as the global temperature evolution through the Holocene [*Liu et al.,* submitted].

6.2 Ice sheet-climate interaction during glacials

In previous studies, it is supposed that the main contribution of continental ice sheets to

global climate is its thermal effect on global cooling due to its high surface albedo reflecting majority of solar radiation back to the space [*Manabe and Broccoli*, 1985], rather its dynamic effect on modifying ocean circulation by changing wind fields. By using a comprehensive fully-coupled model, it is shown that in general the higher NHIS causes the relatively stronger AMOC. This is due to the fact that changes in the height of ice sheet over North America divides the westerly winds into a northern and southern branch that flow in different directions, leading to changes in gyre circulation and sea-ice coverage and then affecting the AMOC. With improved representation of model physics in CCSM4, the dynamic effect of the NHIS on promoting glacial ocean circulation surpasses its thermal effect, in contrast to its older version CCSM3 [*Brady et al.*, 2013]. In addition, via a series of sensitivity experiments, Abe-Ouchi [2013] propose that the simulated glacial AMOC depends critically on the subtle balance between the strengthening of the AABW formation caused by the enhanced sea-ice formation in the Southern Ocean associated with CO_2-induced global cooling and the strengthening of the NADW formation as a consequence of the growing northern hemisphere ice sheets. Thus, better representing the NHIS in the future will be one effective approach for paleoclimate modelers to simulate realistic ocean circulation changes during the LGM in addition to sensitivity of Southern Ocean to global cooling.

During glacials of the Late Pleistocene, many paleoclimate archives document the existence of large and repeated, millennial-scale climate changes (i.e. DO events and HEs) [e.g. *Dansgaard et al.*, 1993; *Hemming*, 2004; *Huber et al.*, 2006]. A variety of mechanisms have been proposed to explain the emergence of such abrupt climate shifts, of which most invoke the existence of nonlinearities in the underlying dynamics of one or more Earth-system components (e.g. AMOC, ice-sheet, sea ice) [e.g. *Ganopolski and Rahmstorf*, 2001; *Schmittner et al.*, 2002; *Li et al.*, 2010]. One common explanation for these events involves changes is the AMOC, usually triggered by freshwater forcing associated with HEs. However, given the uncertainty on the origin, timing and magnitude of freshwater perturbation, it is hard to address whether the freshwater forcing acts as a trigger or responds as a consequence during the abrupt climate shifts (see details in Chapter 1.2). Li et al. [2010], by prescribing different sea-ice extents as surface boundary in an atmosphere-alone model, propose an important role of variations of sea-ice cover in

the Nordic sea on the recorded warming over the Greenland during DO events. In addition, Dokken et al., (2013), by analyzing one marine sediment core in the Nordic Sea, suggest that ocean-sea ice interactions internal to the Nordic seas can trigger the DO cycle, which is subsequently supported by a heuristic columnar model demonstrating the corresponding mechanism without the control of variation in AMOC [*Singh et al.*, 2013]. Nevertheless, lack of atmosphere-ocean interaction in their models is still not able to clarify the cause of these rapid climate shifts, e.g. sea-ice variations. In fact, one fundamental characteristic of DO variability, that is almost all events occurred during glacial periods when global ice volume was varying at intermediate levels [*Dansgaard et al.*, 1993; *McManus et al.*, 1999; *Schulz et al.*, 1999; *Barker et al.*, 2011], suggests a potential relationship between the intermediate ice sheets and the existence of millennial scale climate variability [*Wunsch*, 2006], possibly offering a profound clue to their origin.

In my thesis, it is shown that the existence of non-linear responses of the glacial ocean to NHIS volume changes in the coupled atmosphere-ocean system can explain the occurrence of rapid glacial climate shifts. The global climate responses, including abrupt warming in the North Atlantic and a shift of the tropical rain belts, etc., are generally consistent with empirical evidence [*Voelker*, 2002]. A hysteresis analysis with respect to changes of the NHIS suggests that two distinct glacial climate modes coexist at identical intermediate ice sheet volumes. In particular, minor shifts in the NHIS and atmospheric carbon dioxide can trigger the rapid climate transitions, which occur due to a local positive atmosphere-ocean-sea ice feedback in the North Atlantic at intermediate ice-sheet volume. During rapid glacial climate changes, a key tempo-spatial shift in internal climate variability is identified, providing a new dynamic framework to explain the recorded sea surface warming and its increased fluctuation during ice-rafting/at the end of stadials in the northern North Atlantic [*Peck et al.*, 2008; *Jonkers et al.*, 2010]. In combination, these results provide the first coherent mechanism accounting for the recorded millennial-scale variability and abrupt climate changes in the coupled atmosphere-ocean system, as well as their linkages to intermediate ice-sheet volume during glacials, e.g. MIS3.

It is noteworthy that the ice sheets in our study are prescribed according to the ice-sheet configuration of the Last Glacial Maximum and thus decoupled from the changes in

atmosphere-ocean system. Further studies with fully coupled climate-ice sheet/shelf models shall explore the ice sheet variability which may be related to internal feedbacks within atmosphere-ocean-cryosphere systems [*Macayeal*, 1993; *Petersen et al*., 2013] and to weak external forcing [*Dima and Lohmann,* 2008].

6.3 Hypothesis for Bølling-Allerød warming and Meltwater Pulse 1a

During the last glacial termination, global climate was punctuated with several rapid climate shifts, e.g. collapse of the AMOC during the HE1, abrupt warming over the Greenland during the BA, etc. Transient modeling studies [e.g. *Liu et al.,* 2009; *Menviel et al.*, 2011] propose that these abrupt changes are associated with the nonlinearity of the AMOC variation caused by the meltwater injection as a consequence of the retreat of northern hemisphere ice sheets during the deglaciation. However, in order to mimic these rapid events, the models were prescribed using different freshwater discharge schemes [*Liu et al.,* 2009; *Menviel et al.*, 2011], largely deviating from the sea-level records [*Peltier and Fairbanks*, 2006]. Furthermore, Bethke et al. [2012] employed the freshwater scheme based on the reconstructed ice-sheet retreat [*Peltier*, 2004] to represent melt-water history in their LDG simulations, but failed to reproduce the abrupt warming during the BA when the meltwater pulse 1a occurred. In addition to the uncertainty on the origin, as well as timing and magnitude of freshwater drainage [e.g. *Carlson and Clark*, 2012], other operating factors associated with the non-linearity of AMOC changes is required to involve in the mechanism accounting for the rapid warming. In this respect, Knorr and Lohmann [2007] proposed that changes in the stability behavior of the AMOC can occur in response to gradual changes in the background climate conditions. This is corroborated by Oka et al. [2012] demonstrating that interaction between surface heat flux and wind stress plays a critical role in controlling the timing when the abrupt change of AMOC occurs during the deglaciation. As of yet no models utilizing fully coupled atmosphere-ocean system corroborate this assertion. However, in this study, it is shown that the bistable window of glacial AMOC can exist by only varying the northern hemisphere ice sheet volume. Providing the uncertainties associated with model performance [*Randall et al.*, 2007] and the reconstructed ice-sheet topography [*Ullman et al.*, 2013], it is plausible that the bistable

window is different in the real world. Accordingly, assuming that the real LGM climate is within or close to the upper end of the bistable window, a conceptual mechanism can be proposed to merit our understanding on the series of climate events which occurred during the deglaciation, in a more consistent way with the proxy reconstructions.

Sea-level records indicate that the LGM sea-level lowstand is abruptly terminated by a rapid sea level rise of 10~15 m at ~19ka BP [e.g. *Clark et al.*, 2004], contemporaneous with a decrease in AMOC [*McManus et al.*, 2004]. This rapid reduction of AMOC can be attributed to meltwater injection to the Nordic Sea [*Jones and Keigwin*, 1988] and/or loss of northern hemisphere ice-sheet volume [Zhang et al., *in revision*]. In parallel, as a consequence of the bipolar thermal seesaw [*Stocker and Johnsen*, 2003], the Southern Hemisphere warms up [*Shakun et al.*, 2012]. In the Northern Hemisphere, the suppressed vertical convection leads to a subsurface warming in the North Atlantic, destabilizing the Hudson Strait Ice Stream grounding line and triggering HE1 at ~17.5ka BP [*Marcott et al.*, 2011]. This IRD event causes the glacial ocean transition from the weak mode to the collapsed mode at ~17.5-17ka BP [*McManus et al.*, 2004], enhancing the warming in the Southern Hemisphere [*Shakun et al.*, 2012]. This effectively reduces the sea-ice cover over the Southern Ocean [*Fischer et al.*, 2007] and promotes the release of carbon dioxide stored in the abyssal ocean via enhanced upwelling [*Anderson et al.*, 2009; *Schmitt et al.*, 2012]. Meanwhile, subsurface warming, as a consequence of the combined effects of increased CO_2, obliquity and sea-ice melting (retreat) [personal communication with Axel Timmerman], destabilizes the grounding line of the Antarctic ice shelves, causing the first large IRD events during the last termination (Antarctic Ice-sheet Discharge 7, AID 7 in [*Weber et al.*, accepted]). The subsequent release of icebergs from the Antarctic ice shelves further dilutes the sea surface salt content, maintaining the local subsurface warming and promoting the collapse of the Antarctic ice shelves [*Weber et al.*, *accepted*]. Directly after HE1 (~ 16ka BP), the glacial ocean circulation is characterized by a weak AMOC mode. Simultaneous with the continuous increase in atmospheric carbon dioxide, the weak AMOC mode approaches or possibly crosses the upper boundary of the bistable window (with respect to the ice sheet volume, as established in Chapter 4). That is, until ~14.8ka BP, when a ~45 ppm increase of atmospheric CO_2 [*Monnin et al.*, 2001] should be enough to trigger the abrupt warming by changing the

ocean stability. However, the onset of the largest Southern Hemisphere LDG IRD event associated with the Antarctic Ice Shelves occurs simultaneously (AID 6 in [*Weber et al.*, *accepted*]) and prohibits the AMOC resumption. Once this southern freshwater injection is significantly reduced at ~14.6ka BP, the AMOC is permitted to recover and causes the recorded BA warming in Greenland. In parallel, global continental shelf flooding associated with abrupt sea-level rise [*Deschamps et al.,* 2012; *Weber et al., accepted*] causes an extra CO_2 increase of 20-35 ppm within ~200 years [*Köhler et al.*, 2011], further promoting the global warming. As a consequence of the BA warming, the NHIS begin to retreat, draining meltwater to the North Atlantic, and gradually weakening the ocean circulation from ~14.5ka BP. The meltwater injection from the NHIS during the BA likely results in a short cooling interval, the Older Dryas at ~14.0ka BP [*Bard et al.*, 1996; *Stanford et al.*, 2006] after which the AMOC resumes its strong mode (interglacial level) owing to the existence of vigorous vertical mixing in the Nordic sea [e.g. *Lohmann and Schulz*, 2000; *Zhang et al*., 2013]. In response to the AMOC resumption, the Southern Hemisphere gradually cools, accompanied by a decrease of CO_2, a period known as the Antarctic Cold Reversal (ACR).

This hypothesis involves an inter-hemispheric melt-water contribution to meltwater-1a, characterized by a preceding meltwater injection from the AIS and a following contribution from the NHIS. This non-synchronicity of the melt-water contributions from AIS and NHIS is consistent with the published dating of sea-level rise in records from Tahiti [*Deschamps et al*., 2012] and Barbados [*Bard et al.*, 1990; *Fairbanks*, 1989]. In particular, the amplitude of sea-level rise is larger in the records from Barbados than Tahiti, indicating the possibility of a combined inter-hemispheric signal in the former. This might be associated with the different response time-scales of Barbados to the southern (far-field) and northern (near-field) meltwater injection events. Further study with regard to this issue is highly desirable to confirm these hypotheses.

Last, but not the least, it is noteworthy that age uncertainty in records is crucial to sequence events occurring in different places, especially during rapid climate changes due to the short time window (e.g. the BA warming, around 14.6~14.3ka BP). Further research regarding improvement of age model will benefit our understanding on this issue.

Reference:

Abe-Ouchi (2013), Southern Ocean as a key for understanding modelling uncertainties in simulating the Glacial AMOC, *talk* in PMIP ocean workship 2013, Corvallis US.

Adkins, J. F., K. McIntyre, and D. P. Schrag (2002), The salinity, temperature, and delta^{18}O of the glacial deep ocean, *Science*, *298*, 1769–1773, doi:10.1126/science.1076252.

Ahn, J., and E. J. Brook (2007), Atmospheric CO_2 and climate from 65 to 30 ka B.P., *Geophys. Res. Lett.*, *34*, L10703, doi:10.1029/2007GL029551.

Ahn, J., and E. J. Brook (2008), Atmospheric CO2 and climate on millennial time scales during the last glacial period, *Science*, *83*, 83–85, doi:10.1126/science.1160832.

Allen, C. S., J. Pike, and C. J. Pudsey (2011), Last glacial–interglacial sea-ice cover in the SW Atlantic and its potential role in global deglaciation, *Quat. Sci. Rev.*, *30*, 2446–2458, doi:10.1016/j.quascirev.2011.04.002.

Anderson, R. F., S. Ali, L. I. Bradtmiller, S. H. H. Nielsen, M. Q. Fleisher, B. E. Anderson, and L. H. Burckle (2009), Wind-driven upwelling in the Southern Ocean and the deglacial rise in atmospheric CO_2, *Science*, *323*, 1443–1448, doi:10.1126/science.1167441.

Banderas, R., J. Alvarez-Solas, and M. Montoya (2012), Role of CO_2 and Southern Ocean winds in glacial abrupt climate change, *Clim. Past*, *8*, 1011–1021, doi:10.5194/cp-8-1011-2012.

Bard, E., B. Hamelin, M. Arnold, L. Montaggioni, G. Cabiochll, G. Faure'll, and F. Rougerie (1996), Deglacial sea-level record from Tahiti corals and the timing of global meltwater discharge, *Nature*, *382*, 241–244.

Bard, E., B. Hamelin, and R. Fairbanks (1990), U-Th ages obtained by mass spectrometry in corals from Barbados: sea level during the past 130, 000 years, *Nature*, *346*, 456–458.

Bard, E., F. Rostek, J.-L. Turon, and S. Gendreau (2000), Hydrological Impact of Heinrich Events in the Subtropical Northeast Atlantic, *Science*, *289*, 1321–1324, doi:10.1126/science.289.5483.1321.

Barker, S., G. Knorr, R. L. Edwards, F. Parrenin, A. E. Putnam, L. C. Skinner, E. Wolff, and M. Ziegler (2011), 800,000 Years of Abrupt Climate Variability., *Science*, *334*, 347–51, doi:10.1126/science.1203580.

Beckmann, A., and R. Döscher (1997), A Method for Improved Representation of Dense Water Spreading over Topography in Geopotential-Coordinate Models, *J. Phys. Oceanogr.*, 27, 581–591.

Bethke, I., C. Li, and K. H. Nisancioglu (2012), Can we use ice sheet reconstructions to constrain meltwater for deglacial simulations?, *Paleoceanography*, *27*, PA2205, doi:10.1029/2011PA002258.

Blunier, T., and E. J. Brook (2001), Timing of millennial-scale climate change in Antarctica and Greenland during the last glacial period., *Science*, *291*, 109–12, doi:10.1126/science.291.5501.109.

Bouttes, N., D. Paillard, D. M. Roche, C. Waelbroeck, M. Kageyama, A. Lourantou, E. Michel, and L. Bopp (2012), Impact of oceanic processes on the carbon cycle during the last termination, *Clim. Past*, *8*, 149–170, doi:10.5194/cp-8-149-2012.

Braconnot, P. et al. (2007), Results of PMIP2 coupled simulations of the Mid-Holocene

and Last Glacial Maximum – Part 1: experiments and large-scale features, *Clim. Past*, *3*, 261–277, doi:10.5194/cp-3-261-2007.

Braconnot, P., S. P. Harrison, M. Kageyama, P. J. Bartlein, V. Masson-Delmotte, A. Abe-Ouchi, B. Otto-Bliesner, and Y. Zhao (2012), Evaluation of climate models using palaeoclimatic data, *Nat. Clim. Chang.*, *2*, 417–424, doi:10.1038/nclimate1456.

Brady, E. C., B. L. Otto-Bliesner, J. E. Kay, and N. Rosenbloom (2013), Sensitivity to Glacial Forcing in the CCSM4, *J. Clim.*, *26*, 1901–1925, doi:10.1175/JCLI-D-11-00416.1.

Broecker, W. (1998), Paleocean circulation during the last deglaciation: A bipolar seesaw?, *Paleoceanography*, *13*, 119–121, doi:10.1029/97PA03707.

Broecker, W., D. Peteet, and D. Rind (1985), Does the ocean-atmosphere system have more than one stable mode of operation?, *Nature*, *315*, 21–26.

Brovkin, V., T. Raddatz, C. H. Reick, M. Claussen, and V. Gayler (2009), Global biogeophysical interactions between forest and climate, *Geophys. Res. Lett.*, *36*, 1–5, doi:10.1029/2009GL037543.

Butzin, M., M. Prange, and G. Lohmann (2005), Radiocarbon simulations for the glacial ocean: The effects of wind stress, Southern Ocean sea ice and Heinrich events, *Earth Planet. Sci. Lett.*, *235*, 45–61, doi:10.1016/j.epsl.2005.03.003.

Carlson, A., and P. Clark (2012), Ice Sheet Sources of Sea Level Rise and Freshwater Discharge Druing the Last Deglaciation, *Rev. Geophys.*, 50, RG4007, 1–72, doi:10.1029/2011RG000371.

Cheng, J., Z. Liu, F. He, B. L. Otto-Bliesner, E. C. Brady, and M. Wehrenberg, (2011) Simulated Two-Stage Recovery of Atlantic Meridional Overturning Circulation During the Last Deglaciation, in: Abrupt Climate Change: Mechanisms, Patterns, and Impacts, American Geophysical Union, 75–92.

Clark, P. U., A. S. Dyke, J. D. Shakun, A. E. Carlson, J. Clark, B. Wohlfarth, J. X. Mitrovica, S. W. Hostetler, and a M. McCabe (2009), The Last Glacial Maximum., *Science*, *325*, 710–4, doi:10.1126/science.1172873.

Clark, P. U., S. J. Marshall, G. K. Clarke, S. W. Hostetler, J. M. Licciardi, and J. T. Teller (2001), Freshwater forcing of abrupt climate change during the last glaciation., *Science*, *293*, 283–7, doi:10.1126/science.1062517.

Clark, P., J. Mitrovica, G. Milne, and M. Tamisiea (2002a), Sea-level fingerprinting as a direct test for the source of global meltwater pulse IA, *Science*, 295, 10–14, doi:10.1126/science.1068797.

Clark, P. U., A. M. McCabe, A. C. Mix, and A. J. Weaver (2004), Rapid rise of sea level 19,000 years ago and its global implications., *Science*, *304*, 1141–4, doi:10.1126/science.1094449.

Clark, P. U., N. G. Pisias, T. F. Stocker, and A. J. Weaver (2002b), The role of the thermohaline circulation in abrupt climate change, *Nature*, *415*, 863–869.

Clement, A., and L. Peterson (2008), Mechanisms of abrupt climate change of the last glacial period, *Rev. Geophys.*, 46, RG4002 1–39, doi:10.1029/2006RG000204.

CLIMAP Members (1981), Seasonal reconstruction of the earth's surface at the last glacial maximum, *Geol. Soc. Am. Map Chart Ser.*, *MC-36*(MC 36), 17.

Crowley, T. (1992), North Atlantic deep water cools the southern Hemisphere, *Paleoceanography*, *7*, 489–497.

Crucifix, M. (2006), Does the Last Glacial Maximum constrain climate sensitivity?,

Geophys. Res. Lett., *33*, 1–5, doi:10.1029/2006GL027137.

Curry, W. B., and D. W. Oppo (2005), Glacial water mass geometry and the distribution of $\delta^{13}C$ of ΣCO_2 in the western Atlantic Ocean, *Paleoceanography*, *20*, 1–13, doi:10.1029/2004PA001021.

Dansgaard, W. et al. (1993), Evidence for general instability of past climate from a 250-kyr ice-core record, *Nature*, *364*, 218–220.

Deschamps, P., N. Durand, E. Bard, B. Hamelin, G. Camoin, A. L. Thomas, G. M. Henderson, J. Okuno, and Y. Yokoyama (2012), Ice-sheet collapse and sea-level rise at the Bølling warming 14,600 years ago., *Nature*, *483*, 559–64, doi:10.1038/nature10902.

Dima, M., and G. Lohmann (2008), Conceptual model for millennial climate variability: a possible combined solar-thermohaline circulation origin for the ~1,500-year cycle, *Clim. Dyn.*, *32*, 301–311, doi:10.1007/s00382-008-0471-x.

Dokken, T. M., K. H. Nisancioglu, C. Li, D. S. Battisti, and C. Kissel (2013), Dansgaard-Oeschger cycles : Interactions between ocean and sea ice intrinsic to the Nordic seas, *Paleoceanography*, *28*, 491–502, doi:10.1002/palo.20042.

Dowsett, H. J. et al. (2013), Sea surface temperature of the mid-Piacenzian ocean: a data-model comparison., *Sci. Rep.*, *3*, 2013, doi:10.1038/srep02013.

Duplessy, J. C., N. J. Shackleton, R. G. Fairbanks, L. Labeyriefi, D. Oppo, and N. Kallel (1988), Deepwater Source Variations during the Last Climatic Cycle and Their impact on the Global Deepwater Circulation, *Paleoceanography*, *3*, 343–360.

Elliot, M., L. Labeyrie, and J. Duplessy (2002), Changes in North Atlantic deep-water formation associated with the Dansgaard – Oeschger temperature oscillations (60 – 10 ka), *Quat. Sci. Rev.*, *21*, 1153–1165.

Fairbanks, R. (1989), A 17, 000-year glacio-eustatic sea level record: influence of glacial melting rates on the Younger Dryas event and deep-ocean circulation, *Nature*, *342*, 637–642.

Fischer, H. et al. (2007), Reconstruction of millennial changes in dust emission, transport and regional sea ice coverage using the deep EPICA ice cores from the Atlantic and Indian Ocean sector of Antarctica, *Earth Planet. Sci. Lett.*, *260*, 340–354, doi:10.1016/j.epsl.2007.06.014.

Ganachaud, a, and C. Wunsch (2000), Improved estimates of global ocean circulation, heat transport and mixing from hydrographic data., *Nature*, *408*, 453–7, doi:10.1038/35044048.

Ganopolski, A., and S. Rahmstorf (2001), Rapid changes of glacial climate simulated in a coupled climate model, *Nature*, *409*, 153–158, doi:10.1038/35051500.

Gent, P., J. Willebrand, T. J. McDougall, and J. C. McWilliams (1995), Parameterizing eddy-induced tracer transports in ocean circulation models, *J. Phys. Oceanogr. 25*, 463–474.

Gersonde, R., X. Crosta, A. Abelmann, and L. Armand (2005), Sea-surface temperature and sea ice distribution of the Southern Ocean at the EPILOG Last Glacial Maximum—a circum-Antarctic view based on siliceous microfossil records, *Quat. Sci. Rev.*, *24*, 869–896, doi:10.1016/j.quascirev.2004.07.015.

Gherardi, J. -M., L. Labeyrie, S. Nave, R. Francois, J. F. McManus, and E. Cortijo (2009), Glacial-interglacial circulation changes inferred from $^{231}Pa/^{230}Th$ sedimentary record in the North Atlantic region, *Paleoceanography*, *24*, 1–14,

doi:10.1029/2008PA001696.

Gong, X., G. Knorr, G. Lohmann, and X. Zhang (2013), Dependence of abrupt Atlantic meridional ocean circulation changes on climate background states, *Geophys. Res. Lett.*, *40*, 3698–3704, doi:10.1002/grl.50701.

Gordon, C., C. Cooper, C. Senior, and H. Banks (2000), The simulation of SST , sea ice extents and ocean heat transports in a version of the Hadley Centre coupled model without flux adjustments, *Clim. Dyn.*, *16*, 147–168.

Gregory, J. M. et al. (2005), A model intercomparison of changes in the Atlantic thermohaline circulation in response to increasing atmospheric CO_2 concentration, *Geophys. Res. Lett.*, *32*, L12703, doi:10.1029/2005GL023209.

Grootes, P. M., M. Stulver, J. W. C. White, S. Johnsen, and J. Jouzel (1993), Comparison of Oxygen isotope records from the GISP2 and GRIP Greenland ice cores, *Nature*, *366*, 552–554.

Gutjahr, M., and J. Lippold (2011), Early arrival of Southern Source Water in the deep North Atlantic prior to Heinrich event 2, *Paleoceanography*, *26*, 1–9, doi:10.1029/2011PA002114.

Hagemann, S., and L. Dümenil (1998), A parametrization of the lateral waterflow for the global scale, *Clim. Dyn.,*14,17-31

Hagemann, S., and L. D. Gates (2003), Improving a subgrid runoff parameterization scheme for climate models by the use of high resolution data derived from satellite observations, *Clim. Dyn.*, *21*, 349–359, doi:10.1007/s00382-003-0349-x.

Hargreaves, J. C., J. D. Annan, M. Yoshimori, and a. Abe-Ouchi (2012), Can the Last Glacial Maximum constrain climate sensitivity?, *Geophys. Res. Lett.*, *39*, L24702, doi:10.1029/2012GL053872.

Hall, I. R., S. B. Moran, R. Zahn, P. C. Knutz, C. C. Shen, and R. L. Edwards (2006), Accelerated drawdown of meridional overturning in the late-glacial Atlantic triggered by transient pre-H event freshwater perturbation. *Geophysical Research Letters*, 33, L16616.

Hemming, S. (2004), Heinrich Events: Massive Late Pleistocene Detritus Layers of the North Atlantic and their global Climate Imprint, *Rev. Geophys.*, *42*, RG1005, doi:10.1029/2003RG000128.

Hesse, T., M. Butzin, T. Bickert, and G. Lohmann (2011), A model-data comparison of $\delta^{13}C$ in the glacial Atlantic Ocean, *Paleoceanography*, *26*, PA3220, doi:10.1029/2010PA002085.

Hibler III, W. (1979), A dynamic thermodynamic sea ice model, *J. Phys. Oceanogr.*, *9*, 815–846.

Hodell, D. A., K. A. Venz, C. D. Charles, and U. S. Ninneman (2003), Pleistocene vertical carbon isotope and carbonate gradients in the South Atlantic sector of the Southern Ocean, *Geochem. Geophys. Geosystems*, *4*, 1004, doi:10.1029/2002GC000367.

Huber, C., M. Leuenberger, R. Spahni, J. Flückiger, J. Schwander, T. F. Stocker, S. Johnsen, A. Landais, and J. Jouzel (2006), Isotope calibrated Greenland temperature record over Marine Isotope Stage 3 and its relation to CH_4, *Earth Planet. Sci. Lett.*, *243*, 504–519, doi:10.1016/j.epsl.2006.01.002.

Huybers, P., and C. Wunsch (2010), Paleophysical Oceanography with an Emphasis on Transport Rates, *Ann. Rev. Mar. Sci.*, *2*, 1–34, doi:10.1146/annurev-marine-120308-

081056.
Indermühle, A., and E. Monnin (2000), Atmospheric CO2 concentration from 60 to 20 kyr BP from the Taylor Dome ice core, Antarctica, *Geophys. Res. Lett.*, *27*, 735–738.
Jonkers, L., M. Moros, M. a. Prins, T. Dokken, C. A. Dahl, N. Dijkstra, K. Perner, and G.-J. a. Brummer (2010), A reconstruction of sea surface warming in the northern North Atlantic during MIS 3 ice-rafting events, *Quat. Sci. Rev.*, *29*, 1791–1800, doi:10.1016/j.quascirev.2010.03.014.
Jones, G. A. and L. D. Keigwin (1988), Evidence from Fram Strait (78° N) for early deglaciation, *Nature,* 336, 56-59.
Jungclaus, J., N. Keenlyside, and M. Botzet (2006), Ocean circulation and tropical variability in the coupled model ECHAM5/MPI-OM, *J. Clim.*, *19*, 3952–3972.
Jungclaus, J. H., S. J. Lorenz, C. Timmreck, C. H. Reick, V. Brovkin, K. Six, J. Segschneider, and M. A. Giorgetta (2010), Climate and carbon-cycle variability over the last millennium, *Clim. Past*, *6*, 723–737, doi:10.5194/cp-6-723-2010.
K-1-Model-Developers (2004), K-1 Coupled (MIROC Description)1, 34 pp.
Kageyama, M., U. Merkel, B. Otto-Bliesner, M. Prange, a. Abe-Ouchi, G. Lohmann, R. Ohgaito, D. M. Roche, J. Singarayer, and D. Swingedouw (2013), Climatic impacts of fresh water hosing under Last Glacial Maximum conditions: a multi-model study, *Clim. Past*, *9*, 935–953, doi:10.5194/cp-9-935-2013.
Kageyama, M., J. Mignot, and D. Swingedouw (2009), Glacial climate sensitivity to different states of the Atlantic Meridional Overturning Circulation : results from the IPSL model, *Clim. Past*, 5, 551–570.
Kageyama, M., A. Paul, D. M. Roche, and C. J. Van Meerbeeck (2010), Modelling glacial climatic millennial-scale variability related to changes in the Atlantic meridional overturning circulation: a review, *Quat. Sci. Rev.*, *29*, 2931–2956, doi:10.1016/j.quascirev.2010.05.029.
Kim, J.-H., O. E. Romero, G. Lohmann, B. Donner, T. Laepple, E. Haam, and J. S. Sinninghe Damsté (2012), Pronounced subsurface cooling of North Atlantic waters off Northwest Africa during Dansgaard–Oeschger interstadials, *Earth Planet. Sci. Lett.*, *339-340*, 95–102, doi:10.1016/j.epsl.2012.05.018.
Kissel, C., C. Laj, L. Labeyrie, and T. Dokken (1999), Rapid climatic variations during marine isotopic stage 3: magnetic analysis of sediments from Nordic Seas and North Atlantic, *Earth Planet. Sci. Lett., 171*, 489–502.
Knorr, G., M. Butzin, a. Micheels, and G. Lohmann (2011), A warm Miocene climate at low atmospheric CO_2 levels, *Geophys. Res. Lett.*, *38*, 1–5, doi:10.1029/2011GL048873.
Knorr, G., and G. Lohmann (2003), Southern Ocean origin for the resumption of Atlantic thermohaline circulation during deglaciation, *Nature*, *424*, 532–536, doi:10.1038/nature01856.1.
Knorr, G., and G. Lohmann (2007), Rapid transitions in the Atlantic thermohaline circulation triggered by global warming and meltwater during the last deglaciation, *Geochemistry Geophys. Geosystems*, *8*, Q12006, doi:10.1029/2007GC001604.
Knutti, R., J. Flückiger, T. F. Stocker, and a Timmermann (2004), Strong hemispheric coupling of glacial climate through freshwater discharge and ocean circulation., *Nature*, *430*, 851–6, doi:10.1038/nature02786.
Köhler, P., G. Knorr, D. Buiron, a. Lourantou, and J. Chappellaz (2011), Abrupt rise in

atmospheric CO_2 at the onset of the Bølling/Allerød: in-situ ice core data versus true atmospheric signals, *Clim. Past*, *7*, 473–486, doi:10.5194/cp-7-473-2011.

Kucera, M. et al. (2005), Reconstruction of sea-surface temperatures from assemblages of planktonic foraminifera: multi-technique approach based on geographically constrained calibration data sets and its application to glacial Atlantic and Pacific Oceans, *Quat. Sci. Rev.*, *24*, 951–998, doi:10.1016/j.quascirev.2004.07.014.

Kuhlbrodt, T., A. Griesel, and M. Montoya (2007), On the driving processes of the Atlantic meridional overturning circulation, *Rev. Geophys.*, 45, RG2001, doi:10.1029/2004RG000166.

Laskar, J., P. Robutel, F. Joutel, M. Gastineau, A. C. M. Correia, and B. Levrard (2004), A long-term numerical solution for the insolation, *Astron. Astrophys.*, *285*, 261–285.

Lea, D. W., D. K. Pak, L. C. Peterson, and K. a Hughen (2003), Synchroneity of tropical and high-latitude Atlantic temperatures over the last glacial termination., *Science*, *301*, 1361–4, doi:10.1126/science.1088470.

LeGrand, P., and C. Wunsch (1995), Constraints from paleotracer data on the North Atlantic circulation during the Last Glacial Maximum, *Paleoceanography*, *10*, 1011–1045, doi:10.1029/95PA01455.

Legutke, S., and E. Maier (2002), The impact of a downslope water-transport parametrization in a global ocean general circulation model, *Clim. Dyn.*, 18, 611–623, doi:10.1007/s00382-001-0202-z.

Levitus, S., T. P. Boyer, M. E. Conkright, T. O'Brien, J. Antonov, C. Stephens, L. Stathoplos, D. Johnson, and R. Gelfeld (1998), NOAA Atlas NESDIS 18, World Ocean Database 1998: Volume 1: Introduction, *U.S. Gov. Print. Off. Wash., D.C.*, 346pp.

Li, C., D. S. Battisti, and C. M. Bitz (2010), Can North Atlantic Sea Ice Anomalies Account for Dansgaard–Oeschger Climate Signals?, *J. Clim.*, *23*(20), 5457–5475, doi:10.1175/2010JCLI3409.1.

Lippold, J., Y. Luo, R. Francois, and S. Allen (2012), Strength and geometry of the glacial Atlantic Meridional Overturning Circulation, *Nat. Geosci.*, *5*, 813–816, doi:10.1038/NGEO1608.

Liu, Z. et al. (2009), Transient simulation of last deglaciation with a new mechanism for Bolling-Allerod warming., *Science*, *325*, 310–314, doi:10.1126/science.1171041.

Liu, Z., S.-I. Shin, R. S. Webb, W. Lewis, and B. L. Otto-Bliesner (2005), Atmospheric CO_2 forcing on glacial thermohaline circulation and climate, *Geophys. Res. Lett.*, *32*, 32–35, doi:10.1029/2004GL021929.

Liu, Z., X. Zhang, J. Zhu, B. Otto-Bliesner, A. Timmermann, R. S. Smith, G. Lohmann, W. P. Zheng and O. Timm, Slow Global Warming in the Last 10,000 Years, *submitted*

Lohmann, G. (1998), The influence of a near-bottom transport parameterization on the sensitivity of the thermohaline circulation, *J. Phys. Oceanogr.*, 28, 2095–2103.

Lohmann, G., and S. Lorenz (2000), On the hydrological cycle under paleoclimatic conditions as derived from AGCM simulations, *J. Geophys. Res.*, *105*, 17417–17436.

Lohmann, G. and M. Schulz (2000): Reconciling Bølling warmth with peak deglacial meltwater discharge. *Paleoceanography*, 15, 537-540.

Lourantou, A., J. V. Lavrič, P. Köhler, J.-M. M. Barnola, D. Paillard, E. Michel, D.

Raynaud, and J. Chappellaz (2010), Constraint of the CO_2 rise by new atmospheric carbon isotopic measurements during the last deglaciation, *Global Biogeochem. Cycles*, *24*, 1–15, doi:10.1029/2009GB003545.

Lynch-Stieglitz, J. et al. (2007), Atlantic meridional overturning circulation during the Last Glacial Maximum., *Science*, *316*, 66–69, doi:10.1126/science.1137127.

Macayeal, D. R. (1993) Binge/Purge Oscillations of the Laurentide Ice Sheet as A Cause of the North Atlantic's Heinrich Events. *Paleoceanography* 8**,** 775–784.

Manabe, S., and A. Broccoli (1985), The influence of continental ice sheets on the climate of an ice age, *J. Geophys. Res., 90*, 2167, doi:10.1029/JD090iD01p02167.

Marchitto, T. M., and W. S. Broecker (2006), Deep water mass geometry in the glacial Atlantic Ocean: A review of constraints from the paleonutrient proxy Cd/Ca, *Geochemistry Geophys. Geosystems*, *7*, doi:10.1029/2006GC001323.

Marcott, S. A. et al. (2011), Ice-shelf collapse from subsurface warming as a trigger for Heinrich events., *Proc. Natl. Acad. Sci. USA*, *108*, 13415–13419, doi:10.1073/pnas.1104772108.

Marsland, S. J., H. Haak, J. H. Jungclaus, M. Latif, and F. Röske (2003), The Max-Planck-Institute global ocean/sea ice model with orthogonal curvilinear coordinates, *Ocean Model.*, *5*, 91–127, doi:10.1016/S1463-5003(02)00015-X.

Marti, O. et al. (2005), The new IPSL climate system model: IPSL-CM4, Paris, Institut Pierre Simon Laplace: 84.

Masson-Delmotte, V. et al. (2013), Information from Paleoclimate Archives, in *Climate Change 2013: The Physical Science Basis. Contribution of Working Group I to the Fifth Assessment Report of the Intergovernmental Panel on Climate Change*, edited by T. F. Stocker, D. Qin, G.-K. Plattner, M. Tignor, S. K. Allen, J. Boschung, A. Nauels, Y. Xia, V. Bex, and P. M. Midgley, pp. 383–464, Cambridge University Press, Cambridge, United Kingdom and New York, NY, USA.

McCave, I., B. Manighetti, and N. Beveridge (1995), Circulation in the glacial North Atlantic inferred from grain-size measurements, *Nature*, *374*, 149–152.

McManus, J. F., R. Francois, J.-M. Gherardi, L. D. Keigwin, and S. Brown-Leger (2004), Collapse and rapid resumption of Atlantic meridional circulation linked to deglacial climate changes., *Nature*, *428*, 834–837, doi:10.1038/nature02494.

McManus, J. F., D. W. Oppo, and J. L. Cullen (1999), A 0.5-Million-Year Record of Millennial-Scale Climate Variability in the North Atlantic, *Science*, *283*, 971–975, doi:10.1126/science.283.5404.971.

Meehl, G. A., et al. (2007), Global Climate Projections in: Climate Change 2007: The Physical Science Basis. Contribution of Working Group I to the Fourth Assessment Report of the Intergovernmental Panel on Climate Change, Methods, 747–845.

Menviel, L., A. Timmermann, O. E. Timm, and a. Mouchet (2011), Deconstructing the Last Glacial termination: the role of millennial and orbital-scale forcings, *Quat. Sci. Rev.*, *30*, 1155–1172, doi:10.1016/j.quascirev.2011.02.005.

Merkel, U., M. Prange, and M. Schulz (2010), ENSO variability and teleconnections during glacial climates, *Quat. Sci. Rev.*, *29*, 86–100, doi:10.1016/j.quascirev.2009.11.006.

Mignot, J., A. Ganopolski, and A. Levermann (2007), Atlantic Subsurface Temperatures: Response to a Shutdown of the Overturning Circulation and Consequences for Its Recovery, *J. Clim.*, *20*, 4884–4898, doi:10.1175/JCLI4280.1.

Monnin, E., a Indermühle, a Dällenbach, J. Flückiger, B. Stauffer, T. F. Stocker, D. Raynaud, and J. M. Barnola (2001), Atmospheric CO_2 concentrations over the last glacial termination., *Science*, *291*, 112–114, doi:10.1126/science.291.5501.112.

Niedermeyer, E. M., M. Prange, S. Mulitza, G. Mollenhauer, E. Schefuß, and M. Schulz (2009), Extratropical forcing of Sahel aridity during Heinrich stadials, *Geophys. Res. Lett.*, *36*, L20707, doi:10.1029/2009GL039687.

Oka, a., H. Hasumi, and a. Abe-Ouchi (2012), The thermal threshold of the Atlantic meridional overturning circulation and its control by wind stress forcing during glacial climate, *Geophys. Res. Lett.*, *39*, 1–6, doi:10.1029/2012GL051421.

Otto-Bliesner, B. L., and E. C. Brady (2010), The sensitivity of the climate response to the magnitude and location of freshwater forcing: last glacial maximum experiments, *Quat. Sci. Rev.*, *29*, 56–73, doi:10.1016/j.quascirev.2009.07.004.

Otto-Bliesner, B. L., E. C. Brady, G. Clauzet, R. Tomas, S. Levis, and Z. Kothavala (2006), Last Glacial Maximum and Holocene Climate in CCSM3, *J. Clim.*, *19*, 2526–2544, doi:10.1175/JCLI3748.1.

Otto-Bliesner, B. L., C. D. Hewitt, T. M. Marchitto, E. Brady, A. Abe-Ouchi, M. Crucifix, S. Murakami, and S. L. Weber (2007), Last Glacial Maximum ocean thermohaline circulation: PMIP2 model intercomparisons and data constraints, *Geophys. Res. Lett.*, *34*, L12706, doi:10.1029/2007GL029475.

Paul, A., and C. Schäfer-Neth (2003), Modeling the water masses of the Atlantic Ocean at the Last Glacial Maximum, *Paleoceanography*, *18*, 1-16, doi:10.1029/2002PA000783.

Peck, V. L., I. R. Hall, R. Zahn, and H. Elderfield (2008), Millennial-scale surface and subsurface paleothermometry from the northeast Atlantic, 55-8 ka BP, *Paleoceanography*, *23*, 1–11, doi:10.1029/2008PA001631.

Peltier, W. (1994), Ice age paleotopography, *Science*, *265*, 195–201.

Peltier, W., and R. Fairbanks (2006), Global glacial ice volume and Last Glacial Maximum duration from an extended Barbados sea level record, *Quat. Sci. Rev.*, *25*, 3322–3337, doi:10.1016/j.quascirev.2006.04.010.

Peltier, W. R. (2004), Global Glacial Isostasy and the Surface of the Ice-Age Earth : The ICE-5G (VM2) Model and GRACE, *Annu. Rev. Earth Planet. Sci.*, *32*, 111–149, doi:10.1146/annurev.earth.32.082503.144359.

Peterson, L. C., G. H. Haug, K. A. Hughen, and U. Roehl (2000), Rapid Changes in the Hydrologic Cycle of the Tropical Atlantic During the Last Glacial, *Science*, *290*, 1947–1951, doi:10.1126/science.290.5498.1947.

Petersen, S. V, Schrag, D. P. & Clark, P. U. (2013) A new mechanism for Dansgaard-Oeschger cycles. *Paleoceanography* 28**,** 24–30.

Pflaumann, U. (2003), Glacial North Atlantic: Sea-surface conditions reconstructed by GLAMAP 2000, *Paleoceanography*, *18*, 1065, doi:10.1029/2002PA000774.

Piotrowski, A. M. et al. (2008), Oscillating glacial northern and southern deep water formation from combined neodymium and carbon isotopes, *Earth Planet. Sci. Lett.*, 272, 394–405.

Praetorius, S. K., J. F. McManus, D. W. Oppo, and W. B. Curry (2008), Episodic reductions in bottom-water currents since the last ice age, *Nat. Geosci.*, *1*, 449–452, doi:10.1038/ngeo227.

Prange, M., V. Romanova, and G. Lohmann (2002), The glacial thermohaline circulation:

stable or unstable? *Geophys. Res. Lett.,* 29, 2028, doi:10.1029/2002GL015337.

Raddatz, T. J., C. H. Reick, W. Knorr, J. Kattge, E. Roeckner, R. Schnur, K.-G. Schnitzler, P. Wetzel, and J. Jungclaus (2007), Will the tropical land biosphere dominate the climate–carbon cycle feedback during the twenty-first century?, *Clim. Dyn.*, *29*, 565–574, doi:10.1007/s00382-007-0247-8.

Rahmstorf, S. (1996), On the freshwater forcing and transport of the Atlantic thermohaline circulation, *Clim. Dyn.*, 12, 799–811.

Rahmstorf, S. (2002), Ocean circulation and climate during the past 120,000 years., *Nature*, *419*, 207–14, doi:10.1038/nature01090.

Rahmstorf, S. et al. (2005), Thermohaline circulation hysteresis: A model intercomparison, *Geophys. Res. Lett.*, *32*, L23605, doi:10.1029/2005GL023655.

Randall, D. A. et al. (2007), Climate Change 2007: The Physical Science Basis. Contribution of working Group I to the Fourth Assessment Report of the intergovernmental Panel on Climate Change, edited by S. Solomon, D. Qin, M. Manning, Z. Chen, M. Marquis, K. B. Averyt, M. Tignor, and H. L. Miller, Cambridge University Press, Cambridge, United kingdom and New York, NY, USA.

Rasmussen, T. L., and E. Thomsen (2004), The role of the North Atlantic Drift in the millennial timescale glacial climate fluctuations, *Palaeogeogr. Palaeoclimatol. Palaeoecol.*, *210*, 101–116, doi:10.1016/j.palaeo.2004.04.005.

Ritz, S. P., T. F. Stocker, J. O. Grimalt, L. Menviel, and A. Timmermann (2013), Estimated strength of the Atlantic overturning circulation during the last deglaciation, *Nat. Geosci.*, *6*, 208–212, doi:10.1038/ngeo1723.

Roberts, W. H. G., P. J. Valdes, and A. J. Payne (2014), A new constraint on the size of Heinrich Events from an iceberg/sediment model, *Earth Planet. Sci. Lett.*, *386*, 1–9, doi:10.1016/j.epsl.2013.10.020.

Roche, D. M., A. P. Wiersma, and H. Renssen (2010), A systematic study of the impact of freshwater pulses with respect to different geographical locations, *Clim. Dyn.*, *34*, 997–1013, doi:10.1007/s00382-009-0578-8.

Roche, D., D. Paillard, and E. Cortijo (2004), Constraints on the duration and freshwater release of Heinrich event 4 through isotope modelling, *Nature*, *432*, 379–382, doi:10.1038/nature03040.1.

Roeckner, E. et al. (2003), Report No . 349 the atmohspheric general circulation model ECHAM5 Part 1: Model description, 1–127.

Rühlemann, C., S. Mulitza, G. Lohmann, A. Paul, M. Prange, and G. Wefer (2004), Intermediate depth warming in the tropical Atlantic related to weakened thermohaline circulation: Combining paleoclimate data and modeling results for the last deglaciation, *Paleoceanography*, *19*, 1–10, doi:10.1029/2003PA000948.

Schmitt, J. et al. (2012), Carbon Isotope Constraints on the Deglacial CO2 Rise from Ice Cores., *Science*, *336*, 711–4, doi:10.1126/science.1217161.

Schmittner, A., and E. D. Galbraith (2008), Glacial greenhouse-gas fluctuations controlled by ocean circulation changes., *Nature*, *456*, 373–376, doi:10.1038/nature07531.

Schmittner, A., M. Yoshimori, and A. J. Weaver (2002), Instability of Glacial Climate in a Model of the Ocean- Atmosphere-Cryosphere System, *Science*, *295*, 1489–1493, doi:10.1126/science.1066174.

Schulz, M., W. H. Berger, M. Sarnthein, and P. M. Grootes (1999), Amplitude variations

of 1470-year climate oscillations during the last 100,000 years linked to fluctuations of continental ice mass, *Geophys. Res. Lett.*, *26*, 3385–3388.

Seidov, D., R. J. Stouffer, and B. J. Haupt (2005), Is there a simple bi-polar ocean seesaw?, *Glob. Planet. Change*, *49*, 19–27, doi:10.1016/j.gloplacha.2005.05.001.

Shakun, J. D., P. U. Clark, F. He, S. a. Marcott, A. C. Mix, Z. Liu, B. Otto-bliesner, A. Schmittner, and E. Bard (2012), Global warming preceded by increasing carbon dioxide concentrations during the last deglaciation, *Nature*, *484*, 49–54, doi:10.1038/nature10915.

Shin, S.-I., Z. Liu, B. L. Otto-Bliesner, J. Kutzbach, and S. J. Vavrus (2003), Southern Ocean sea-ice control of the glacial North Atlantic thermohaline circulation, *Geophys. Res. Lett.*, *30*, 1096, doi:10.1029/2002GL015513.

Siddall, M., E. J. Rohling, W. G. Thompson, and C. Waelbroeck (2008), Marine Isotope Stage 3 Sea Level Fluctuations: Data Synthesis and New Outlook, *Rev. Geophys.*, *46*, RG000226, doi:10.1029/2007RG000226.1.

Singarayer, J. S., and P. J. Valdes (2010), High-latitude climate sensitivity to ice-sheet forcing over the last 120kyr, *Quat. Sci. Rev.*, *29*, 43–55, doi:10.1016/j.quascirev.2009.10.011.

Singh, H. A., D. S. Battisti, and C. M. Bitz (2013), A heuristic Model of Dansgaard-Oeschger Cycles: Description, Results and Sensitivity Studies: Part I, *J. Clim.*, in press, doi:10.1175/JCLI-D-12-00672.1.

Stanford, J. D., E. J. Rohling, S. E. Hunter, A. P. Roberts, S. O. Rasmussen, E. Bard, J. McManus, and R. G. Fairbanks (2006), Timing of meltwater pulse 1a and climate responses to meltwater injections, *Paleoceanography*, *21*, PA4103, doi:10.1029/2006PA001340.

Stauffer, B., T. Blunier, A. Dällenbach, A. Indermuhle, J. Schwander, T. F. Stocker, J. Tschumi, J. Chappellaz, D. Raynaud, C. U. Hammer and H. B. Clausen (1998), Atmospheric CO_2 concentration and millennial-scale climate change during the last glacial period, *Nature*, *392*, 59-62.

Stepanek, C., and G. Lohmann (2012), Modelling mid-Pliocene climate with COSMOS, *Geosci. Model Dev.*, *5*, 1221–1243, doi:10.5194/gmd-5-1221-2012.

Stocker, T. F., and S. J. Johnsen (2003), A minimum thermodynamic model for the bipolar seesaw, *Paleoceanography*, *18*, 1–9, doi:10.1029/2003PA000920.

Stouffer, R. J. et al. (2006), Investigating the Causes of the Response of the Thermohaline Circulation to Past and Future Climate changes, *J. Clim.*, *19*, 1365–1387.

Stouffer, R., D. Seidov, and B. Haupt (2007), Climate response to external sources of freshwater: North Atlantic versus the Southern Ocean., *J. Clim.*, 20, 436–448.

Toggweiler, J. R., and B. Samuels (1995), Effect of Drake Passage on the global thermohaline circulation, *Deep Sea Res. I*, *42*, 477–500.

Ullman, D. J., A. N. LeGrande, A. E. Carlson, F. S. Anslow, and J. M. Licciardi (2013), Assessing the impact of Laurentide Ice-Sheet topography on glacial climate, *Clim. Past Discuss.*, *9*, 3239–3306, doi:10.5194/cpd-9-3239-2013.

Varma, V., M. Prange, U. Merkel, T. Kleinen, G. Lohmann, M. Pfeiffer, H. Renssen, a. Wagner, S. Wagner, and M. Schulz (2012), Holocene evolution of the Southern Hemisphere westerly winds in transient simulations with global climate models, *Clim. Past*, *8*, 391–402, doi:10.5194/cp-8-391-2012.

De Vernal, a., a. Rosell-Melé, M. Kucera, C. Hillaire-Marcel, F. Eynaud, M. Weinelt, T.

Dokken, and M. Kageyama (2006), Comparing proxies for the reconstruction of LGM sea-surface conditions in the northern North Atlantic, *Quat. Sci. Rev.*, *25*, 2820–2834, doi:10.1016/j.quascirev.2006.06.006.

Voelker, A. H. L. (2002), Global distribution of centennial-scale records for Marine Isotope Stage (MIS) 3: a database, *Quat. Sci. Rev.*, *21*, 1185–1212, doi:10.1016/S0277-3791(01)00139-1.

De Vries, P., and S. L. Weber (2005), The Atlantic freshwater budget as a diagnostic for the existence of a stable shut down of the meridional overturning circulation, *Geophys. Res. Lett.*, *32*, 1–4, doi:10.1029/2004GL021450.

Waelbroeck, C. et al. (2009), Constraints on the magnitude and patterns of ocean cooling at the Last Glacial Maximum, *Nat. Geosci.*, *2*, 127–132, doi:10.1038/ngeo411.

Weaver, A. J., O. a Saenko, P. U. Clark, and J. X. Mitrovica (2003), Meltwater pulse 1A from Antarctica as a trigger of the Bølling-Allerød warm interval., *Science*, *299*, 1709–1713, doi:10.1126/science.1081002.

Weber, M. E., P. U. Clark, G. Kuhn, A. Timmermann, D. Sprenk, R. Gladstone, X. Zhang, G. Lohmann, L. Menviel, M. O. Chikamoto, T. Friedrich, C. Ohlwein, Millennial-scale variability in Antarctic ice-sheet discharge during the last deglaciation, *Nature*, *accepted*.

Weber, S. L., S. S. Drijfhout, A. Abe-Ouchi, M. Crucifix, M. Eby, A. Ganopolski, S. Murakami, B. Otto-Bliesner, and W. R. Peltier (2007), The modern and glacial overturning circulation in the Atlantic ocean in PMIP coupled model simulations, *Clim. Past*, *3*, 51–64, doi:10.5194/cp-3-51-2007.

Wei, W., and G. Lohmann (2012), Simulated Atlantic Multidecadal Oscillation during the Holocene, *J. Clim.*, 25, 6989-7002, doi:10.1175/JCLI-D-11-00667.1.

Wei, W., G. Lohmann, and M. Dima (2012), Distinct modes of internal variability in the Global Meridional Overturning Circulation associated with the Southern Hemisphere westerly winds, *J. Phys. Oceanogr.*, 42, 785-801, doi:10.1175/JPO-D-11-038.1.

Wunsch, C. (2006), Abrupt climate change: an alternative view, *Quat. Res.*, *65*, 191-203.

Yu, E., R. Francois, and M. P. Bacon (1996), Similar rates of medern and last glacial ocean thermohaline circulation inferred from radiochemical data, Nature, 379, 689-694, doi:10.1038/379689a0

Yu, Y., R. Yu, X. Zhang, and H. Liu (2002), A flexible coupled ocean- atmosphere general circulation model, Adv. Atmos. Sci., 19, 169–190, doi:10.1007/s00376-002-0042-8.

Yu, Y., X. Zhang, and Y. Guo (2004), Global coupled ocean-atmosphere general circulation models in LASG/IAP, Adv. Atmos. Sci., 21, 444–455, doi:10.1007/bf02915571.

Zahn, R., H. Erlenkeuser, P. Grootes, and A. Abstract (1997), Thermohaline instability in the North Atlantic during meltwater events : Stable isotope and ice-rafted detritus records from core SO75-26KL, Portuguese margin, *Paleoceanography*, *12*, 696–710.

Zhang, R., and T. L. Delworth (2005), Simulated Tropical Response to a Substantial Weakening of the Atlantic Thermohaline Circulation, *J. Clim.*, 18, 1853–1860, doi: http://dx.doi.org/10.1175/JCLI3460.1

Zhang, X., G. Lohmann, G. Knorr, and C. Purcell, Control of rapid glacial climate shifts by variations in intermediate ice-sheet volume, *Nature*, *in revision*

Zhang, X., G. Lohmann, G. Knorr, and X. Xu (2013), Different ocean states and transient characteristics in Last Glacial Maximum simulations and implications for deglaciation, *Clim. Past*, *9*, 2319–2333, doi:10.5194/cp-9-2319-2013.